(2)

NAVAL POSTGRADUATE SCHOOL

Monterey, California

THESIS

ANALYSIS OF IN-FLIGHT STRUCTURAL FAILURES
OF P-3C WING LEADING EDGE SEGMENTS

by

Dennis A. Lott

June 1992

Thesis Advisor: Louis V. Schmidt

Approved for public release; distribution is unlimited

REPORT DOCUMENTATION PAGE

1a. REPORT SECURITY CLASSIFICATION UNCLASSIFIED	1b. RESTRICTIVE MARKINGS
2a. SECURITY CLASSIFICATION AUTHORITY 2b. DECLASSIFICATION/DOWNGRADING SCHEDULE	3. DISTRIBUTION/AVAILABILITY OF REPORT Approved for public release; distribution is unlimited.
4. PERFORMING ORGANIZATION REPORT NUMBER(S)	5. MONITORING ORGANIZATION REPORT NUMBER(S)
6a. NAME OF PERFORMING ORGANIZATION Naval Postgraduate School 6b. OFFICE SYMBOL (*If applicable*) AA	7a. NAME OF MONITORING ORGANIZATION Naval Postgraduate School
6c. ADDRESS (*City, State, and ZIP Code*) Monterey, CA 93943-5000	7b. ADDRESS (*City, State, and ZIP Code*) Monterey, CA 93943-5000
8a. NAME OF FUNDING/SPONSORING ORGANIZATION 8b. OFFICE SYMBOL (*If applicable*)	9. PROCUREMENT INSTRUMENT IDENTIFICATION NUMBER
8c. ADDRESS (*City, State, and ZIP Code*)	10. SOURCE OF FUNDING NUMBERS Program Element No. / Project No. / Task No. / Work Unit Accession Number

11. TITLE (*Include Security Classification*)
ANALYSIS OF IN-FLIGHT STRUCTURAL FAILURES OF P-3C WING LEADING EDGE SEGMENTS

12. PERSONAL AUTHOR(S) Dennis A. Lott

13a. TYPE OF REPORT	13b. TIME COVERED	14. DATE OF REPORT (*year, month, day*)	15. PAGE COUNT
Master's Thesis	From To	June 1992	118

16. SUPPLEMENTARY NOTATION
The views expressed in this thesis are those of the author and do not reflect the official policy or position of the Department of Defense or the U.S. Government.

17. COSATI CODES			18. SUBJECT TERMS (*continue on reverse if necessary and identify by block number*)
FIELD	GROUP	SUBGROUP	Aeroelasticity, span-load analysis, panel methods, finite-element analysis, stress levels, stress concentrations, structural failure.

19. ABSTRACT (*continue on reverse if necessary and identify by block number*)

A quantative analysis was carried out to determine the stresses present in the leading-edge segment of a P-3C aircraft operating within and outside the normal operating envelope of the aircraft. The purpose of the analysis was to ascertain whether a specific weakness may exist in the leading-edge structure which might endanger future operating flight crews. A three-step process consisting of a static aeroelastic span-load analysis, an inviscid two-dimensional panel-method analysis, and finite-element analysis was employed in the course of the evaluation. Lift-coefficient distributions from the wing span-load analyses were used in the two-dimensional panel method to determine the pressure distribution around the leading edge, which was then used as input to the finite-element analysis. Additionally, static aeroelastic-derived wing-twist effects were included in the structural model. The results of the analysis suggest that the leading edge segment studied may experience stress levels sufficient to cause failure within the normal operating envelope.

20. DISTRIBUTION/AVAILABILITY OF ABSTRACT	21. ABSTRACT SECURITY CLASSIFICATION	
☒ UNCLASSIFIED/UNLIMITED ☐ SAME AS REPORT ☐ DTIC USERS	UNCLASSIFIED	
22a. NAME OF RESPONSIBLE INDIVIDUAL Louis V. Schmidt	22b. TELEPHONE (*Include Area code*) (408) 646-2972	22c. OFFICE SYMBOL AA/Sc

DD FORM 1473, 84 MAR — 83 APR edition may be used until exhausted; All other editions are obsolete — SECURITY CLASSIFICATION OF THIS PAGE: UNCLASSIFIED

Approved for public release; distribution is unlimited.

ANALYSIS OF IN-FLIGHT STRUCTURAL FAILURES OF P-3C WING LEADING EDGE SEGMENTS

by

Dennis A. Lott
Lieutenant Commander, United States Navy
B.S., Arizona State University, 1974

Submitted in partial fulfillment
of the requirements for the degree of

MASTER OF SCIENCE IN AERONAUTICAL ENGINEERING

from the

NAVAL POSTGRADUATE SCHOOL
June, 1992

Author: 

Dennis A. Lott

Approved by: 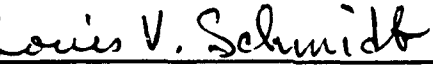

Louis V. Schmidt, Thesis Advisor

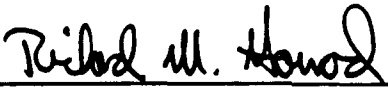

Richard M. Howard, Second Reader

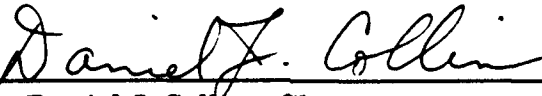

Daniel J. Collins, Chairman
Department of Aeronautics and Astronautics

ABSTRACT

A quantitative analysis was carried out to determine the stresses present in the leading-edge segment of a P-3C aircraft operating within and outside the normal operating envelope of the aircraft. The purpose of the analysis was to ascertain whether a specific weakness may exist in the leading-edge structure which might endanger future operating flight crews. A three-step process consisting of a static aeroelastic span-load analysis, an inviscid two-dimensional panel method, and finite-element analysis was employed in the course of the evaluation. Lift-coefficient distributions from the wing span-load analyses were used in the two-dimensional panel method to determine the pressure distribution around the leading edge, which was then used as input to the finite-element analysis. Additionally, static aeroelastic-derived wing-twist effects were included in the structural model. The results of the analysis suggest that the leading edge segment studied may experience stress levels sufficient to cause failure within the normal operating envelope.

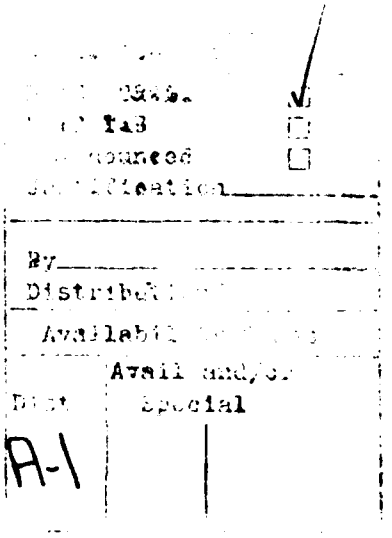

THESIS DISCLAIMER

Although certain commercial software products are referred to in the body of this thesis, such references do not constitute recommendations for use or endorsements of the products.

TABLE OF CONTENTS

ACKNOWLEDGEMENT

This thesis would not have been possible without the help and support of many. Foremost among these are the members of my family, Fran, Casey and Ryan, who have endured my absences, aggravation and absent-mindedness. Your love has sustained me.

To the scholar from who's seemingly endless reserve of talent and patience I have drawn for many months, I can only say, "Thank you, Professor Lou Schmidt".

Thanks also to those who have provided help, inspiration, equipment and time in this endeavor: LCDR Rick Bobbitt who brought this topic to my attention and gave of his time and advice; Dr. Hank Smith who co-sponsored Rick's proposal; Professor Rick Howard who helped with the simulator run and photography, as well as scholarly advice; Professor Ed Wu for his inspiration and aid in the area of finite element analysis; Professor Gerald Lindsey for his help in structural analysis; and Nam Phan and Li Chen, who provided the foundation and support for the finite element model.

I. INTRODUCTION

On 13 February 1988, a U.S. Navy (USN) P-3C Update I Orion aircraft experienced an in-flight failure of a wing leading-edge section during a high-speed, low-altitude maneuver. The aircraft was able (with some difficulty) to return to its departure point and make a safe landing. Some three years later, on 27 April 1991, an Orion operated by the Royal Australian Air Force (RAAF) suffered a similar but more extensive in-flight failure when it lost three wing leading-edge sections during a maneuver similar to the U.S. Navy mishap. The Australian crew was unable to return to the runway due to the loss of lift available from the damaged wings. The aircraft impacted the ocean surface short of its island destination in a nose high-attitude with maximum power set on all four engines. One crewmember was killed when a propeller tore loose from its engine and entered the fuselage where he was sitting.

The leading edge is the rounded front portion of the wing which is physically attached to the front wing spar and is essential in the production of lift by an airfoil. Loss of a leading-edge segment results in a dramatic reduction in wing lift capability combined with a corresponding increase in

drag. The P-3 has three of these leading-edge segments on each wing, separated by the engine nacelles. They are best referred to as inboard, center and outboard sections. Figure 1 shows the P-3 aircraft. The inboard sections are those between the fuselage and the inboard engines on this four-engine turboprop aircraft. The center sections (blackened) span the distance between the inboard and outboard engine nacelles, while the outboard sections cover the remaining distance from the outboard engines to the wing tips. The length (fore and aft) of these leading-edge sections is 15% of the chord (total fore and aft distance) of the wings.

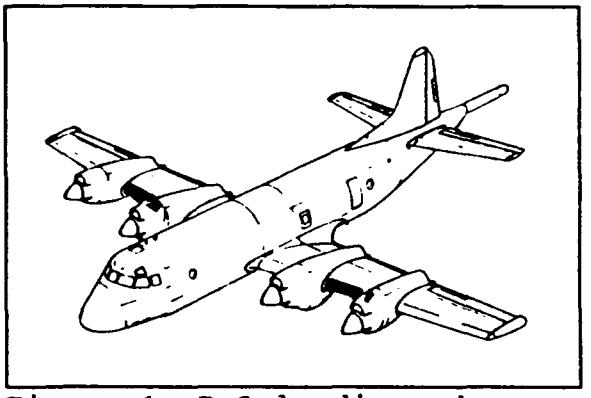

Figure 1. P-3 leading edges.

The USN P-3 lost the starboard wing center leading-edge section while the RAAF aircraft lost both of its center sections and the starboard inboard section. This study focuses on the center leading edge sections.

While both of these mishaps were investigated by the appropriate authorities, the cause of the failures were undetermined, though widely suspected to be the result of aircraft overstress due to pilot error. In both cases, the pilots did not feel that they had exceeded the normal operating envelope (this envelope will be detailed later) for

the aircraft. Even if the aircraft were operated outside the authorized envelope, the question remains as to why the leading edge sections failed before some other component.

This thesis was undertaken for the purpose of studying the aerodynamic loading and structural response of a leading edge section due to operation within and outside the normal flight envelope. Ultimately, its aim was to determine whether there may be a need to further restrict the operating envelope or recommend some modification to the existing structure in order to prevent a further recurrence of the in-flight failure.

II. GENERAL AERODYNAMICS

A. MISHAP AIRCRAFT SPECIFICATIONS

The configurations and operational parameters of the mishap aircraft were similar in that both were at high gross weight (RAAF at 127,000 pounds, USN at 135,000 pounds) and operating at high airspeeds (RAAF approximately 380 knots, USN approximately 350 knots). Both aircraft executed a pullup maneuver from an altitude of less than 400 feet at the time of leading edge failure. The RAAF maneuver was a straight pullup (wings level), while the USN maneuver was a starboard rolling pullup (meaning that the aircraft was banked to the right as the pullup maneuver was executed). Interviews with some USN crewmembers indicate that the failure of their leading-edge section may have begun a few seconds earlier as the aircraft rolled from a right bank to wings level while inbound for the above stated pullup. This, they said, was reported to them by ground observers. Table 1 presents the relevant P-3C dimensional data used during this analysis while Table 2 delineates the aircraft performance parameters. Figure 2 shows the operating flight envelope for the aircraft in a flaps-up, gear-up configuration.

TABLE 1. DIMENSIONAL DATA [Refs. 1,2,3]

Wing		
Area, S (ft^2)		1300
Span, b (theoretical, ft)		99
MAC, cbar (ft)		14.1
Aspect Ratio, A		7.5
Taper Ratio, λ		0.4
Dihedral, ($.25c_w$, degrees)		5.0
Incidence, Root (degrees)		3.0
Tip		0.5
Airfoil Section, Root	NACA0014-1.10 40/1.051	cl_i=.3,a=.8
Tip	NACA0014-1.10 40/1.051	cl_i=.4,a=.8
Straight Element		0.15c
Chord, Root (ft)		18.9
Tip		7.6
Aileron		
Area, S_a (ft^2)		45.5
Hinge Line (c_w)		0.725
Deflection Limit, Up (degrees)		-23.3
Down		+16.2
Horizontal Tail		
Area, S_t (ft^2)		321.8
Tail Length ($.25cbar_w$ to $.25cbar_t$, ft)		49.8

TABLE 2. PERFORMANCE PARAMETERS [Refs. 1,2,3]

Flight Design Gross Weight (pounds)	135000
Load Factor (through 135,000 pounds, G)	-1.0 to +3.0
Maximum Operating Speed, Sea Level (knots)	405
Center of Gravity Limits (135,000 lbs, %MAC)	21.5 to 31.0
Maximum Shaft Horsepower (per engine)	4600
Maximum Lift Coefficient, C_{Lmax} (power off)	1.30
Lift Curve Slope, $C_{L\alpha}$, Tail Off (power off)	4.84
Tail On (power off)	5.50
Moment Slope, C_{mCL}, Tail Off, c.g @ $0.25cbar_W$	0.19

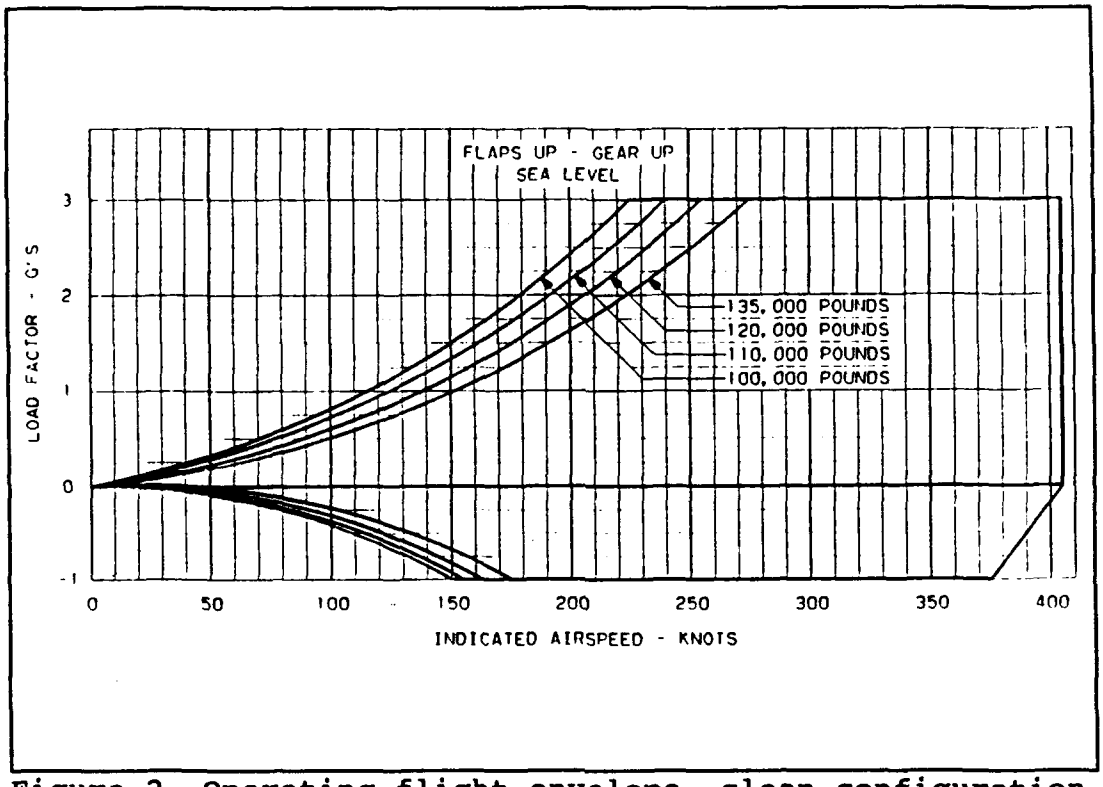

Figure 2. Operating flight envelope, clean configuration [Ref. 2].

B. PROBLEM STATEMENT

Accurate analysis of the problem within limited time and budget constraints available for completion of the work served to restrict the options for solution methods. While instrumented flight and laboratory tests would probably be more precise, these choices were not feasible. It was necessary to develop an analytic method which could provide credible results within the academic environment.

Determination of the loads applied and their effect upon the leading edge structure was accomplished by a three-step process. The first step was to conduct a static aeroelastic

span-load analysis of the wing using a computer program to determine the section lift coefficients and structural twist on the P-3 wing. Next, a two-dimensional panel method was employed to find the pressure distribution around the leading edge. Finally, the forces derived from the pressure distribution were used as the loads applied in a finite element analysis computer application. In addition, consideration was given to the aeroelastically-derived spanwise wing twists which were introduced as torsion-like deflections in the finite element analysis.

C. ASSUMPTIONS

Certain assumptions were made in conducting the analysis. While static aeroelasticity effects upon the wing were accounted for, the fuselage and tail were assumed as rigid structures. In addition, the effect of fuselage interference on wing lift distribution was neglected. That is, the wing was taken to be fully effective in producing lift even in the central region where it is influenced by the fuselage. The unswept, straight-tapered wing with an aspect ratio of 7.5 was modeled structurally in the span-load analysis by an elastic axis. Chordwise bending of the wing was neglected. Inviscid solution methods were employed in the span-load and airfoil analysis programs. It was felt that these assumptions would model the flowfield without inducing an unacceptable level of error in the overall outcome, and that this analysis was a

preferable method of solution to performing a computational-fluid-dynamics analysis where static aeroelastic influence could not be included. Static aeroelastic effects upon wing loadings were suspected of playing a large role in the problem because of the location of the wing's elastic axis at a constant 40 percent of chord, according to available information. This is well aft of the 25 percent of chord location at which a majority of the aerodynamic loadings are presumed to act, creating the potential for a significant coupling influence by structural deflection during the development of lift.

III. WING SPAN-LOAD ANALYSIS

A. THEORY

Because the P-3 wing (as well as nearly all others) is flexible, the aerodynamic-load distribution varies from that which would be seen when considering the wing as a rigid structure. Allowing for structural deflection of the wing increases the accuracy of the result in the attempt to model the true physics of the problem. The computer program used for this analysis, written in Microsoft Quick BASIC®, was based upon the work of Schmidt [Ref. 4]; c.f. Appendix A. The basic concepts employed in the program are presented below.

Defining a set of linear, simultaneous equations for the span-load solution on a wing at a specified angle of attack starts with the following:

$$a_{i1}(\ell/q)_1 + a_{i2}(\ell/q)_2 + \ldots + a_{in}(\ell/q)_n = \alpha_i$$

where the wing is cut into a series of spanwise stations and

- a_{ij} = aerodynamic influence coefficient of (ℓ/q) at station "j" upon induced angle at control station "i"
- ℓ = running span-load ($lb\text{-}in^{-1}$)
- q = freestream dynamic pressure ($lb\text{-}in^{-2}$)
- α_i = geometric angle of attack at control station "i".

The relationship states that the span-load-induced downwash velocities satisfy flow tangency at a control point. Expressed as a matrix equation this system becomes:

$$[A]\{\ell/q\} = \{\alpha\}$$

where,

- $[A]$ = square (n x n) matrix of aerodynamic influence coefficients (length^{-1})
- $\{\ell/q\}$ = column (n x 1) matrix of span-load values (length)
- $\{\alpha\}$ = column (n x 1) matrix of angle-of-attack input (radian)

In similar fashion, a matrix equation relating the structural twist at a wing station "i" to the span-loading may be developed from:

$$s_{i1}\ell_1 + s_{i2}\ell_1 + \ldots + s_{in}\ell_n = \Delta\alpha_{si}$$

or, $$q\{s_{i1}(\ell/q)_1 + s_{i2}(\ell/q)_2 + \ldots + s_{in}(\ell/q)_n\} = \Delta\alpha_{si}$$

which may be stated to apply to all the wing stations as before to yield the matrix equation,

$$q[S]\{\ell/q\} = \{\Delta\alpha_s\}$$

where,

- $[S]$ = square (n x n) matrix of structural influence coefficients (length-force^{-1})
- $\{\Delta\alpha_s\}$ = column (n x 1) matrix of effective angle-of-attack changes due to structural twist (radian)

Next, the two matrix equations may be combined to generate a single equation for an elastic wing as follows:

$$[A]\{\ell/q\}_E = \{\alpha\}_R + \{\Delta\alpha\}_S$$

$$[A]\{\ell/q\}_E = \{\alpha\}_R + q[S]\{\ell/q\}_E$$

$$\left[[A] - q[S] \right] \{\ell/q\}_E = \{\alpha\}_R$$

yielding the span-load solution for the elastic wing,

$$\{\ell/q\}_E = \left[[A] - q[S] \right]^{-1} \{\alpha\}_R$$

where the subscript "E" is used to mean elastic and "R" to mean rigid.

The concept of mathematical symmetry may be employed to develop equations for a symmetric and anti-symmetric load case by considering the wing to be divided into left and right hand wing panels at the spanwise centerline. This process allows a superposition of linear aerodynamic solutions such as the combination of a symmetric pullup and anti-symmetric roll rate to yield the total solution for a rolling pullup. It also reduces computing time since the size of the matrices is half the original required for the total wing. In employing this technique it is necessary to distinguish between the symmetric and anti-symmetric forms of the aerodynamic influence coefficients.

The approach employed for developing the aerodynamic influence coefficients involves use of a technique known as the "Modified Weissinger" approach, wherein the wing is divided into a series of spanwise stations with swept bound vortices attached at the local quarter-chord point, giving rise to horseshoe vortices extending downstream to infinity in accordance with Helmholtz' laws. The vortex strengths are

determined in accordance with the Biot-Savart law, such that the induced downwash angle at all local three-quarter chord points (from the summation of all vortices) are equivalent to the local geometric angle of attack. The three-quarter chord points are termed "control points". Enforcement of the stated boundary conditions replicates the occurrence of tangential flow over the surface of the wing. Application of the Biot-Savart and Kutta-Jukowski laws to the geometric relationships of the horseshoe vortices and control points results in development of the symmetric and anti-symmetric aerodynamic influence coefficient matrices,

$$[A_s] = \left[[A]_{RH} + [A]_{LH} \right]$$

$$[A_a] = \left[[A]_{RH} - [A]_{LH} \right]$$

where the subscripts "RH" and "LH" denote the right and left hand wing panels, respectively. These influence coefficient matrices may next be substituted in the previously-developed equations to yield,

$$[A_s]\{\ell/q\} = \{\alpha_s\}$$

$$[A_a]\{\ell/q\} = \{\alpha_a\}$$

Subsonic compressibility effects were included in the development of the aerodynamic influence coefficients using the Prandtl-Glauert planform distortion approach [Ref. 5]. In this method, the chordwise dimension of the planform is increased according to the relationship,

$$x' = \frac{x}{\sqrt{1-M^2}}$$

The "Modified Weissenger" approach was altered to a panel form for this analysis in that the wing half was divided into five chordwise and ten spanwise stations, requiring manipulation of (50 x 50) matrices. A representative sketch of the method employed is shown in Figure 3. The vector U in the figure represents the free stream velocity while Γ is the circulation strength of the vortex filament.

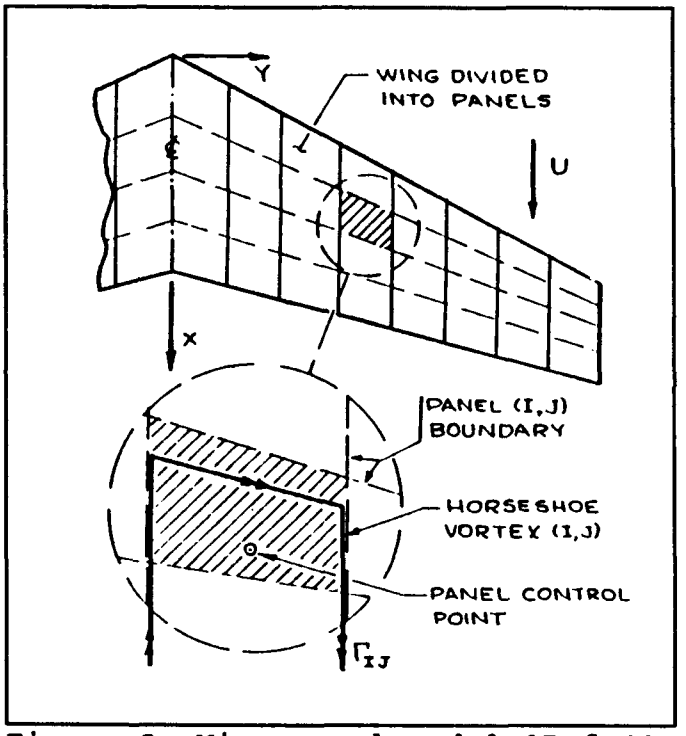

Figure 3. Wing panel model [Ref 4].

Development of the structural influence coefficient matrix in the program is accomplished through determination of the moments exerted about the longitudinal (X) and lateral (Y) axes of the wing at points along the wing elastic axis as shown in Figure 4. These points correspond to the mid-span locations of the individual panels, along the elastic axis. These moments are found by solving the matrix equations:

$\{M_y\}=q(B/N)[t]\{\ell/q\}$

$\{M_x\}=q(B/N)^2[m]\{\ell/q\}$

Where B is the span, N is the number of spanwise local stations, [t] is a torsional matrix and [m] is a bending moment matrix. From these equations, a coordinate axis rotation can be performed as follows:

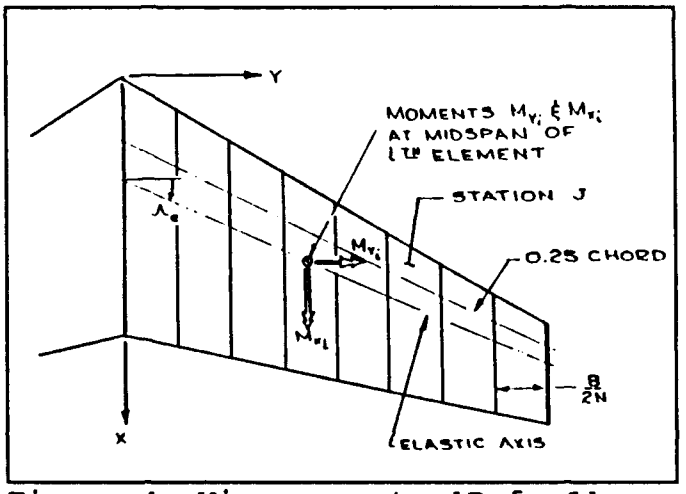

Figure 4. Wing moments [Ref. 6]

$$\{T\} = \cos\Lambda_e\{M_y\} + \sin\Lambda_e\{M_x\}$$

$$\{M\} = -\sin\Lambda_e\{M_y\} + \cos\Lambda_e\{M_x\}$$

Next, torsional and bending stiffness (GJ and EI) values along the elastic axis are employed to determine the angular deflections resulting from the torsion and bending moments from the equations,

$$\Theta_t(y) = \int_0^{\frac{y}{\cos\lambda_e}} \frac{T(z)}{GJ(z)}dz \qquad \Theta_t(m) = \int_0^{\frac{y}{\cos\lambda_e}} \frac{M(z)}{EI(z)}dz$$

These are then discretized as,

$$\Delta\Theta_m(I) = \frac{B}{2N\cos\Lambda_e}\left(\sum_{J=I+1}^{N} \frac{M(J)}{EI(J)} + \frac{M(I)}{EI(I)}\right)$$

$$\Delta\Theta_t(I) = \frac{B}{2N\cos\Lambda_e}\left(\sum_{J=I+1}^{N} \frac{T(J)}{GJ(J)} + \frac{T(I)}{GJ(I)}\right)$$

or expressed in matrix form,

$$\{\Theta_t\} = \frac{B}{2N\cos\Lambda_e}[u]\left[\frac{1}{GJ}\right]\{T\} \qquad \{\Theta_m\} = \frac{B}{2N\cos\Lambda_e}[u]\left[\frac{1}{EI}\right]\{M\}$$

The angle-of-attack column vector may then be found as,

$$\{\Delta\alpha_s\} = \cos\Lambda_e\{\theta_t\} - \sin\Lambda_e\{\theta_m\}$$

which is also: $\{\Delta\alpha_s\} = q[S]\{1/q\}$.

The preceding equations may then be tied together to form the equation for the structural influence matrix,

$$[S] = (B/2N)^2[u][1/GJ]\left[\cos\Lambda_e[t] + \sin\Lambda_e(B/2N)[m]\right]$$
$$+ \tan\Lambda_e(B/2N)^2[u][1/EI]\left[\sin\Lambda_e[t] - \cos\Lambda_e(B/2N)[m]\right]$$

B. USAGE OF THE SPAN-LOAD PROGRAM

Application of the wing span-load program required the determination of the following influences:

- Additional loading distribution due to wing angle of attack
- Built-in geometric twist
- Airfoil camber distribution
- Dead-weight induced wing twists due to propulsion system weight
- Aileron float angle
- Propeller slipstream effects
- Aileron control deflection
- Roll helix angle

The last two influences involved anti-symmetric wing span-load solutions. The total wing span-load distribution, which provided a measure of wing lift coefficient (C_L), moment coefficient (C_{mCG}) and section lift coefficient (C_ℓ), was obtained by an appropriate linear combination of the above influences. These influences were incorporated in the program as discrete angle of attack adjustments at the control points. Finally, a specified airplane lift coefficient required an estimate of the tail lift contribution before the representative wing C_L could be estimated. The tail lift contribution was based upon trimming the P-3 airplane for a specified flight condition and the assumption that the body and horizontal tail behaved approximately as rigid structures.

1. Additional Loading

Static aeroelastic effects upon wing span-loading due to geometric angle of attack were incorporated in the program as a selectable input from the operator at the computer terminal. Calculation of the appropriate angle of attack for a given flight condition was based on the fundamental equation

$$C_L = C_{L0} + C_{L\alpha}\alpha,$$

with appropriate modification for tail lift contribution as delineated in subsection nine of this Chapter.

Early in the analysis, it was found that static aeroelastic effects had a dramatic impact on additional loading. Solutions were obtained using the span-load program

for a wide range of dynamic pressures. The **q** equals zero solution corresponded to a rigid-wing case. A dynamic pressure of 3.7 psi corresponded too the aircraft operating at a Mach number (M) of 0.6 at sea level. The variation of wing-alone $C_{L\alpha}$ with dynamic pressure, shown in Figure 5, indicates a 41 percent increase due to static aeroelastic influences at the sea level flight condition. The increase in lift-curve slope is associated with a spanwise variation of structural twist as shown in Figure 6. At a Mach number of 0.6 for sea-level flight, each degree of geometric angle-of-attack input at the wing root results in 1.95 degrees of α at the tip, with the added 0.95 degrees being due to the structural twist component in the α direction. The static aeroelastic influence upon the wing aerodynamic center was determined as

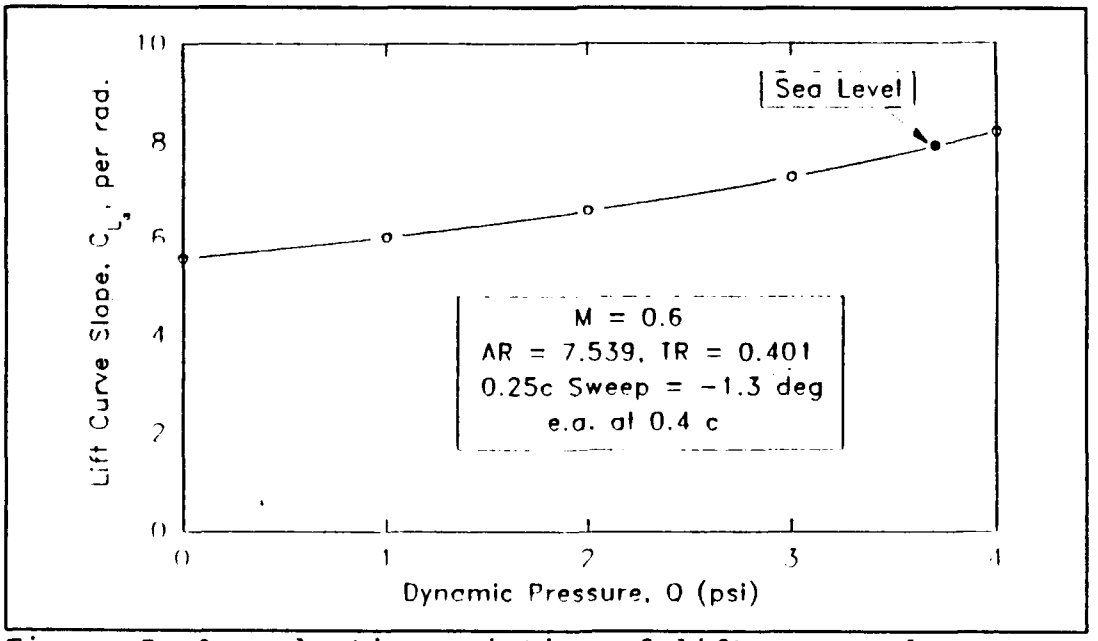

Figure 5. Aeroelastic variation of lift-curve slope [Ref. 6]

being negligible, a result which may be attributed to the wing 0.25 chord line having a small sweep angle.

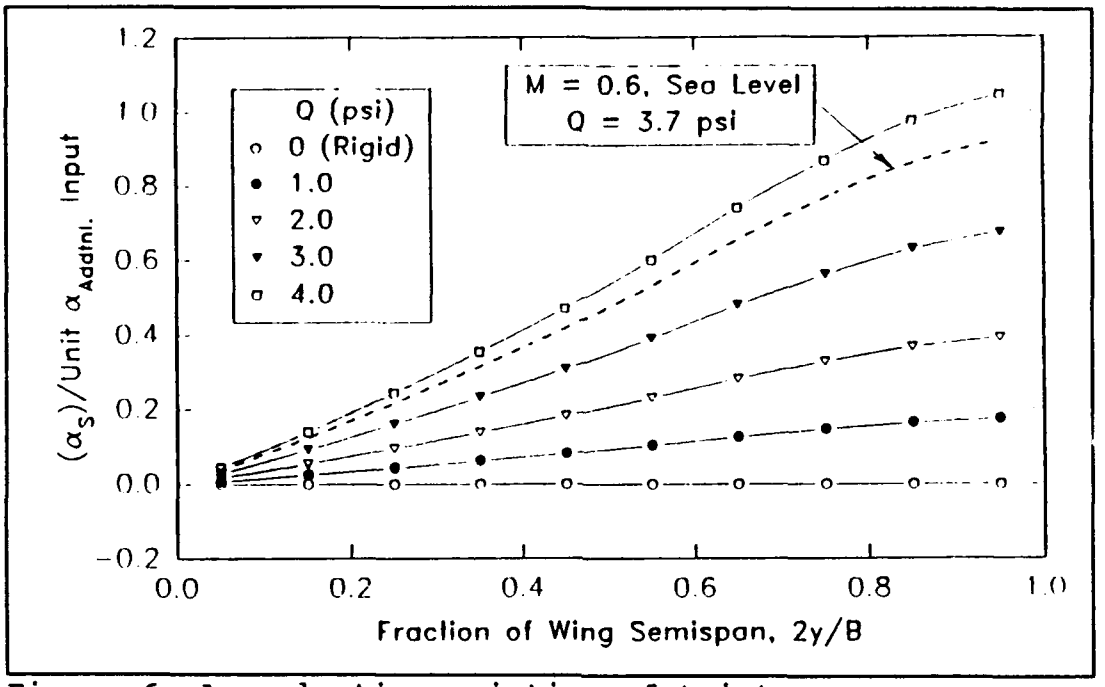

Figure 6. Aeroelastic variation of twist [Ref. 6]

2. Built-in Geometric Twist

The effect of 2.5 degrees of washout was included in the program by linearly varying the local (panel) angle of attack moving outward from zero at the root to -2.5 degrees at the tip. Figure 7 depicts the effect of washout on section lift and twist distribution for the rigid and elastic P-3 wing cases. The magnitude of the negative section C_ℓ values is seen, in Figure 7, to increase by 21 percent while the wing tip experiences a 1.5-degree negative twist due to aeroelastic influences.

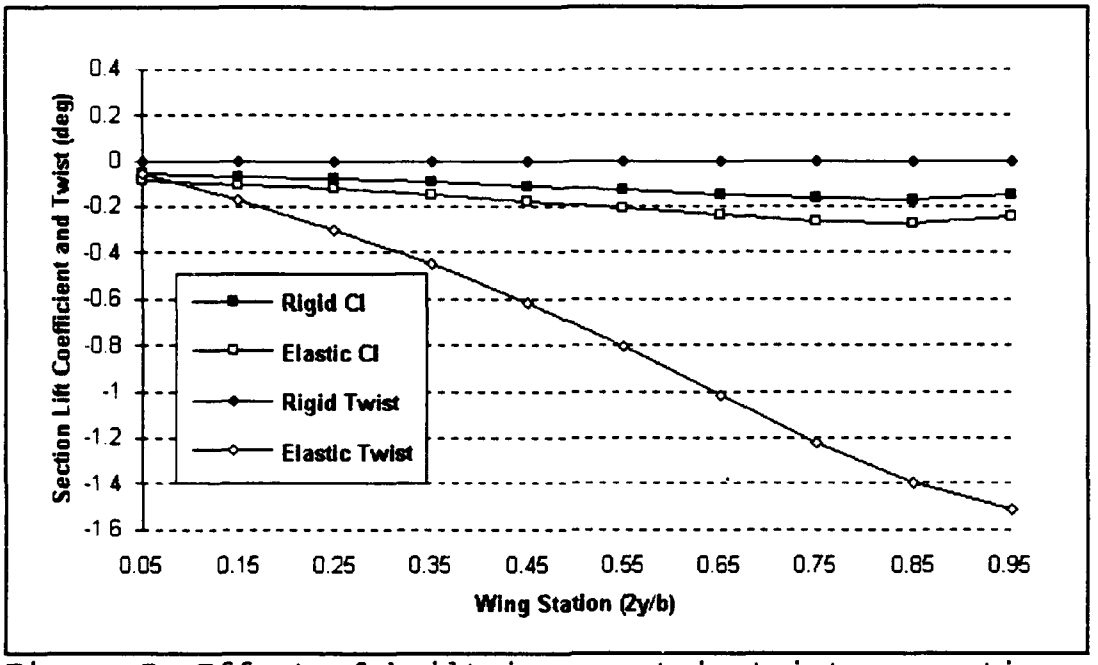

Figure 7. Effect of built-in geometric twist on section lift coefficient and twist distribution.

3. Engine Dead-weight Twist

A separate version of the span-load program was developed and run to determine the wing twist induced per G due to the effect of engine dead-weight moment. Output information was generated in terms of discretized angle-of-attack adjustments and included in the basic span-load program. An engine and propeller assembly weight of 3974 pounds was assumed to act at the (x,y) coordinates (coordinate system as shown in Figures 3 and 4) of (-51", 187") and (-45", 357") for the inboard and outboard engines, respectively. Figure 8 shows the effect of engine dead-weight twist on the elastic twist distribution at three G's and 405 knots. The

wing is twisted to a maximum of -4.5 degrees at the tip under this load condition.

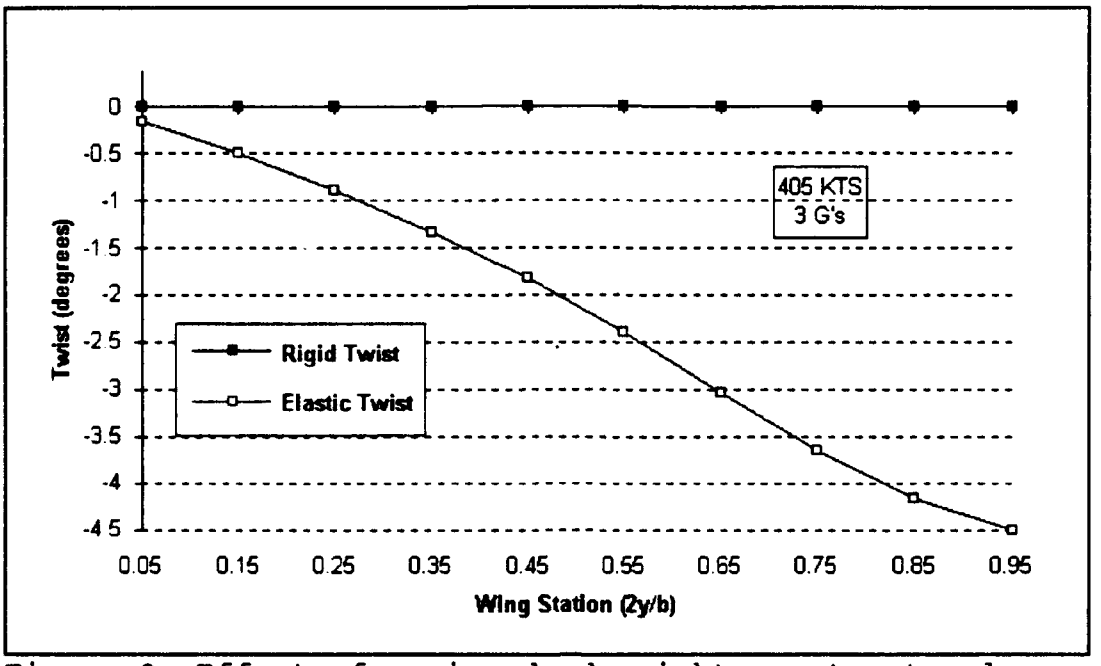

Figure 8. Effect of engine dead-weight on structural twist.

4. Camber

Although listed in Table 1 as a NACA 0014 which tapers to a NACA 0012, the airfoil used for the P-3 wing is not a symmetric section, as indicated by available data [Ref. 8, p. 2-470]. It is, in fact, a hybrid with considerable camber. The wing camber has an effect on aeroelastic behavior and was included in the analysis by determination of camber-line slope at the five chordwise control points which make up the wing model and entering the negative of this value as an adjustment to the station angle of attack.

5. Aileron Float

The span-load analysis included the effect of aileron float as given in a graph of aileron angle versus airspeed in a Lockheed report [Ref. 9, p. 123]. An equation curve fit for the 50-pound control-wheel-force curve was developed and incorporated in the program. Deflected aileron surface area was matched by a selection of panels on the wing model for varying degrees of deflection in order to closely emulate the aircraft control-surface deflection and aeroelastic effect.

6. Aileron Deflection Angle

Using the same process as that used for the aileron float angle, the effect of aileron deflection for consideration of anti-symmetric solutions to emulate roll maneuvering was also included. A curve fit to the data given for available 50-pound control-wheel-force deflection in the same report [Ref. 9, p. 123] was used to generate the deflection angles.

7. Roll Helix Angle

Data [Ref. 9, p. 118] for available tip helix-angle (pb/2V) variation with airspeed were curve fitted and incorporated as another control point angle-of-attack variation in the program. A roll helix angle of 2.63 degrees provided roll moment equilibrium with the available 9.3 degrees of aileron deflection at 275 knots equivalent airspeed, at a control wheel force of 50 pounds. At 405

knots, the roll helix angle was 1.03 degrees for roll equilibrium with an aileron deflection of 8.2 degrees. The merging of the anti-symmetric input due to aileron deflection with the symmetric pullup solution allowed a comprehensive analysis of the static aeroelastic effect of a rolling pullout maneuver as described in part A of this Chapter. An example of the individual and combined effects of these components on wing section lift coefficient (C_ℓ) distribution is shown in Figure 9, where the outer corner of the operating envelope for roll maneuvering (405 knots, 2.4 G's) was examined.

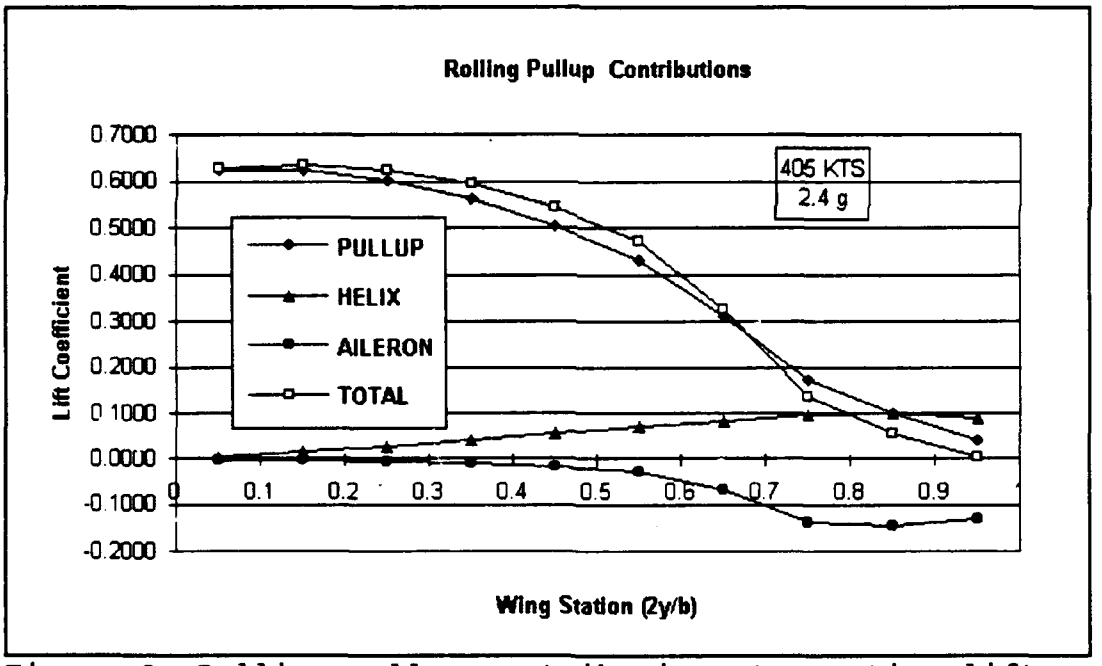

Figure 9. Rolling pullup contributions to section lift distribution.

8. Propeller Slipstream Effect

The increase in dynamic pressure over the wing due to the propellers was calculated using momentum theory as stated

in Glauert [Ref. 10, p. 200] according to the following formula:

$$T = A\rho(V + v_1)v_1$$

where,

- T = propeller thrust (pounds)
- A = propeller disk area (ft^2)
- V = freestream velocity (ft/sec)
- v_1 = velocity increase behind the propeller, determined from known thrust.

The velocity increase, v_1, was converted to a dynamic pressure boost and incorporated in the span-load program in the area behind the propellers.

9. Tail Contribution

Horizontal tail and fuselage moment effects on wing span-load distribution resulted in an adjustment to the wing angle-of-attack value used as input to the program. This adjustment was calculated according to the relationship,

$$C_L = C_{Ladd} + C_{Lt} + C_{L0}$$

where,

- C_L = lift coefficient required for flight condition
- C_{Ladd} = lift coefficient due to additional loading (due to angle of attack)
- C_{Lt} = tail contribution to lift coefficient
- C_{L0} = tail-off lift coefficient at zero angle of attack (due to camber, wing twist and dead-weight twist)

and,

$$C_{Lt} = -\Delta C_{mt}(cbar/\ell_t)$$

where,

- ΔC_{mt} = tail-moment coefficient
- cbar = mean aerodynamic chord of the wing
- ℓ_t = distance from .25cbar$_w$ to .25cbar$_t$

Additionally, at airframe trim ($C_{mCG} = 0$),

$$C_{mt} = C_{m0} + C_{mCL}C_{Ladd}$$

where,

- C_{m0} = moment coefficient at zero angle of attack
- C_{mCL} = tail-off airplane dC_m/dC_L, c.g. = 0.25cbar

The above was assembled and solved for C_{Ladd} to give,

$$C_{Ladd} = \frac{[C_L - C_{L0}] - \frac{cbar}{l_t} C_{m0}}{1 + \frac{cbar}{l_t} C_{mCL}}$$

The value of tail-off C_{mCL} for the aircraft was found from wind tunnel data to be approximately 0.19 [Ref. 3, p. 20]. The value of C_{Ladd} for any given flight condition was then used to solve for the angle of attack in the span-load program according to the formula:

$$\alpha = C_{Ladd}/C_{L\alpha}$$

The value of $C_{L\alpha}$ was available as an output, for the elastic wing, from the program for any given airspeed by entering one radian for the angle of attack input.

A correction of +0.03 to C_{m0} due to fuselage effect was made after finding that the value C_{m0} in the wind tunnel data and that from the program differed by this amount. This correction was verified by calculations made in accordance with Etkin [Ref. 7, p. 334] concerning the effect of body and engine nacelles on neutral point location.

C. EFFECTS NOT INCLUDED

Two other factors were considered as possible contributors to the static aeroelastic problem, but were found to have no significant impact and therefore not included in the span-load program. These factors were propeller gyroscopic effects and the effect of moments due to wing fuel.

1. Propeller Gyroscopic Moment

This phenomenon was investigated using the following formulation from [Ref. 11]:

$$M = 2I_p\omega\Omega$$

$$I_p = mk^2$$

where,

- M = moment due to gyroscopic precession (lb-ft)
- I_p = polar moment of inertia of each blade (lb-ft sec^2)
- ω = rotation rate of the propeller (rad-sec^{-1})

- Ω = pitch rate of the aircraft (rad-sec^{-1})
- m = mass of propeller blade (slugs)
- k = radius of gyration (ft)

The analysis showed that, allowing for a five-degree-per-second aircraft pitch rate, the moment developed by each propeller was 1225 lb-ft in a counterclockwise direction as viewed from above the propeller. This moment was considered insignificant since it is applied in the lateral plane and does not influence the static aeroelastic span-load solution.

2. Wing Fuel Moment

Analysis of the fuel tank geometry and location revealed that the center of mass of the fuel (with full wing tanks) lies nearly coincident with the elastic axis. Any torsional moment derived from this source would be negligible.

D. APPLICATION

Linear summation of the contributing factors addressed earlier in this Chapter resulted in a prediction of the total span-load distribution for the P-3 wing under any given flight condition. The primary flight conditions of concern in this analysis were those encountered during the aircraft mishaps as discussed in the introduction. The basic premise applied was to examine limit loads at the edge of the operating envelope and then expand the analysis to regions outside the envelope, at the ultimate load condition. In addition it was decided to

first examine the loads encountered in a symmetric pullup of three G's at 275 knots. This speed was chosen because of an observed higher load on the leading edge than determined at the upper right corner of the flight envelope, at 405 knots. (A further discussion of this loading phenomenon will be presented in Chapter IV.) Following that, the target flight condition was extended to 4.5 G's at 325 knots, which represented an approximate extension of the envelope using a value for C_{Lmax} of 1.3. Next, the effect of anti-symmetric loading in the form of a starboard and then a port rolling pullup were considered in order to assess the contributions of aileron deflection and roll helix angle. Rolling pullup analyses were done at 2.4 G's and 275 knots to remain inside the envelope and maintain some congruity with the symmetric loading case. Presented in this section are plots of the impact of some of the various flight maneuvers on section lift coefficient and twist distribution, using the fully-developed, tail-on solution with all contributing factors included. Figures 10 and 11 show the 275-knot, 3-G symmetric condition, and compare section lift coefficient and structural twist for the rigid-wing and elastic-wing cases. In Figures 12 and 13, the same distributions are depicted for the 275-knot, 2.4-G rolling pullup load condition.

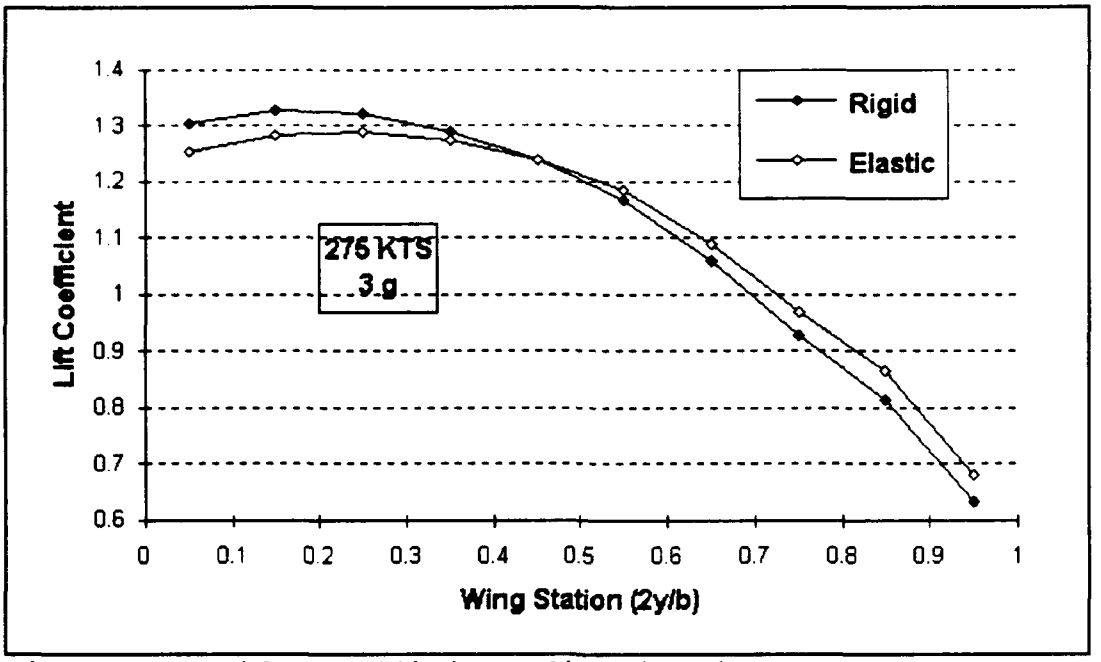

Figure 10. Lift coefficient distribution at 275 knots, 3-G, symmetric pullup.

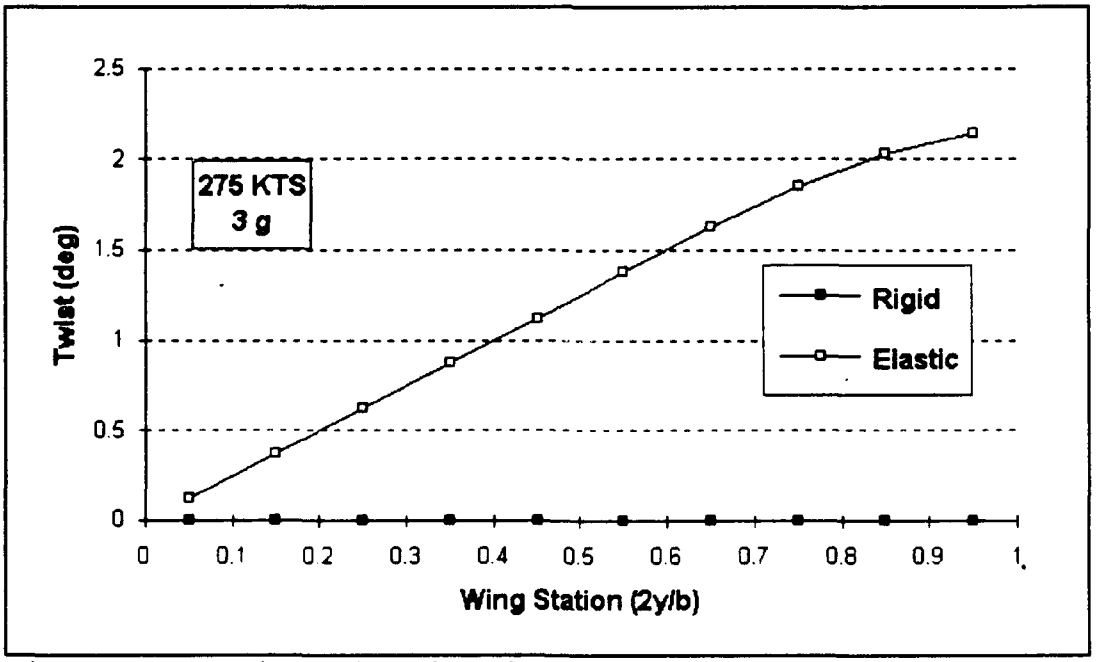

Figure 11. Twist distribution at 275 knots, 3-G, symmetric pullup.

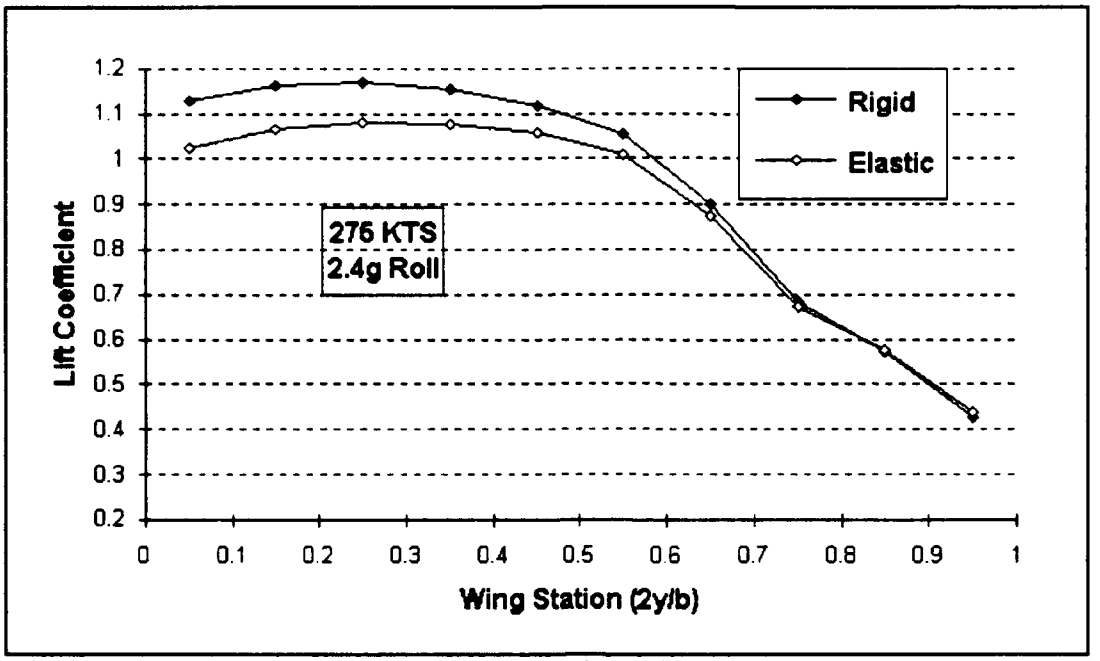

Figure 12. Lift coefficient distribution at 275 knots, 2.4-G, rolling pullup.

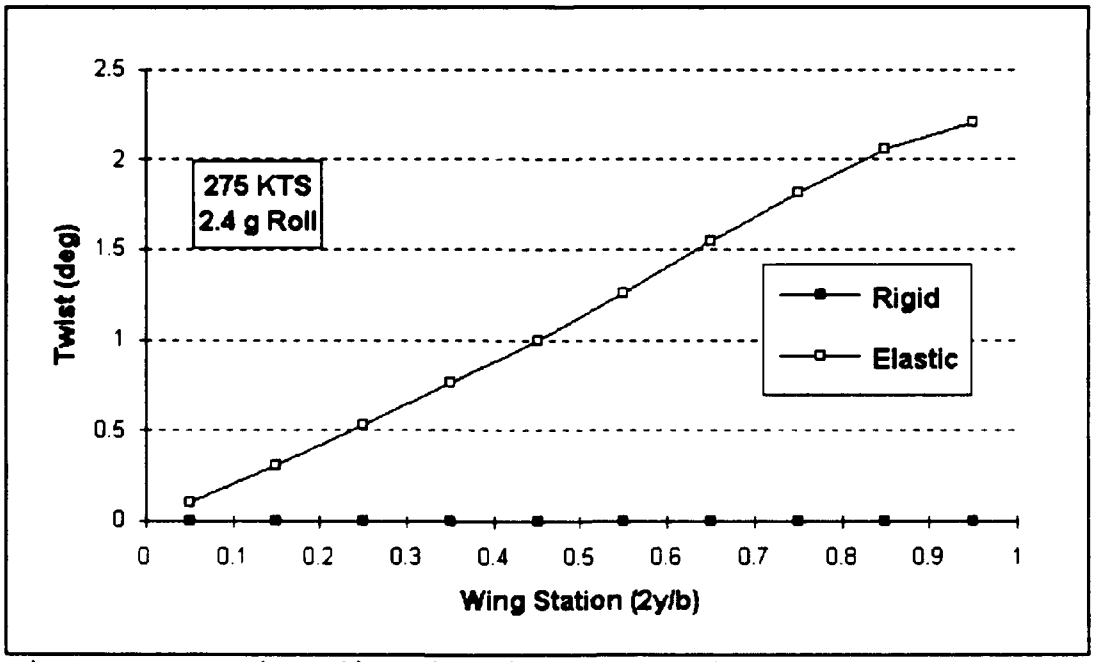

Figure 13. Twist distribution at 275 knots, 2.4-G, rolling pullup.

IV. TWO-DIMENSIONAL PRESSURE ANALYSIS

A. THEORY

Like the static aeroelastic span-load analysis, the two-dimensional pressure analysis employed in this thesis involves the application of linear superposition. This is a consequence of the pressure analysis being based upon a solution to the LaPlace equation, a linear, homogeneous second-order partial differential equation. Linearity allows the problem to be subdivided into three separate elements (which will be described later in this Chapter) and added together. The actual application was based upon a panel method similar to the technique used in the preceding Chapter except that now, instead of dividing a wing planform into chordwise panels, a two dimensional (**x,y**) airfoil is divided into panels along the perimeter of its surface. Camber is defined in the airfoil shape, instead of being added on as a discretized variation of angle of attack, as before. The analysis now concerns a vertical plane or cross-section. Steady (no variation in the flow field with time), inviscid, incompressible flow is assumed to exist. The panel method and formulation employed is documented in a Naval Postgraduate School thesis by Teng [Ref. 12].

1. Coordinate Axis and Panel Numbering System

The airfoil is considered to be fixed in an **(x,y)** coordinate system with its origin at the point of intersection of the chord line with the leading edge. The positive **x** axis points aft to the trailing edge while positive **y** is up. The panels which make up the airfoil surface are of varying lengths, depending mostly on the radius of curvature, and are numbered from **1** through **n** starting at the lower surface of the trailing edge and proceeding clockwise to the upper surface at the trailing edge. Delineating the end points of these panels are nodes which begin with the number **1** at the trailing edge and proceed along the same numbering path as the panels. The trailing edge point is counted twice, giving **n+1** nodes in all.

2. Flow Formulation

Consider some panel **j** on the surface of the airfoil. On this surface there exists a pair of singularity distributions, known as a source distribution q_j and a vorticity distribution γ. The strength of the source distribution varies from panel to panel while the vortex strength is the same for all panels. These singularity distributions satisfy LaPlace's equation and the far field boundary condition.

Applying superposition, the overall flow field is considered to be made up of three individual flows and is represented by the equation,

$$\Phi = \phi_\infty + \phi_s + \phi_v$$

where ϕ_∞ is the potential of the freestream flow,

$$\phi_\infty = V_\infty(x \cos\alpha + y \sin\alpha)$$

ϕ_s is the velocity potential of the source distribution of strength q(s) per unit length (s) and is calculated by,

$$\phi_s = \int \frac{q(s)}{2\pi} \ln(r) ds$$

where (r) is the radial distance from some point at which a source and vortex flow exist, to the midpoint of the panel in consideration. In addition, ϕ_v is the velocity potential of a vorticity distribution of strength λ(s) per unit length and is given by,

$$\phi_v = -\int \frac{\gamma(s)}{2\pi} \theta ds$$

where θ is the angle formed by a line drawn along the radial distance (r) and the panel in question.

Each of the preceding equations is integrated along the straight line which makes up each of the panels, where q_j and λ are constant. The individual effects are then summed to give the total effect of the sources and vortices from all panels, as given in the equation,

$$\Phi = V_\infty(x\cos\alpha + y\sin\alpha) + \sum_{j=1}^{n} \int_{panel(j)} [\frac{q_j}{2\pi} \ln(r) - \frac{\gamma}{2\pi} \theta] ds$$

The calculation of Φ requires solution of the (n+1) unknowns, q_j (j = 1,2,...,n) and γ. This is accomplished numerically in the computer program. Once Φ is known, the velocity can be found by taking the gradient (∇) of Φ. The total velocity vector is found as,

$$V_{total} = \nabla\Phi = \nabla\phi_\infty + \nabla(\phi_s + \phi_v)$$

Next, the coefficient of pressure is found from the Bernoulli equation in the incompressible form,

$$C_p = 1 - \left(\frac{V_{total}}{V_\infty}\right)^2$$

3. Boundary Conditions

Both the condition of flow tangency at the surface and the Kutta trailing edge condition must be satisfied as boundary conditions. As in the span-load analysis, control points are designated at which flow tangency is satisfied, except here the control point is taken as the mid point of the panel. It is stipulated that each control point will have tangential velocity, $(V^t)_i$, but that all normal velocities, $(V^n)_i$, will be exactly zero.

The Kutta condition requires that the pressures on the upper and lower surface at the trailing edge be equal. Using Bernoulli's equation for steady potential flow, this state of pressure equilibrium is found to exist when the tangential velocities in the downstream direction are equal at the upper

and lower trailing-edge panels. In equation form this is written,

$$(V^t)_1 = -(V^t)_n$$

The task then becomes one of using the boundary conditions to solve for the (n+1) unknowns.

4. Influence Coefficients

The concept of influence coefficients is again employed in this portion of the analysis, as it was in the span-load analysis. Here, the influence coefficients take the form of induced normal and tangential velocities at the control point of a given panel. These velocities are induced by the source and vorticity distributions of the other panels, and it is from this influence that they receive their designations:

- A^n_{ij} = normal velocity induced at the i^{th} panel control point by the source distribution on the j^{th} panel.
- A^t_{ij} = tangential velocity induced at the i^{th} panel control point by the source distribution on the j^{th} panel.
- B^n_{ij} = normal velocity induced at the i^{th} panel control point by the vorticity distribution on the j^{th} panel.
- B^t_{ij} = tangential velocity induced at the i^{th} panel control point by the vorticity distribution on the j^{th} panel.

These influence coefficients are calculated through application of the geometric relationships which exist between the panels in conjunction with the formulas for the source and vorticity velocity potentials as given above.

5. Numerical Solution Method

Using the influence coefficients, the boundary conditions can now be employed to write (n+1) equations which may be solved in matrix form for the (n+1) unknowns. The set of **n** equations comes from enforcement of the flow tangency boundary condition in the form,

$$\sum_{j=1}^{n} [A^{n}_{ij} q_j] + \gamma \sum_{j=1}^{n} B^{n}_{ij} + V_\infty \sin(\alpha - \theta_i) = 0$$

Next may be written the enforcement of the Kutta boundary condition as,

$$-\sum_{j=1}^{n} [A^{t}_{1j} q_j] - \gamma \sum_{j=1}^{n} B^{t}_{1j} - V_\infty \cos(\alpha - \theta_1) = \sum_{j=1}^{n} [A^{t}_{nj} q_j] + \gamma \sum_{j=1}^{n} B^{t}_{nj} + V_\infty \cos(\alpha - \theta_1)$$

The negative signs on the left side of the equation are due to the defined orientation of the tangential velocities as positive in the downstream direction.

These equations may then be expressed in matrix form with the (n+1) unknowns (i.e., q_j (j=1,2,...,n) and γ) arranged as a column (nx1) matrix multiplied by the $A_{n+1,n+1}$ (n+1 x n+1) influence coefficient matrix and set equal to a B_{n+1} column matrix. From this point, a Gaussian Elimination numerical technique may be employed to solve for the (n+1) unknowns [Ref. 13].

6. Velocity and Pressure Distribution

Once the q_j and γ are found, the tangential velocities at the control points can be solved for according to the equation:

$$V_{total} = \sum_{j=1}^{n} [A^t_{ij} q_j] + \gamma \sum_{j=1}^{n} B^t_{ij} + V_\infty \cos(\alpha - \theta_i)$$

where i = 1,2,...,n. From this, the individual pressure coefficients may be solved using the equation,

$$(C_p)_i = 1 - (V^t)_i^2, \quad i=1,2,...,n$$

At this point, the forces at work on the airfoil may be found by first integrating forces in the airfoil coordinate system as follows,

$$C_y = -\sum_{i=1}^{n} (C_p)_i (x_{i+1} - x_i)$$

$$C_x = \sum_{i=1}^{n} (C_p)_i (y_{i+1} - y_i)$$

Performing a coordinate axis rotation to re-align with that of the freestream yields the lift coefficient,

$$C_\ell = C_y \cos\alpha - C_x \sin\alpha$$

For this application, the values of C_x an C_y are found in discretized form at each panel as $(C_x)_i$ and $(C_y)_i$, i = 1,2,...,n, and then multiplied by the chord length and freestream dynamic pressure to arrive at the normal and chordwise force exerted at each panel. From this, the

leading-edge panels are selected and their forces collected for application as point loads in the finite element analysis portion.

B. APPLICATION

1. P-3 Airfoil Section

As mentioned in Chapter III, the airfoil shape used in this application is as delineated by [Ref. 8]. Surface coordinate locations were solved using the tables and equations provided therein relative to a "wing reference plane" which appeared to correspond to a water line (i.e. the angle of incidence at the root was included in the definition). These coordinates were then rotated to an (**x,y**) coordinate system aligned with the chord of the airfoil as required in this panel method. The result was an airfoil consisting of some 48 panels, which was increased to 52 panels (53 node points) due to observed roughness of the leading edge shape when plotted. This smoothing of the leading edge shape was achieved by applying the specified leading edge radius to create intermediate node points. The basic shape of the airfoil, though not precisely to scale, is depicted in Figure 14. The locations of the node points are also shown.

2. Program Inputs and Outputs

The desired output from the two-dimensional panel method program was a collection of forces and boundary constraints to be applied at node locations in the finite

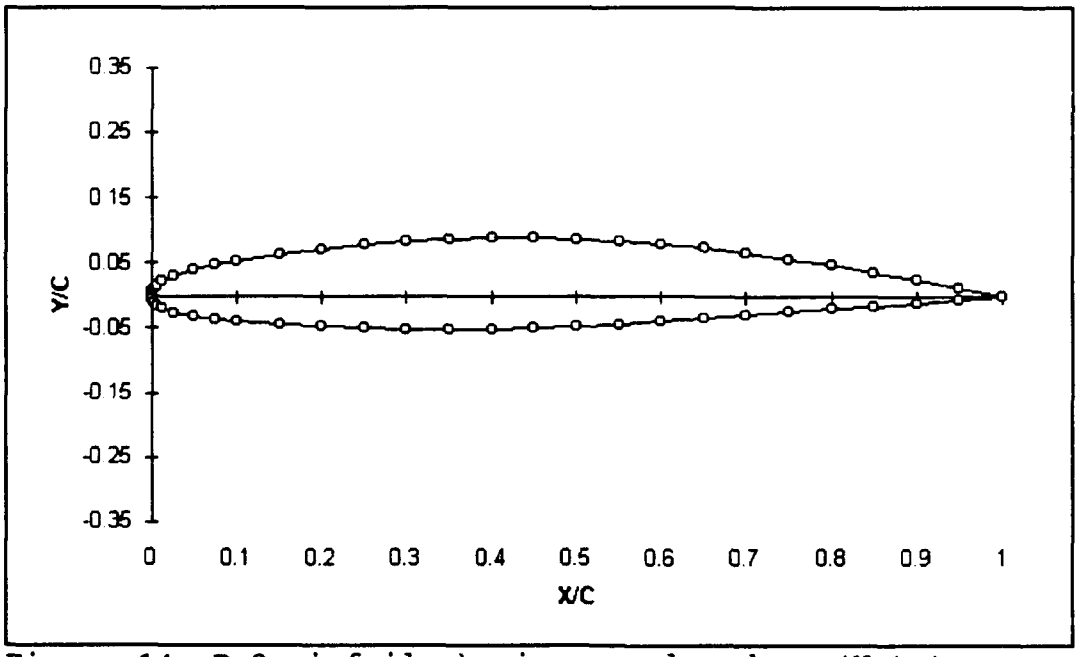

Figure 14. P-3 airfoil showing panel nodes. (Not to scale)

element analysis phase. In order to achieve this, the program was altered considerably from the initial state as outlined earlier in this Chapter. The final FORTRAN code is available in Appendix B. Since it was necessary to develop loads to be applied to a three-dimensional model, the program was set up to iteratively compute the force distribution at a series of two-dimensional airfoil sections which ranged in location from the inboard end of the finite element model at wing station (WS) 256 to the outboard end at WS 320. (These locations correspond to the outboard 64 inches of the wing center section leading edge, located between the nacelles.) This section force distribution was scaled up from a chord-normalized airfoil shape to a full-sized airfoil as described above, then multiplied by a scaling factor equal to the

distance between the section locations. Section locations consisted of 24 wing-station positions along the leading-edge model, including the nine ribs and 15 intermediate points as determined by finite element model node locations.

The first of the inputs to the program consisted of the airfoil geometry definition as described above. Next, a tabular file of wing station locations was read in together with the section lift coefficient for that spanwise location as found by the span-load program. These section lift coefficients, initially found for the .35, .45 and .55η locations (where $\eta = 2y/b$) were curve-fitted using the Cricket Graph™ plotting software in order to achieve a high degree of accuracy in determining the individual C_ℓ's at stations which were no more than three inches apart. Also included in this input file was a list of spanwise multiplication factors for scaling up the load as described above. Additional input files consisted of the finite element node numbers which were matched with their respective **x** and **y** direction loads in the program. Read in from the terminal were the airspeed under consideration and the twist angles of the wing box as determined from the span-load program.

Output consisted primarily of the load file which included not only the loads at the finite element node points, but also the constraints and twist displacements for the upper flange and lower hinge node points of the leading-edge finite element model. The twist displacements were calculated within the

panel program using formulas based on geometric considerations of the height of the wing spar at the inboard and outboard ends of the leading-edge segment, and the net twist displacement of the front spar from the inboard to the outboard end of the model. That is, the finite element model was assumed to have undergone a rigid-body rotation to the degree of twist which was found to exist at the inboard end (WS 256). Therefore, twist displacements at the inboard end were set to zero, followed by application of the subsequent net twist distribution that occurred at the other wing stations while proceeding outboard to WS 320. This net twist distribution was equal to the difference between the outboard and inboard twist amounts, applied linearly over the 24 stations. This twist amounted to approximately 0.3 degrees in the 275-knot, 3-G symmetric pullup. The displacements generated for application at the node points were in the longitudinal (x) and vertical (z) directions on the three-dimensional model. Twist rotation of the front spar was taken to be about its vertical mid point, and the structural wing box was assumed to have no chordwise distortion as it rotated about the .40c elastic axis location. Other output took the form of files to examine C_p distributions and to tabulate loads by wing station and two-dimensional node point for verification of the load file. In addition, output was generated which approximated the total normal and chordwise loads applied to the entire wing leading-edge center section

located between the engine nacelles. This estimation was accomplished by computing the load on the leading-edge portion of the airfoil at WS 274 and multiplying by the length of the leading-edge segment (92 inches).

3. Program Operation

After reading in the coordinate information for the airfoil along with the wing station, C_ℓ and load multiplication factor, the FORTRAN program calculated the chord length at the particular station based upon the 0.40 taper ratio. It also determined the thickness fraction of the airfoil section at that station by assuming a linear taper from 14% maximum thickness at the root to 12% at the wing tip. This thickness factor was then used to recalculate the **y** coordinate position of each node point to redefine the shape of the airfoil. An initial angle of attack of one degree was set and the process described in the theory section of this Chapter took place, wherein the C_x, C_y, and C_ℓ were calculated for that angle of attack. This C_ℓ value was then compared to that required (as input with the wing station), and an iterative cycle commenced in which the angle of attack was varied up or down by an amount based on the product of the C_ℓ deviation multiplied by a preset angular value. An accuracy test of .0001 was applied to reach an acceptable value for C_ℓ, at which time the process started over with the next wing station. Forces in the **x** and **y** direction were matched with

the appropriate finite element node points and written to the load file for each iterative cycle. After all loads were calculated and stored, the twist displacements and zero boundary constraints were calculated and appended to the load file.

4. Verification of the Program

The accuracy of the two-dimensional panel method was verified by comparison with published empirical data for tangential velocity and/or pressure coefficient distributions for the NACA 0012 and Eppler E64 airfoils before its use in this application. Results were nearly identical to the published data with only a small deviation seen near the trailing edge of the program tangential velocity distribution for the Eppler airfoil. No difference from the NACA 0012 C_p data could be identified.

5. Flight Regime Selection

It was found in the course of running the program at various airspeeds and angles of attack that the highest loads on the leading-edge segment were generated at slower airspeeds and higher angles of attack as a constant G load was maintained on the aircraft. This result seemed contrary to conventional opinion that the highest loads would most likely occur at or near the high speed end of the operating envelope. A brief study was undertaken to determine the cause of this phenomenon and a hypothesis is given here.

a. Method Employed

In an effort to study the effect of dynamic pressure (airspeed) and angle of attack on the leading edge of an airfoil, the variation of net C_p distribution on the leading edge at various angles of attack was first examined. These C_p values were the numerical sum of the difference between the upper and lower C_p's, integrated over the chordwise distances occupied by their respective panels. These data obtained were then curve fitted with a third order polynomial and used in a spreadsheet to calculate the C_p distribution at varying angles of attack. These angles of attack were generated by varying the airspeed from 275 to 425 knots, calculating dynamic pressure (**q**) for a 3-G wing loading from the Bernoulli equation, and then converting these **q**'s to angles of attack required using the basic lift formula, altered by the equation,

$$C_L = C_{L0} + C_{L\alpha}\alpha$$

to give,

$$\alpha = 3W/C_{L\alpha}qS \quad \text{and} \quad \alpha = 3W/C_{L\alpha}qS - C_{L0}/C_{L\alpha}$$

for the symmetrical NACA 0012 and cambered P-3 airfoil, respectively. These angles of attack were then used as inputs to the polynomial curve fits, from which a corresponding set of C_p values were calculated. Next the product of C_p and **q** were found, to give the pressure acting on the leading edge, corresponding to a matched set of **q** and angle of attack. This

information was then plotted as seen below in Figures 15 and 16.

b. Symmetric Airfoil

Figure 15 shows the distribution of the various parameters on a relative scale as airspeed increases for the case of a symmetric airfoil. Note that the pressure acting on the leading edge is nearly constant, showing only a slight **increase** with increasing airspeed.

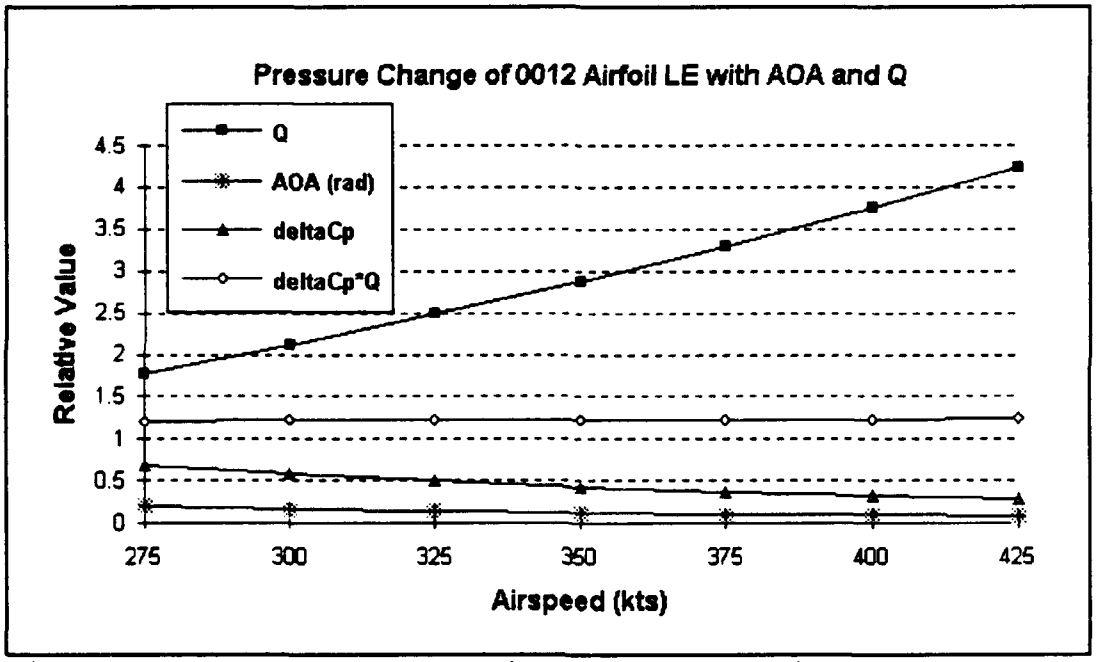

Figure 15. Pressure analysis of 0012 leading edge.

c. Cambered P-3 Airfoil

Next the same information is plotted for the P-3 airfoil in Figure 16. Note that the pressure on the leading edge undergoes a marked decline as airspeed increases (AOA decreases).

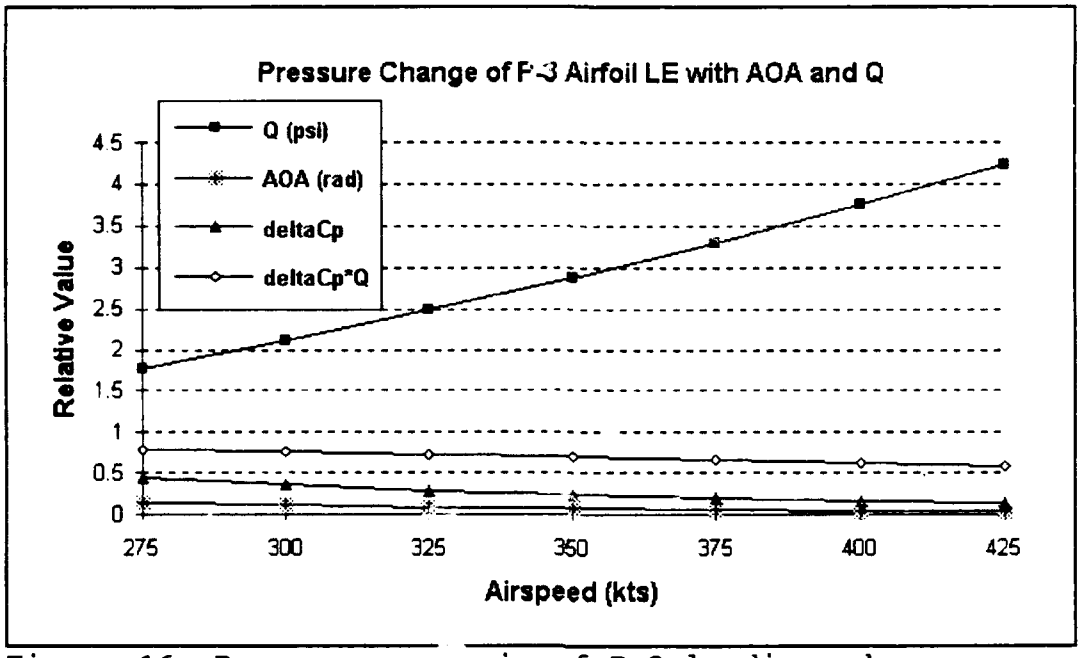

Figure 16. Pressure analysis of P-3 leading edge.

d. Analysis

Because of the apparent drop in pressure on the cambered airfoil, it was concluded that the effect of camber was to shift the loading of the wing in a way that caused angle of attack to become the dominant influence rather than dynamic pressure. It was also observed that if the lift equation applied in the program was that of a cambered airfoil (i.e. $C_{\ell 0}$ had some positive value as the lift curve was displaced upward), this loading phenomenon was present. If $C_{\ell 0}$ were zero, the load on the leading edge was approximately the same at various angles of attack and airspeeds. Because of this observation, it was decided to select the 275-knot, 3-G flight position as the maximum loading position in the normal operating envelope.

V. FINITE ELEMENT ANALYSIS

A. THEORY

The method of finite element analysis is a means of simulating the structural behavior of a continuous physical system by a discretized representation of that system. Structures are represented by discrete node points which are connected by structural elements. The nodes form a grid which details the general shape of the structure while the elements, although they appear as only lines, are mathematically given the physical properties of the portion of the structure which they are there to represent. A physical structure is thus transformed into a mathematical representation for the purpose of analyzing some behavior of the structure. This analysis may be in the area of dynamic response, heat transfer, or, as is the case here, static loading response. This method of analysis is widely proven to be highly accurate and has been used in many engineering fields, including aerospace, automotive, civil and mechanical applications. With the increased capability, speed and data storage capacity of microcomputers, this analysis technique is no longer limited to mainframe applications, as was the case a few years ago.

1. Accuracy

The accepted rule of thumb in finite element modeling is that the use of more node points results in a more accurate solution. Convergence tables have been developed which show that the use of fewer nodes increases the stiffness of the model . The main drawback to using a large number of nodes is that it greatly increases computation time and requires larger amounts of storage space than a model of the same structure using fewer nodes [Ref. 14]. The finite element analysis software used for this thesis is called MSC/pal 2® and is a product of the MacNeal-Schwendler Corporation, the company which also creates the highly respected NASTRAN® finite element application for VAX/VMS work stations and mainframe operations. The accuracy of MSC/pal 2® has been tested and documented by the manufacturer [Ref. 15]. In addition, the manufacturer recommends simple hand calculations to verify that results obtained for a given model are reasonable (i.e. within the same order of magnitude). This was done by calculating simple beam bending stress with constant area cross sections approximating the rib legs of the model. Results established that the finite element model produced a solution which was well within expected norms.

2. Equations

The number of equations to be solved in the finite element analysis is equal to the number of degrees of freedom in the model. Each node point has six degrees of freedom: three translational (in each of the **(x,y,z)** coordinate directions, and three rotational (about each of the coordinate axes). Stiffness equations are generated for the stiffness of each connecting element, based on the specified material properties (Young's modulus, shear modulus, mass density, tensile yield stress are specified) and the geometric configuration of the element. Elements may take the form of beams, triangles, quadrilaterals and others. These nodal stiffnesses are combined to form a system stiffness matrix, **[K]**, of size **(NxN)** where **N** is the number of equations. Degrees of freedom may be eliminated by setting them to zero in the model definition phase (a way of applying boundary constraints) or fully retained as was done in this application. (Here, boundary constraints were applied in the load as discussed in Chapter IV. This application allows variation of the boundary displacements from one load to the next and allows recovery of reaction forces at the constrained nodes.) Once the stiffness matrix has been formed, the static analysis may be performed according to the following equation:

$$[K]\{U\} = \{F\}$$

where,

- {F} = column vector of applied loads (Nx1)
- {U} = resultant column vector of nodal displacements (Nx1)

Gaussian elimination is employed to solve the matrix equation. In large models, as is the case here, matrix partitioning takes place prior to solution.

Once the displacements are known, stress-strain relationships are employed to compute stress values throughout the structure. These stresses are available to the user in the form of major and minor principal axis stresses, Von Mises stress concentrations and maximum shear stresses. In addition, output of displacements and rotations are accessible.

B. STRUCTURAL REPRESENTATION

1. The Leading Edge Structure

The leading edge segment considered for this analysis was the port wing, center section, located between the number three and four engine nacelles. Figure 17 shows a cutaway view of the structure. The segment is composed of 12 vertical ribs supporting a double (inner, outer) skin. The outer skin is .040 inches thick and the inner is a stamped corrugation of .016 inches. Assembly of the outer and inner skins provides a series of ducts approximately .25 inches in height and two

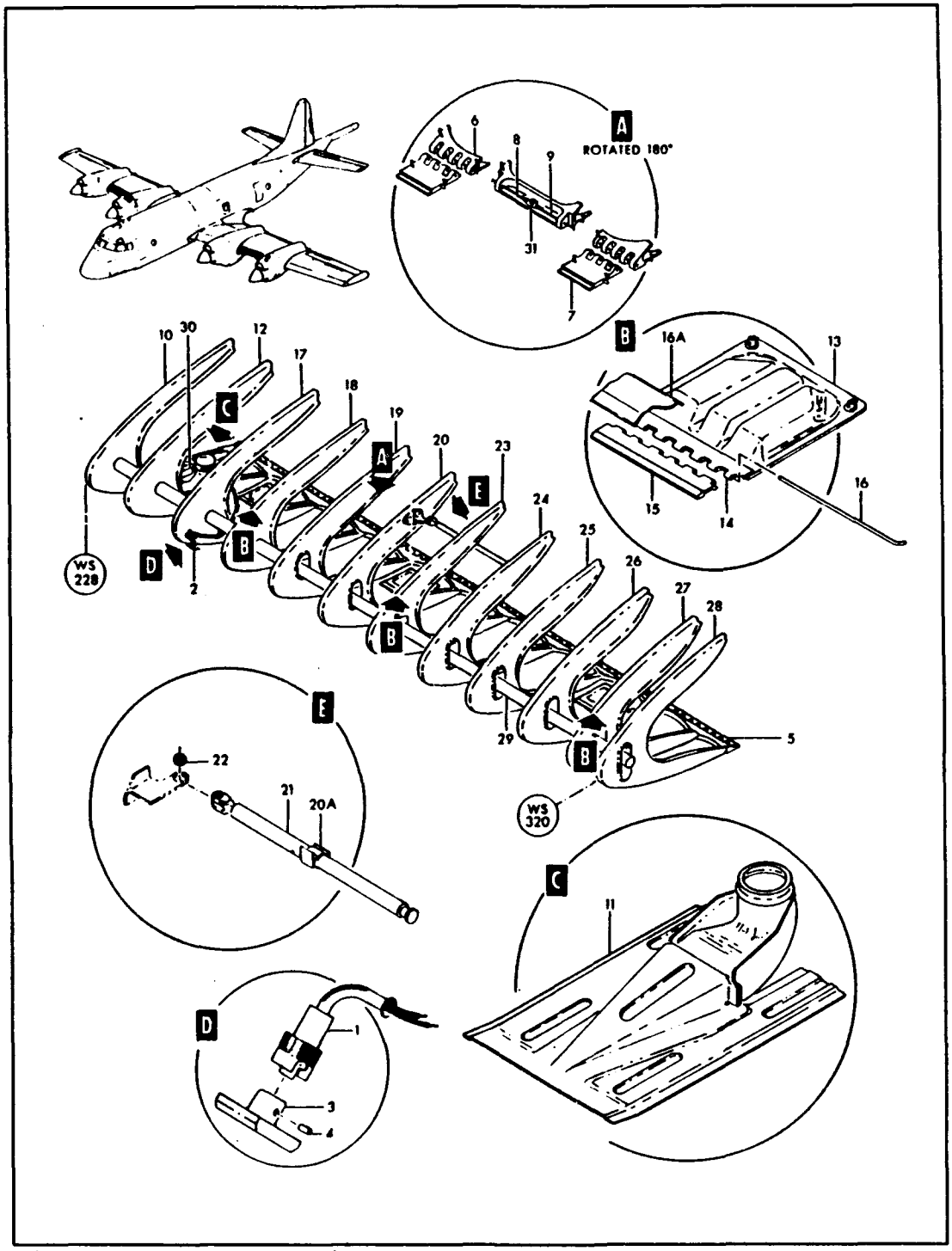

Figure 17. P-3 leading edge structure [Ref 16].

inches wide each. These ducts run longitudinally along the inner surface of the leading edge and are continuous over the

spanwise length of the leading edge. The purpose of this series of ducts is to provide a channel through which bleed air may travel to heat the leading edge. The tube seen extending through the structure delivers the bleed air to the ducts. The leading edge segment is secured to the front spar of the wing by a full-length piano hinge at the bottom edge and a screwed-down spar cap flange at the top. This arrangement provides access to the area for maintenance functions.

2. The Model

The basic finite element model used in this analysis was obtained through translation of a NASTRAN® finite element model using a function in the MSC/pal 2® application called NASPAL®. NASPAL® reads the NASTRAN® text file for the model and rewrites it in the format used by MSC/pal 2®. The NASTRAN® model file was obtained from Aerostructures, Inc. through contact with NAVAIR's AIR-530 office. Because the NASTRAN® model consisted of 2749 nodes, it was necessary to reduce the model size to meet the MSC/pal 2® limitation of 2000 nodes. This reduction was done by entering a set of geometric coordinates during the NASPAL® translation and instructing the translator to consider only the outboard 64 inches of the model. In effect, the leading edge section was severed between WS 247 and WS 256, or between the third and fourth ribs from the left end as shown in Figure 17. The

remaining portion of the model was translated from the fully defined model. This approach was considered to provide a more accurate solution than increasing the spacing between nodes, keeping the highest available level of detail in the model (again, more nodes mean better accuracy for the same structure). In doing so, it was necessary to modify the inboard end rib of the structure (WS 256) since the end ribs were constructed differently than the intermediate ribs. The end ribs are closed in the front and have single, riveted flanges on their interior (Figure 18, bottom), while the intermediate ribs (Figure 18, top) have an open front to allow access for the bleed air "pump cap" assembly which leads to the double skin described earlier. The intermediate ribs also have double flanges as shown.

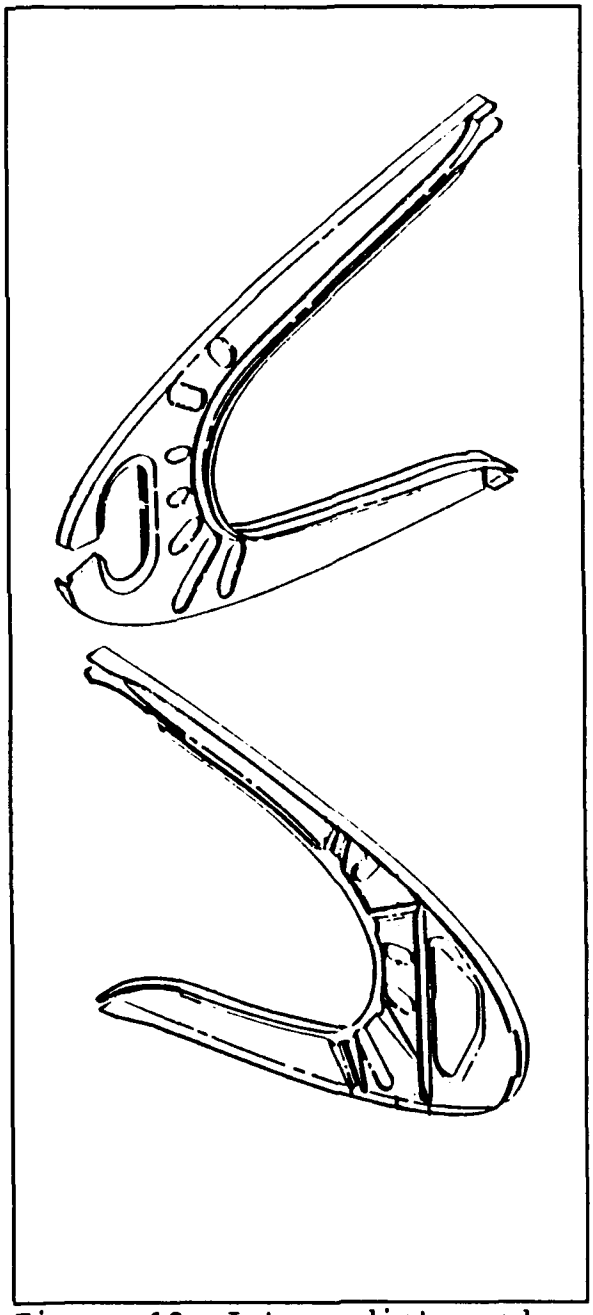

Figure 18. Intermediate and end rib detail.

These changes to the model were made in the rib at WS 256 (now the inboard end rib of the model) by adding node points and quadrilaterals to close the front and by rearranging the beam element properties within the MSC/pal® 2 model definition text file. In this way, the model was altered to represent a shortened leading edge segment with properly defined ribs. The model was constructed as an all-aluminum structure, and as stated in Chapter IV, the loads applied were generated for each specific wing station and scaled according to the spanwise distance between the node points. In this way, the model detailed here received a scaled-down load for its scaled-down size. The upper and lower surface views of the model are presented in Figures 19 and 20. The end views of the model are shown in Figure 21.

The lower hinge is replicated in the model by leaving the Y-axis rotation unrestrained. The upper flange of the model is secured in all six degrees of freedom. Displacements for front spar twist are incorporated in the upper and lower constraints as detailed in the previous Chapter. All of these boundary conditions are input through the "Displacements Applied" command section of the load file.

Another difference between this model and the original NASTRAN® code developed for NAVAIR is that the original did not incorporate stiffness generation in the skin of the model. The skin thickness of the NASTRAN® model was .056 inches, which is the sum of the outer and inner skin thicknesses but

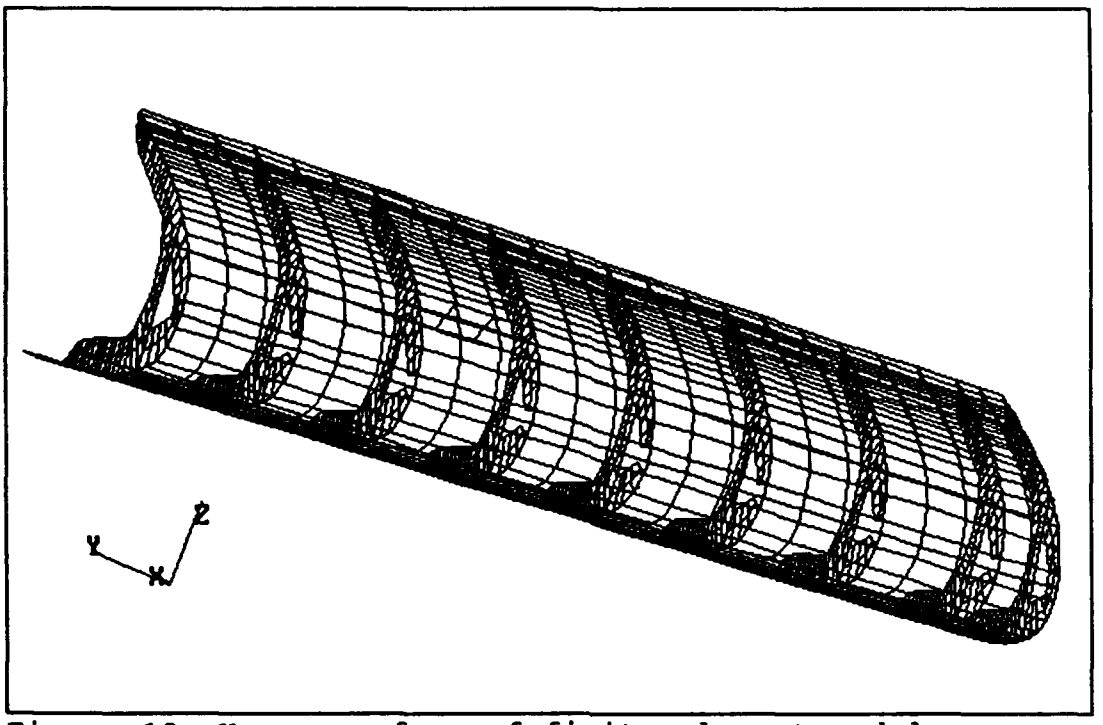

Figure 19. Upper surface of finite element model.

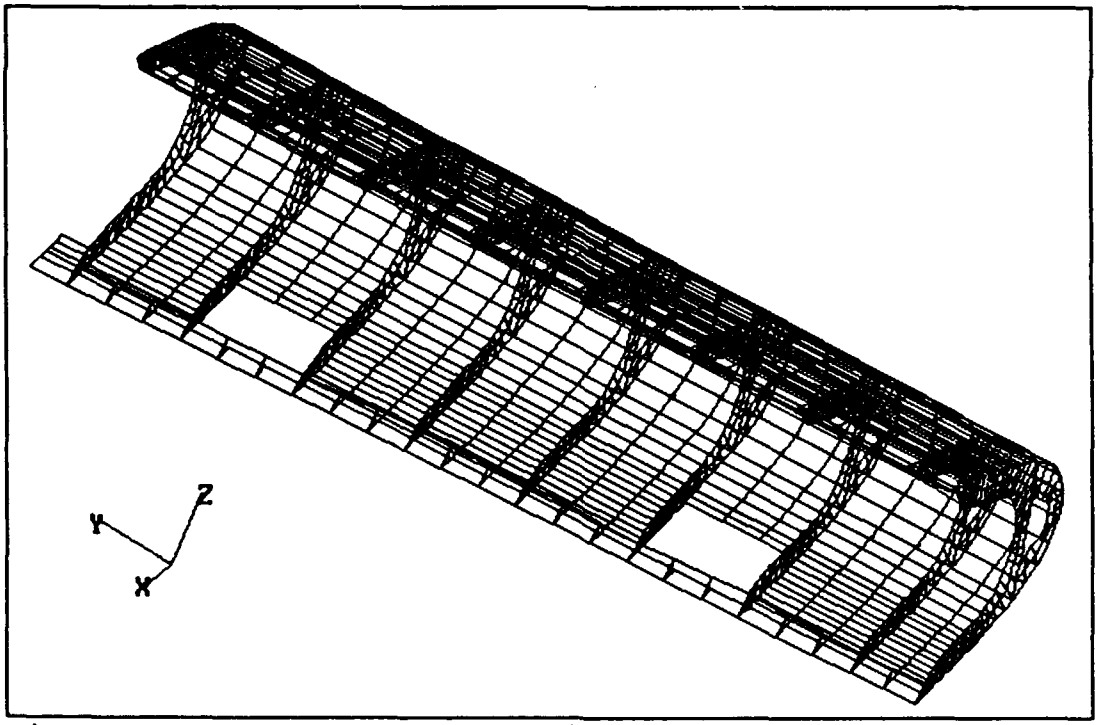

Figure 20. Lower surface of finite element model.

without the stiffness generation enabled in the model definition file, the skin would have no stiffness. In effect, it would act as a non-loadbearing membrane. In the MSC/pal 2® model, stiffness generation was enabled, but when loaded, this resulted in excessive deformation of the skin. It was decided that the .056 inch thick skin did not accurately model the combined effect of the inner and outer skin combination since the corrugated inner skin would be much stiffer than its mere thickness (.016 inches) would represent. Although there is a variable stiffness

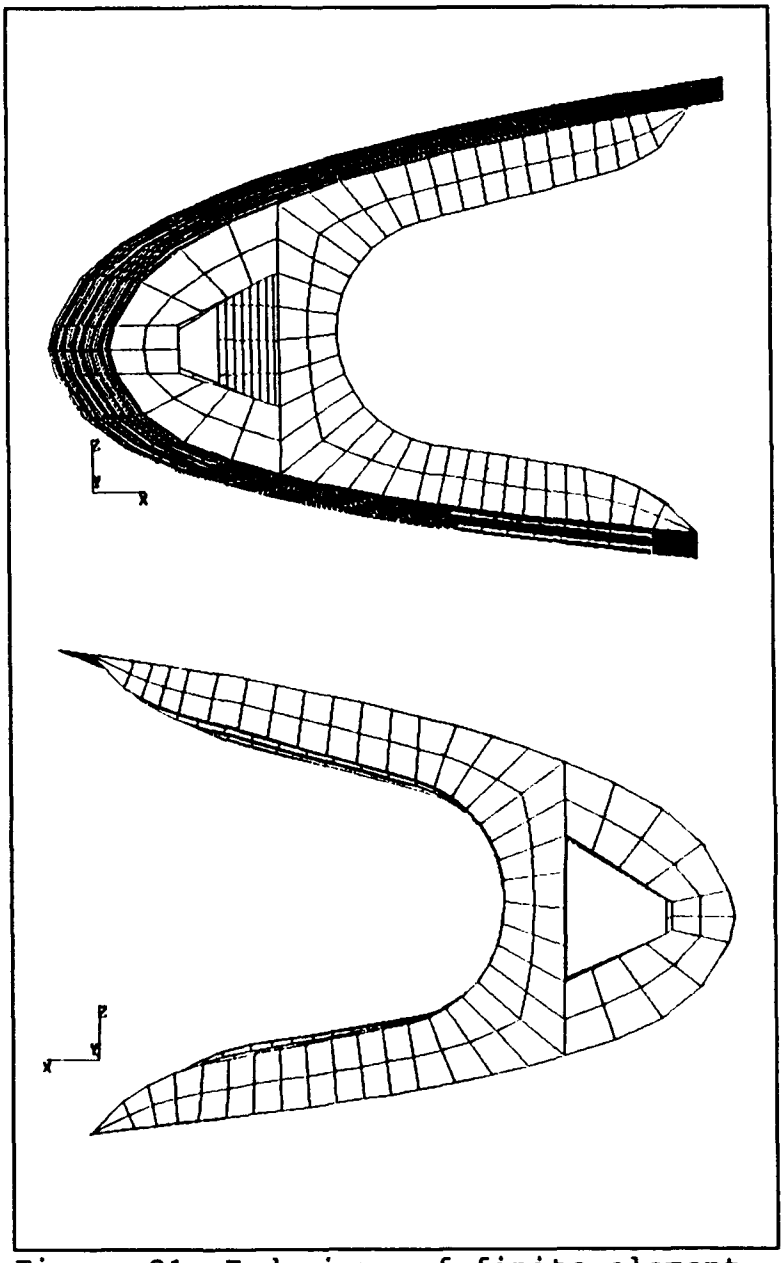

Figure 21. End views of finite element model (outboard, inboard).

factor in the MSC/pal 2® application, available references on finite element analysis did not detail the calculation of this factor. Therefore, it was decided to increase the skin thickness to an equivalent thickness which would accurately replicate the behavior of the corrugated skin combination. This thickness was calculated by equating the moment of inertia of a box beam formed by a single corrugation and outer skin combination with that of a solid cross section about the same reference axis (at the upper surface). After allowing for spaces between the corrugations where the two skins are riveted together, an equivalent skin thickness of .1838 inches was determined and employed. This action reduced the deformation of the skin under load to reasonable norms.

Loads were applied to the model at spanwise rows of selected node points which most nearly corresponded to the mid points of the panels in the two-dimensional panel method. These point loads were applied in the vertical (Z) and horizontal (X) directions in units of pounds force.

Material properties used to represent the 2024-T6 aluminum structure in the construction of the model were as follows:

- Young's modulus (E) = 1.06E+07 psi [Ref. 17]
- Shear modulus (G) = 4.0E+06 psi [Ref. 17]
- Poisson's ratio (υ)= 3.25E-01
- Tensile yield strength (σ_{ys}) = 4.7E+04 psi [Ref. 18]

where Poisson's ratio (υ) was calculated according to the standard formula:

$$G=\frac{E}{2(1+\nu)}$$

C. APPLICATION

Many load conditions were examined in the course of this thesis. Presented here are the six load cases which give the best overall illustration of the observed effects of static aerodynamic loading, both with and without static aeroelastic effects included. In this way, the effect of wing box twist may be seen, along with the combined effect of angle of attack and dynamic pressure. In Table 3, the features of the six load cases are given. The **L/R** column provides a distinction between a wings level (**L**) pullup or a rolling (**R**) pullup. The effect of rolling into a turn during the application of G loading (as in a climbing breakaway maneuver) is not the same as that of rolling out of a turn during G application (as in rolling to wings level while pulling out of a dive). Since it was found that the loading effect in terms of both twist and air loading was greater during the former (due to the combined effect of roll helix angle, aileron deflection and air load), the former was chosen for presentation here in the rolling load cases. All load cases were generated at 135,000 pounds gross weight except for number 4 which was done at 110,000 pounds. In load case number 1, the effect of twist was

eliminated from the load solution by setting the MSC/pal 2® displacements to zero so that the effect of wing torsional twist may be seen by comparison with load case 2.

TABLE 3. LOAD CASES EMPLOYED

Load Case	Airspeed(kts)	Load Factor	L or R	Comment
1	275	3.0	Level	No twist.
2	275	3.0	Level	
3	275	2.4	Roll	
4	240	3.0	Level	110,000 #
5	350	2.4	Roll	
6	325	4.5	Level	

1. Input Data

Presented in Table 4 are the input data sets for each of the load cases. These are given for the three pertinent non-dimensional spanwise wing stations (2y/b) as generated by the span load program. The 24 actual wing stations (2y/b = 0.4322 through 0.5397) employed for the two-dimensional panel program were solved by curve fitting the lift coefficients bounded by these extremes, as described in Chapter IV. The 92-inch loads are the approximate longitudinal (positive aft) and vertical (positive up) total loads which would be seen by a complete center section leading edge segment on the aircraft. The total load applied to the shortened finite element model would be some 69.6 percent of this stated load.

TABLE 4. FINITE ELEMENT ANALYSIS INPUT DATA

Load Case	2y/b	Cℓ	Twist (deg)	92" Load (lbs)
1	.35	1.2726	0.0000	FX = -5157
	.45	1.2379	0.0000	FZ = 13155
	.55	1.1834	0.0000	
2	.35	1.2726	0.8736	FX = -5157
	.45	1.2379	1.1221	FZ = 13155
	.55	1.1834	1.3764	
3	.35	1.0778	0.7605	FX = -3657
	.45	1.0569	0.9966	FZ = 11069
	.55	1.0090	1.2572	
4	.35	1.3465	0.7216	FX = -4454
	.45	1.3118	0.9272	FZ = 10666
	.55	1.2575	1.1375	
5	.35	0.7109	0.5673	FX = -2103
	.45	0.6723	0.7335	FZ = 10540
	.55	0.6100	0.9169	
6	.35	1.3789	1.2997	FX = -5982
	.45	1.3247	1.6613	FZ = 16742
	.55	1.2453	2.0279	

2. Finite Element Analysis Results

a. Load Case 1

In looking at the 275 knot load without static aeroelastic twist, it was noted that the largest stress concentrations in the structure were located in the rib legs, with the lower legs experiencing approximately 15 ksi in tension along their upper flanges and the upper legs seeing about -14 ksi (compression) along the lower flanges. These stresses were evenly distributed, as may be seen by the values in Figures 22, 23 and 24 where the major principal axis stress (σ_I) contours are shown. The minor principal (σ_{II}) stresses, Von Mises and shear stresses show a similarly even distribution, with all stress levels well below the yield

stress value (σ_{ys} = 47 ksi) for the material. It should be noted that the apparent deformations in the plot are exaggerated and not to scale. This scaling provides the viewer with a better perception of the direction of displacement occurring, although in reality, the displacements are only on the order of 0.06 inches for this load case as determined by MSC/pal 2®.

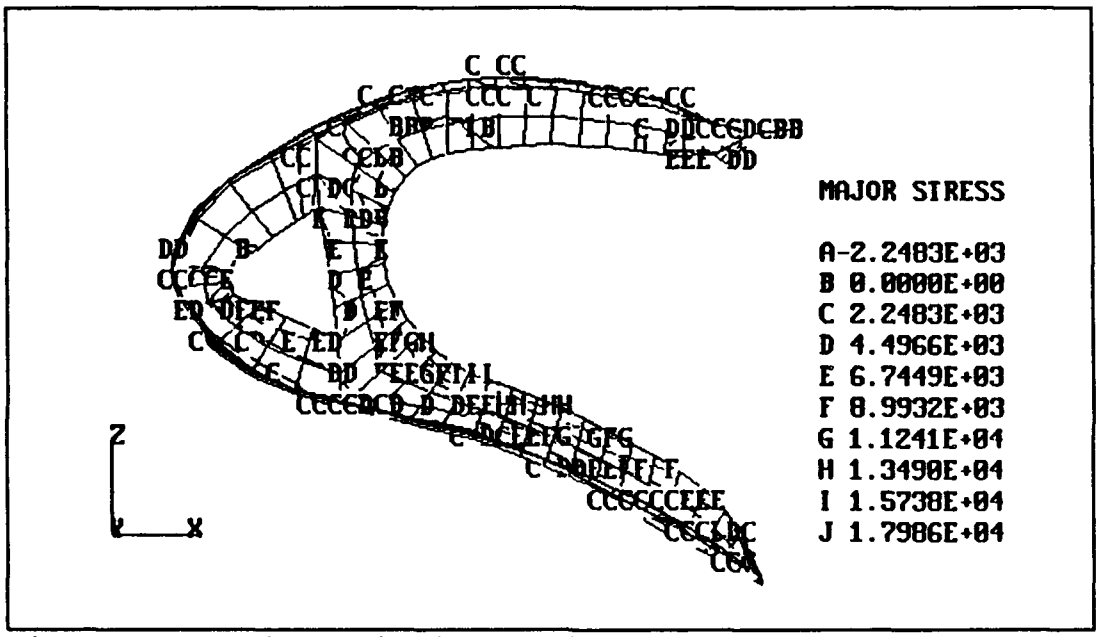

Figure 22. Major principal axis stress contours on inboard (WS256) end rib in untwisted condition (Case 1).

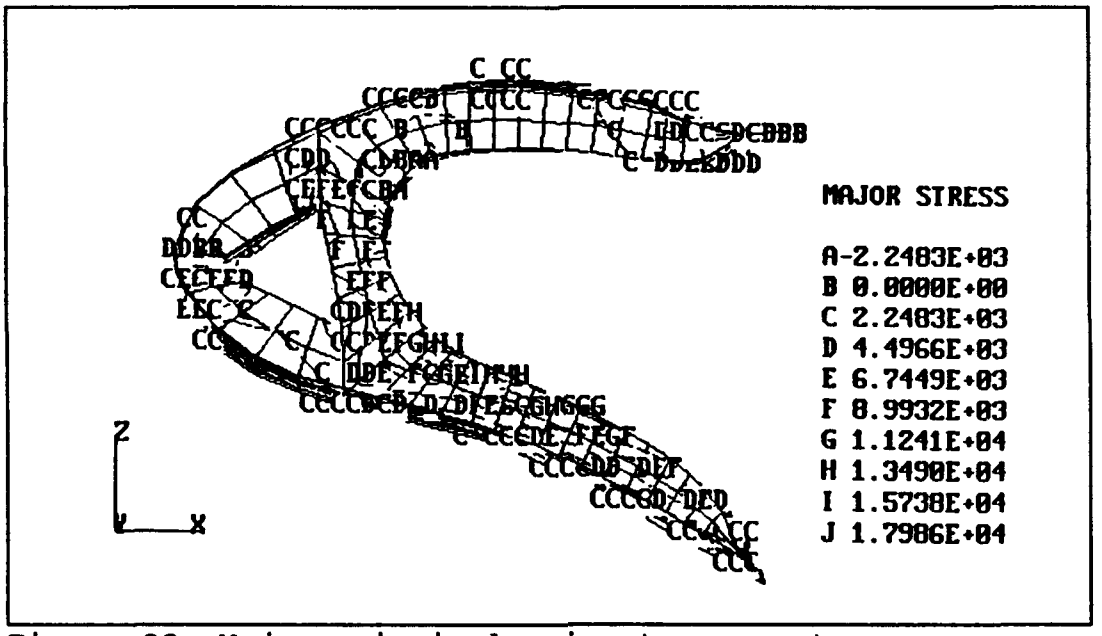

Figure 23. Major principal axis stress contours on middle (WS282) rib in untwisted condition (Case 1).

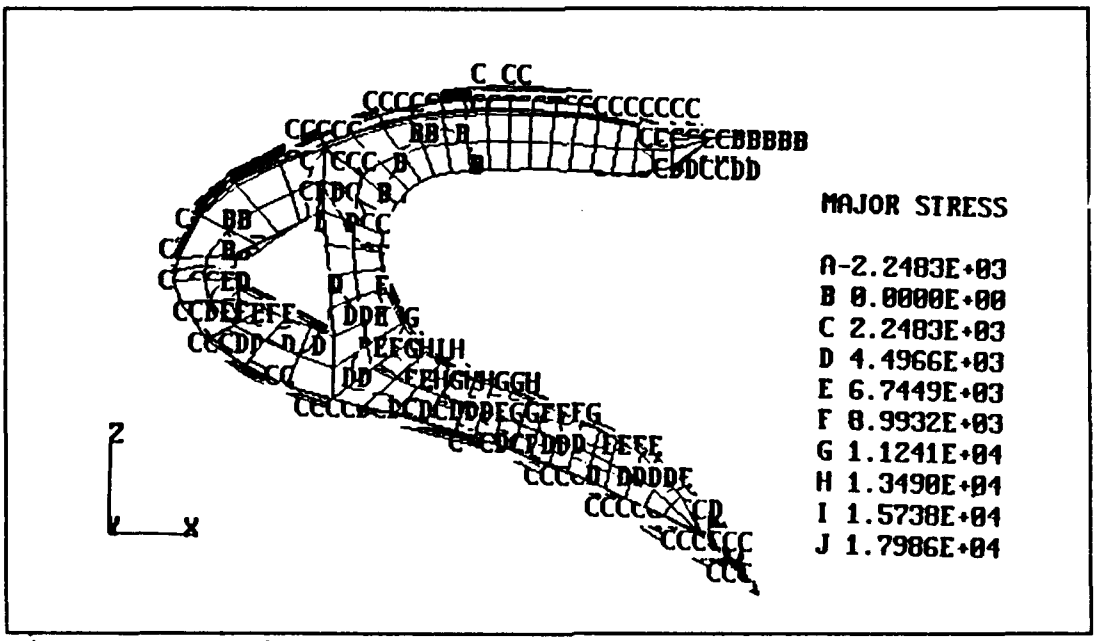

Figure 24. Major principal axis stress contours on outboard (WS320) rib in untwisted condition (Case 1).

The untwisted load case (case 1) does not accurately reflect the behavior of the leading edge since it does not include the effect of aeroelastic-induced spanwise twisting (torsion) of the wing. The stress contours in Figures 22, 23 and 24 were presented for comparison to load case 2.

b. Load Case 2

A dramatic difference in the observed stress contours occurred when the finite element model was subjected to the net twist occurring in the wing box as determined by the static aeroelastic span load analysis. It should be noted that the displacement input to the model equated to only about 0.3 degrees of front spar rotation from WS 256 to WS 320. The same set of stress contour plots as above are given in Figures 25, 26 and 27. A striking contrast existed between the first and second load cases, with the case 2 major principal axis stress distribution very unevenly spread between the inboard and outboard ends. As may be seen in Figure 25, the inboard end rib (WS 256) experienced more than double the stress concentration in its lower leg with 34.8 ksi being the highest level contour shown. Moving outboard, WS 282 (Figure 26) showed a maximum of about 20 ksi in its lower leg while the stress in the same leg on the outboard (WS 320) rib went to zero. (A stress level of 2.9 ksi in the saddle and upper leg of the rib may still be seen.)

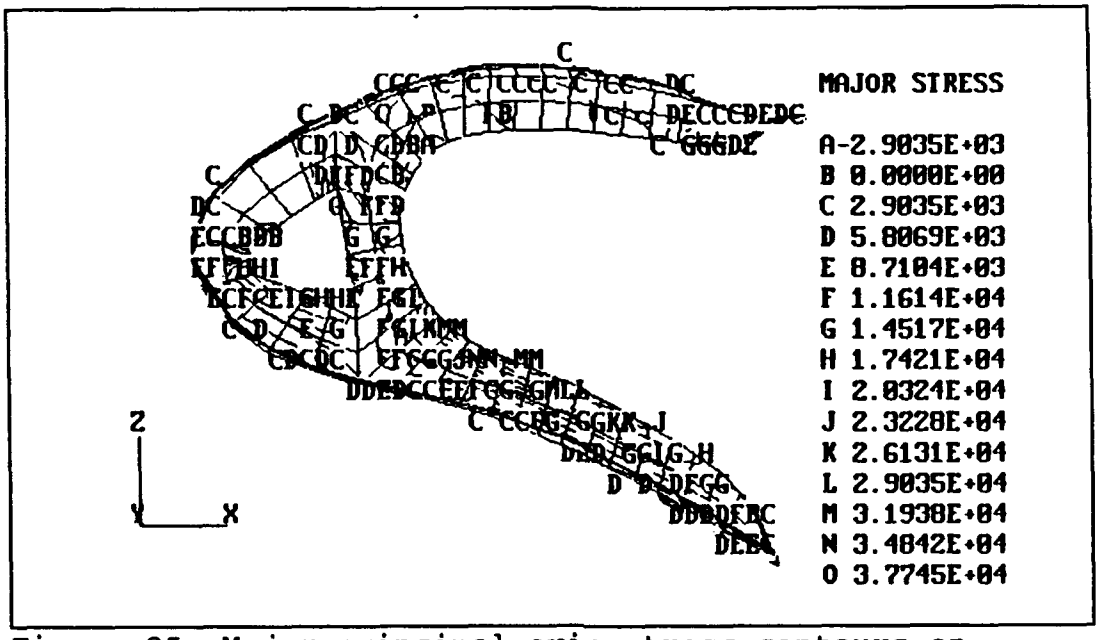

Figure 25. Major principal axis stress contours on inboard (WS256) end rib with twist applied (Case 2).

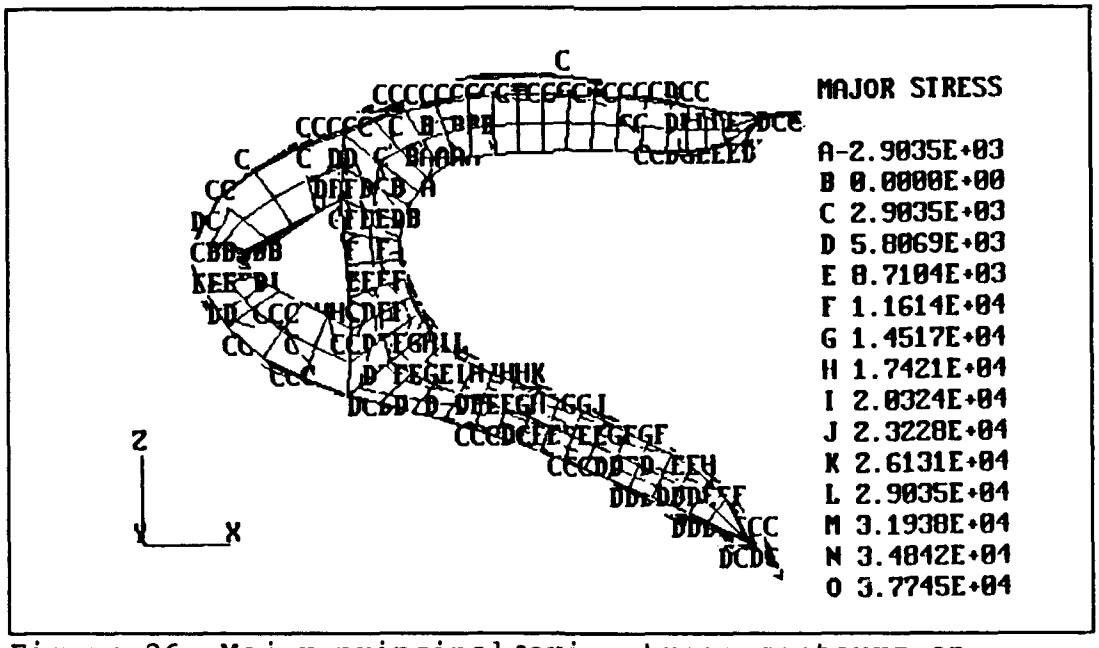

Figure 26. Major principal axis stress contours on middle (WS282) rib with twist applied (Case 2).

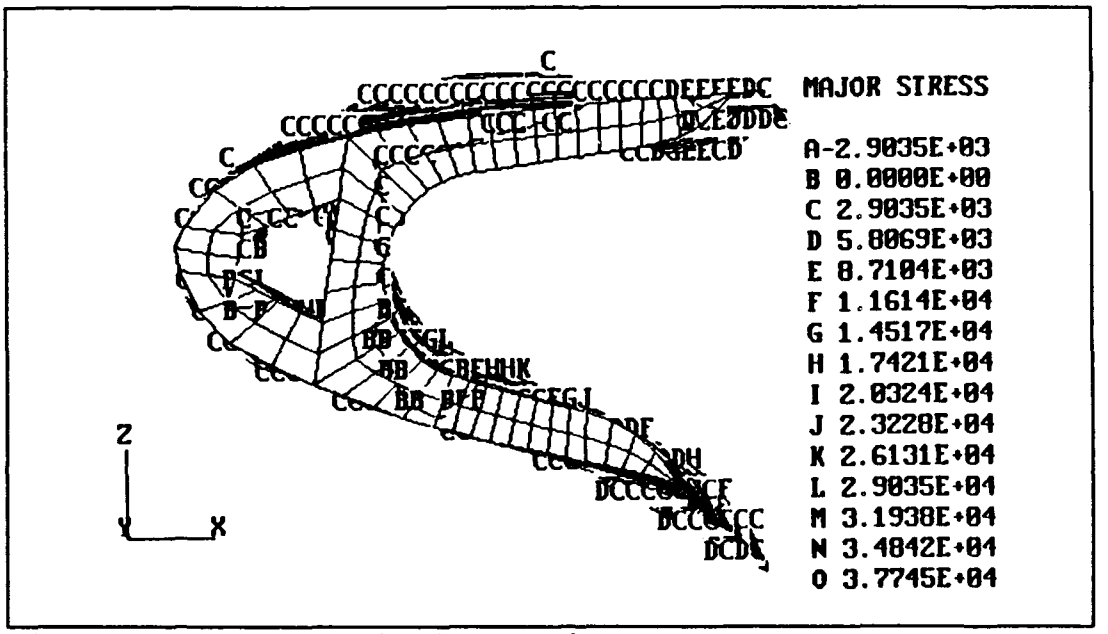

Figure 27. Major principal axis stress contours on outboard (WS320) rib with twist applied (Case 2).

Since it was observed that this same pattern of stress distribution occurred for the minor principal axis, Von Mises and maximum shear stresses, only the inboard end (WS 256) contours are shown in Figures 28, 29 and 30. This pattern is to be expected since they are all geometrically related. The major and minor principal stresses occur on planes on which there is no shear stress and are oriented perpendicularly to each other, while the maximum shear stress occurs on planes which are at angles of 45 degrees to the principal planes. Von Mises stresses (σ_V) are derived from a criterion known as the Maximum Distortion Energy Criterion and may be found from the equation,

$$\sigma_V^2 = \sigma_I^2 - \sigma_I\sigma_{II} + \sigma_{II}^2$$

which is based on the determination of the energy associated with changes in shape of a given material. These relationships are valid under the assumption of a plane stress condition in the material. This means that the metal is thin in comparison to its other dimensions so that the stresses across the thickness of the metal may be considered as negligible. This plane stress condition is the case for most aircraft structural components since they are made of sheet material, and is valid here. [Ref. 19, 20]

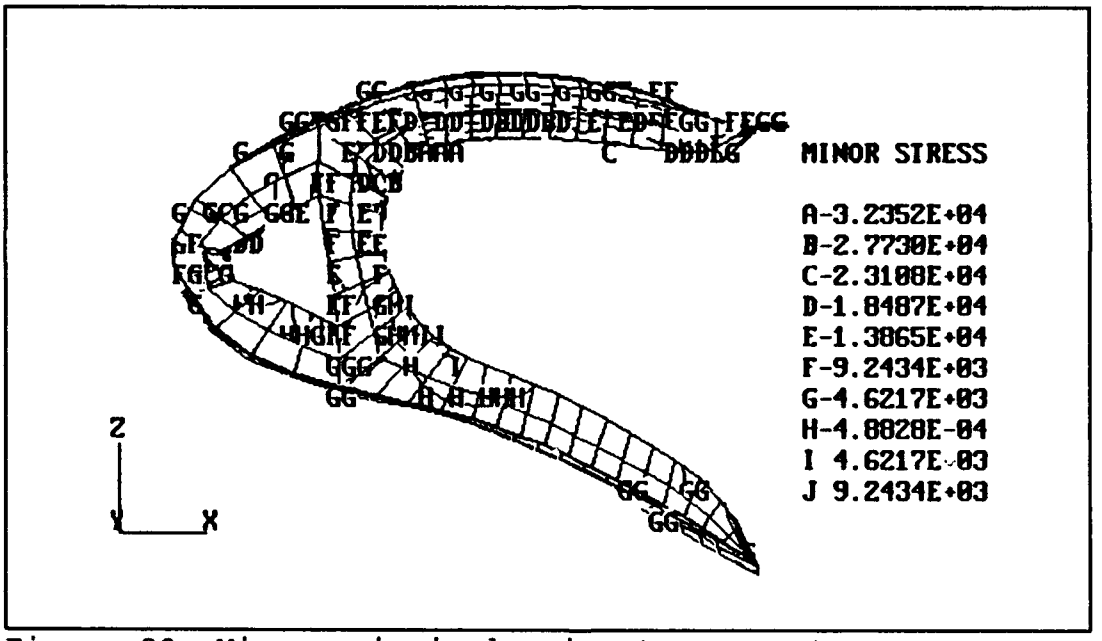

Figure 28. Minor principal axis stress contours on inboard (WS256) end rib with twist applied (Case 2).

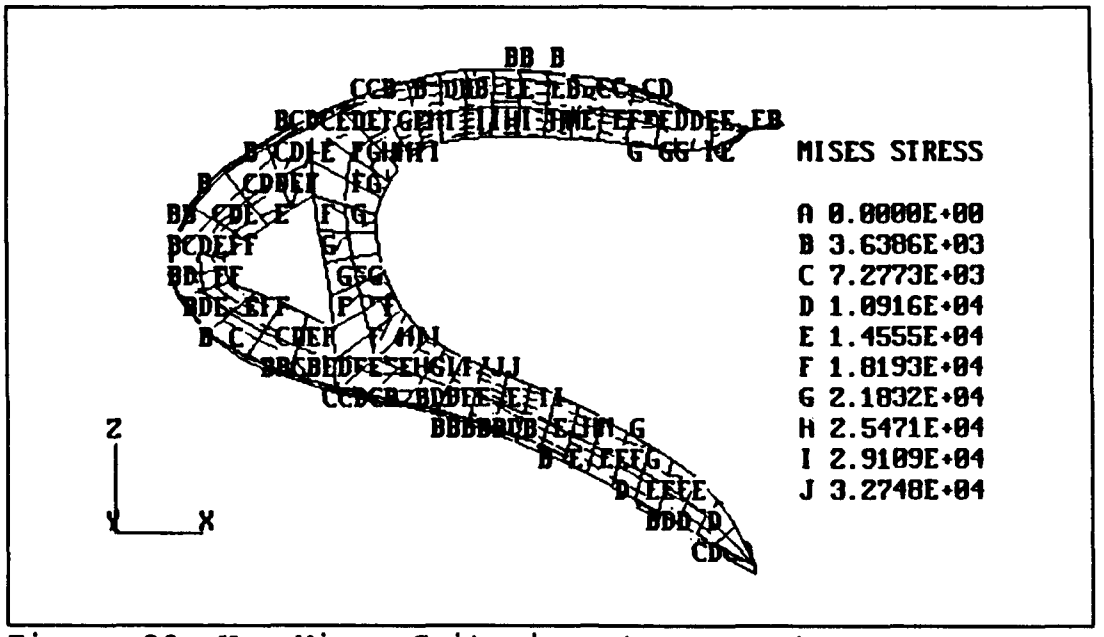

Figure 29. Von Mises Criterion stress contours on inboard (WS256) end rib with twist applied (Case 2).

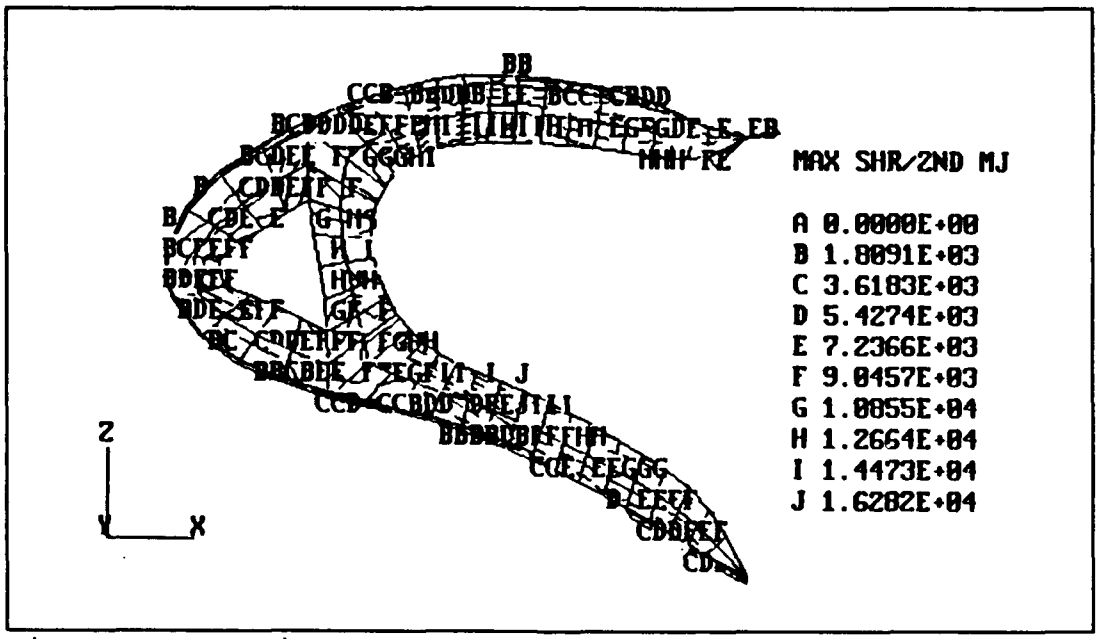

Figure 30. Maximum shear stress contours on inboard (WS256) end rib with twist applied (Case 2).

In Figures 31 through 36, the **x** and **z** displacements of the ribs are shown in pairs from inboard to outboard. Note

the small displacements occurring in the upper flange and lower hinge due to twist of the front spar.

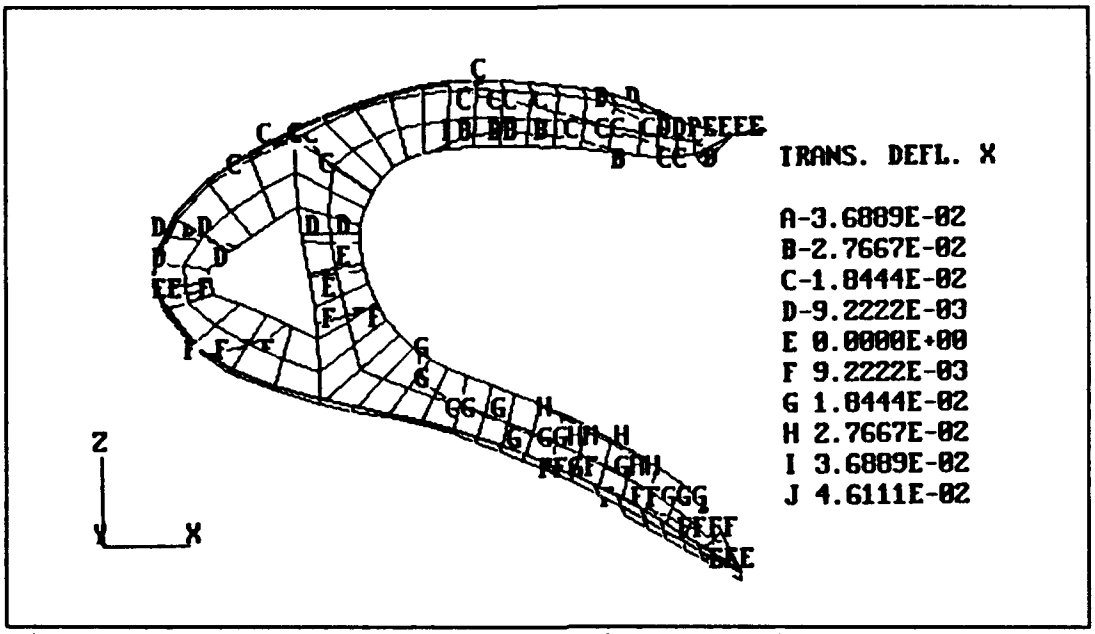

Figure 31. Displacement (x) at inboard rib (WS256).

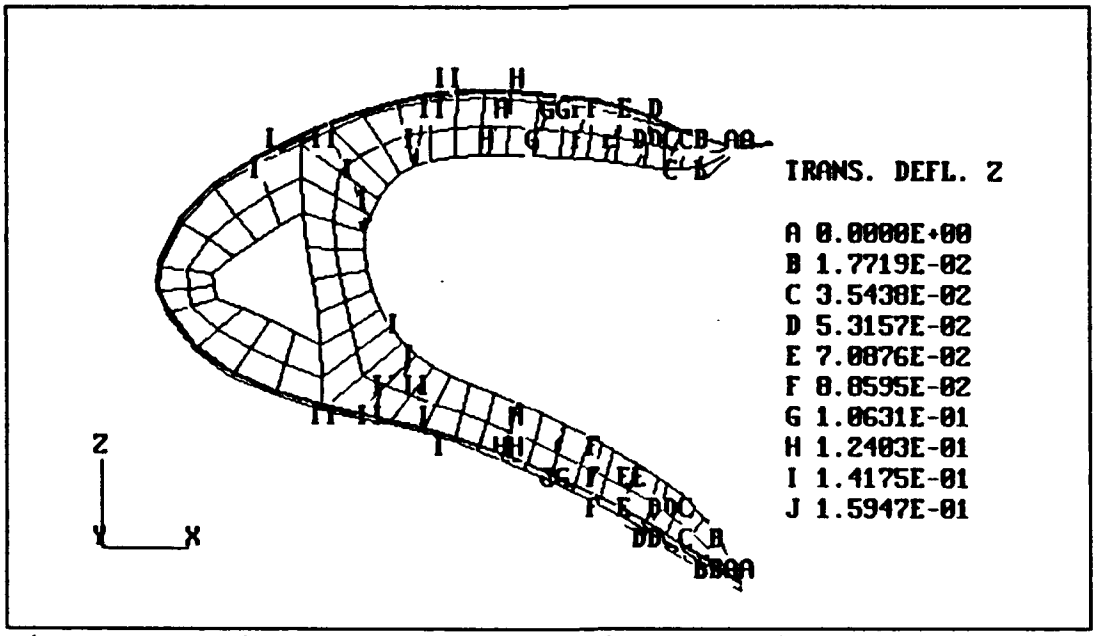

Figure 32. Displacement (z) at inboard rib (WS256).

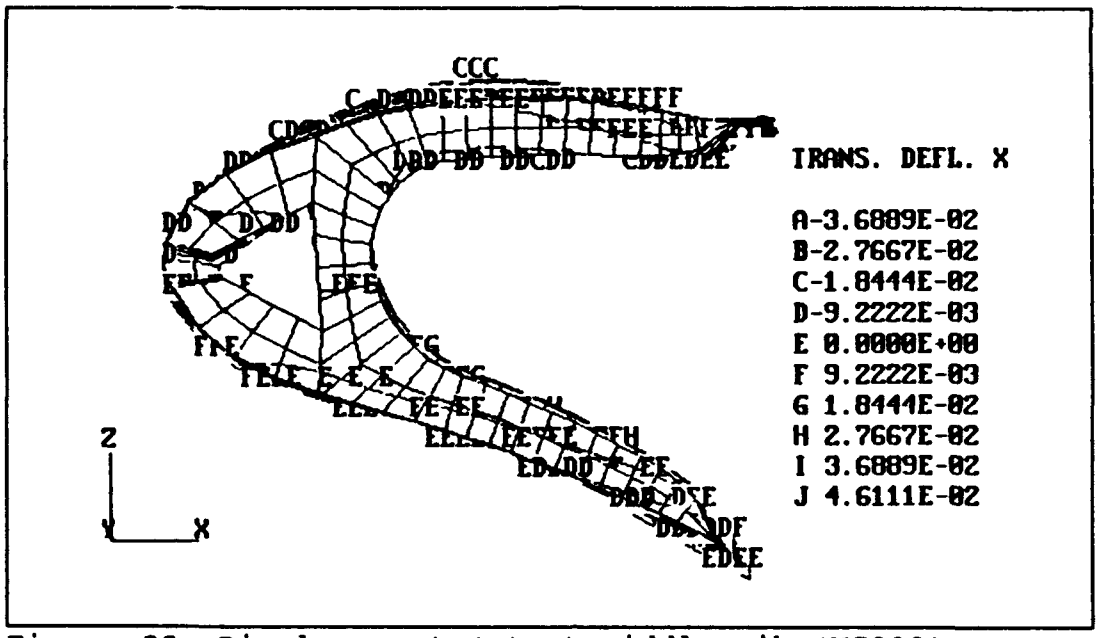

Figure 33. Displacement (x) at middle rib (WS282).

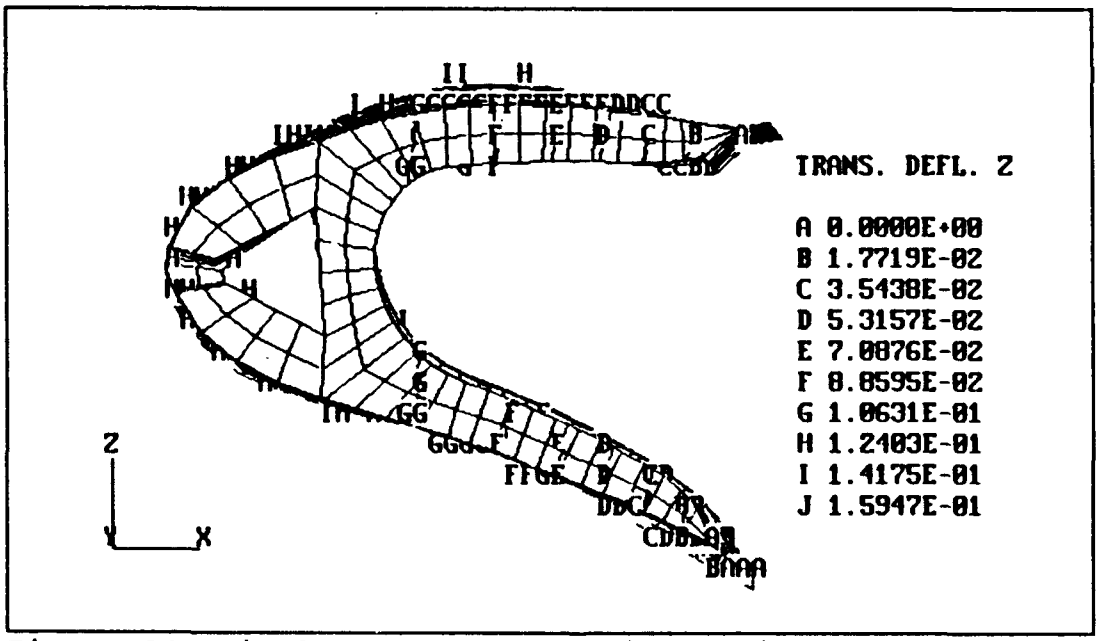

Figure 34. Displacement (z) at middle rib (WS282).

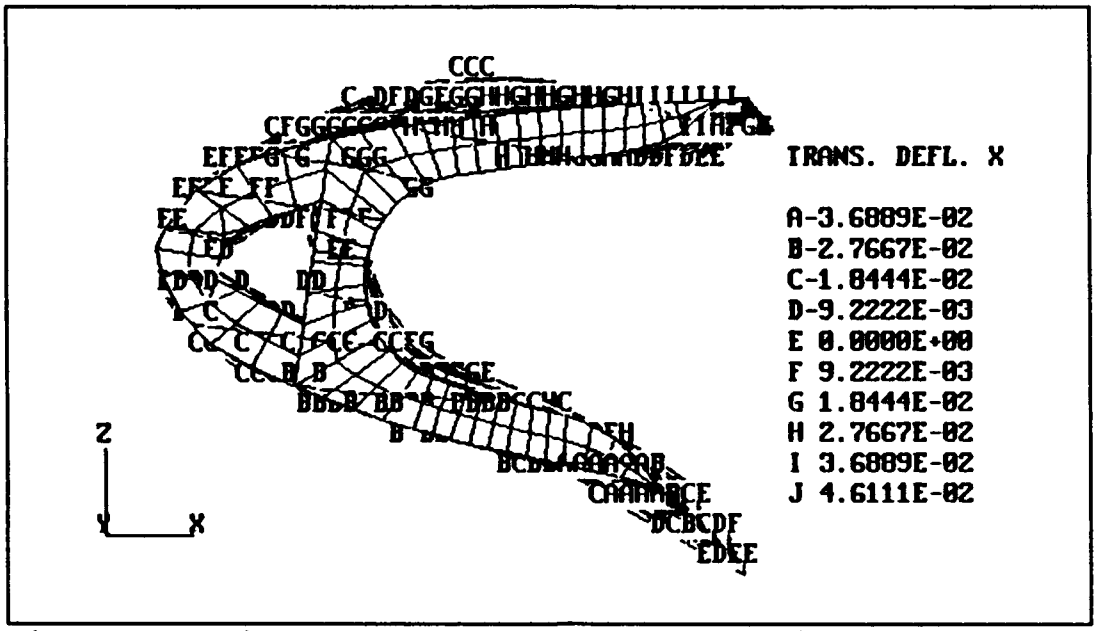

Figure 35. Displacement (x) at outboard rib (WS320).

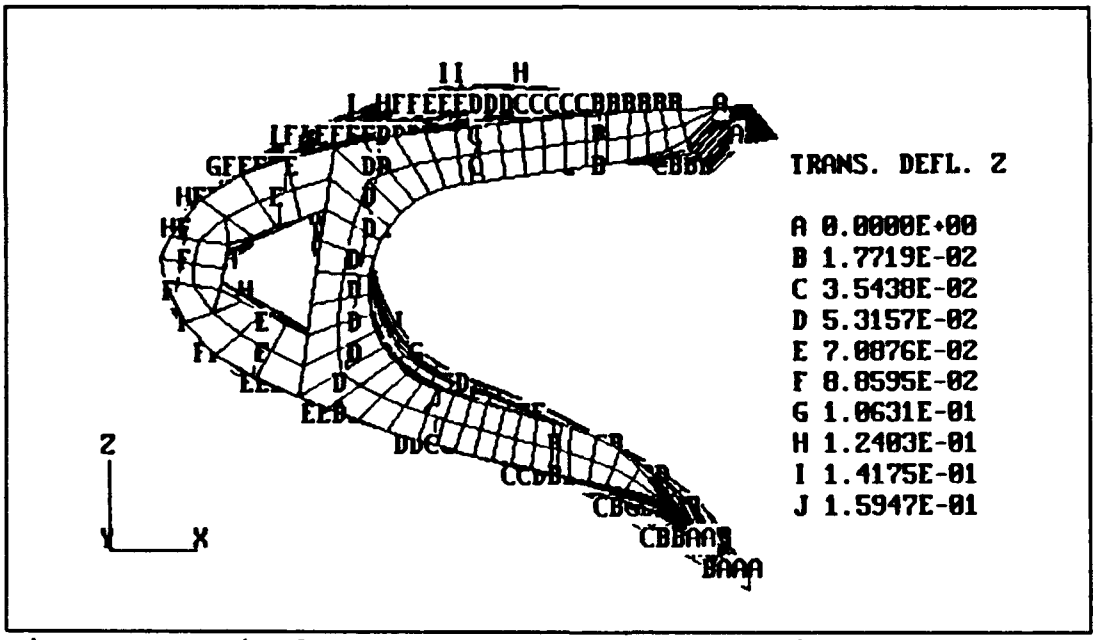

Figure 36. Displacement (z) at outboard rib (WS320).

Another available representation of the stress concentrations present in the structure is an X-Y plot of all four stresses together in a form resembling a frequency scatter on an oscilloscope. This plot for the case 2 load

condition is presented in Figure 37. While this is a rather cluttered plot it does serve to provide, at a glance, the maximum and minimum stress concentrations in the structure. Since the stress contours of individual members in the structure have been examined and it has been found that the highest stresses are in the rib legs, the peak stresses depicted may be attributed to these locations. The positive (upper) portion of the plot is a combination of the major principal, Von Mises and shear stresses while the lower half depicts the minor principal axis stresses. For the sake of

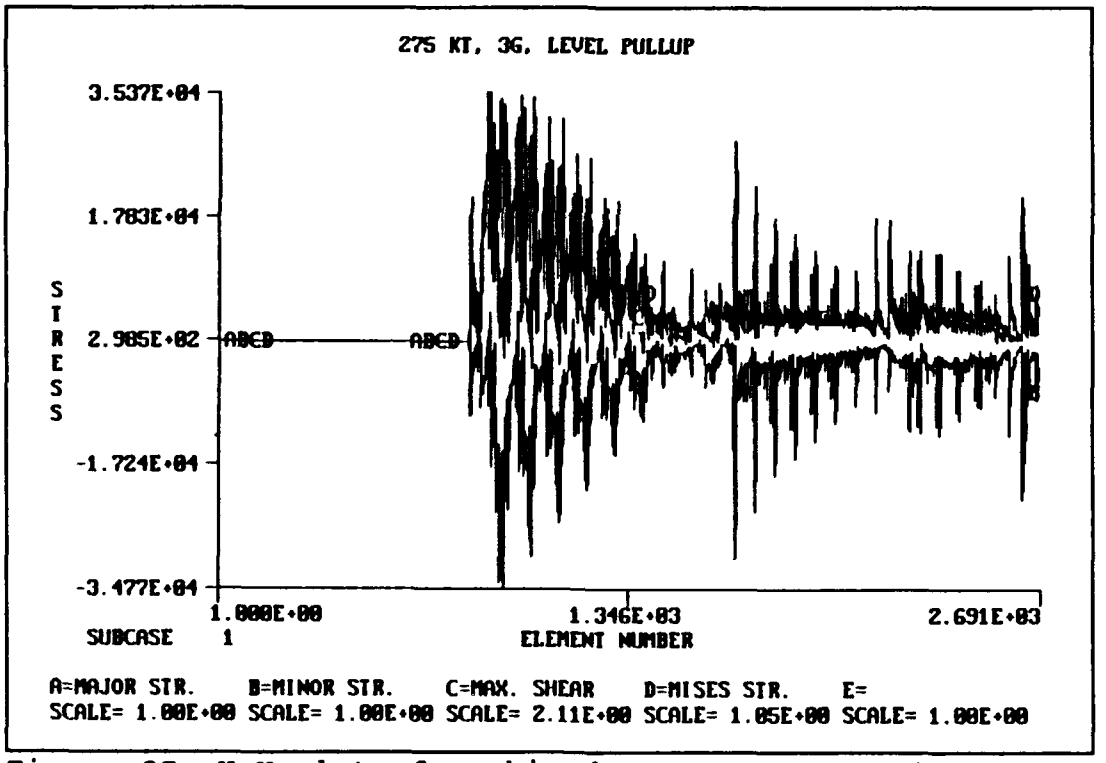

Figure 37. X-Y plot of combined stresses (Case 2).

brevity, and since the contour plots of the individual ribs retain the same relative form as those presented for cases 1

and 2, the stress levels for the remaining load cases will be presented in this form.

c. Load Case 3

For the 275-knot, 2.4-G rolling pullup, the maximum stress levels observed are approximately 33 ksi on the descending wing as shown in Figure 38. The loads on the leading edge of the ascending wing are lower than those for the descending wing. This speed was chosen because of the relationship which was shown to exist between leading edge loading, angle of attack and dynamic pressure. The result of

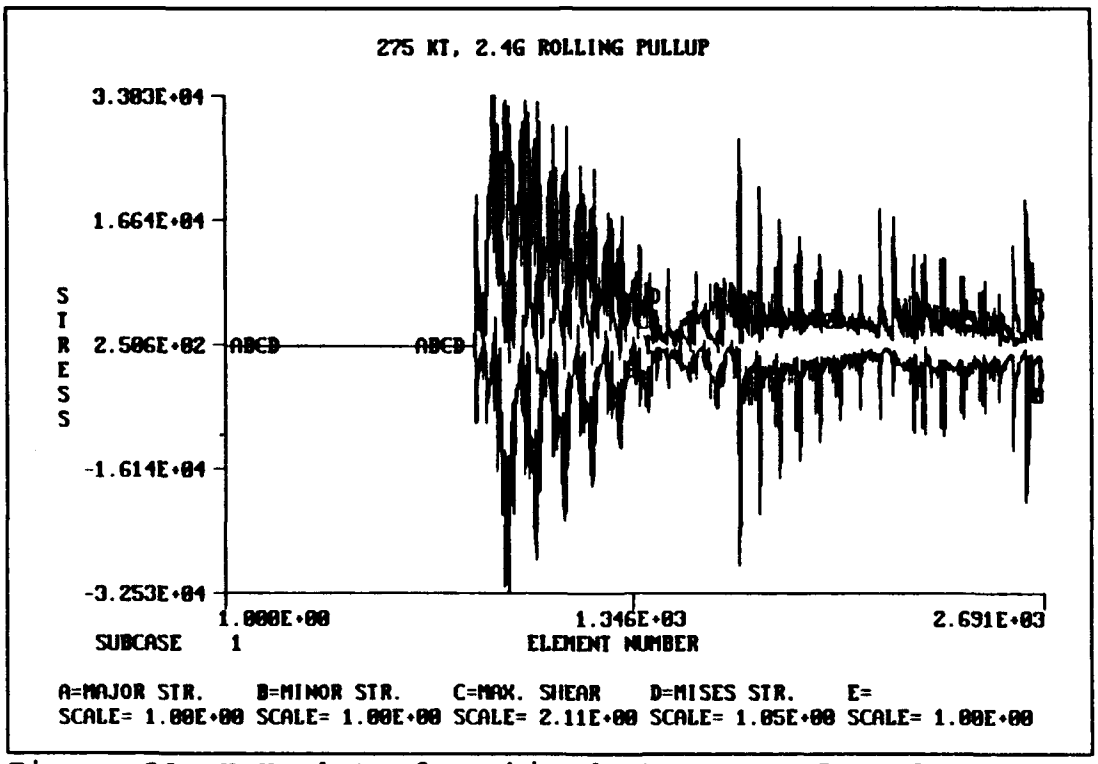

Figure 38. X-Y plot of combined stresses (Case 3).

higher airspeed at the same aircraft load factor may be see in part e of this Chapter.

d. Load Case 4

The 110,000 pound weight condition was chosen for this load case in order to examine the reduction in leading edge stress when operating within the normal flight envelope at less than maximum gross weight. The 240-knot airspeed is the approximate "corner" speed at a load factor of 3G for this weight. The maximum stress values seen under this condition are 28.8 ksi in tension and 28.3 ksi in compression as seen in Figure 39.

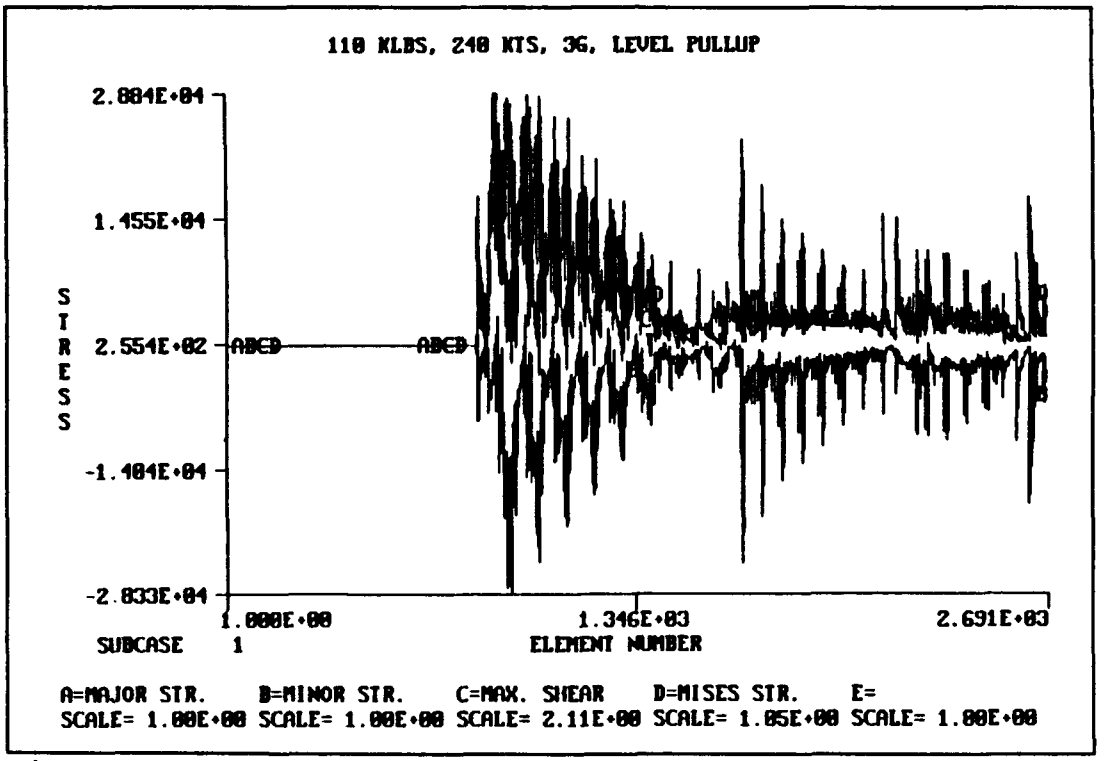

Figure 39. X-Y plot of combined stresses (Case 4).

e. Load Case 5

In load case 5, the effect of a 2.4-G rolling pullup at 135,000 pounds gross weight at a true airspeed of 350 knots was examined. In Figure 40, it may be seen that the maximum stress values are approximately 26 ksi, which is approximately 7 ksi less than the same maneuver at 275 knots (load case 3).

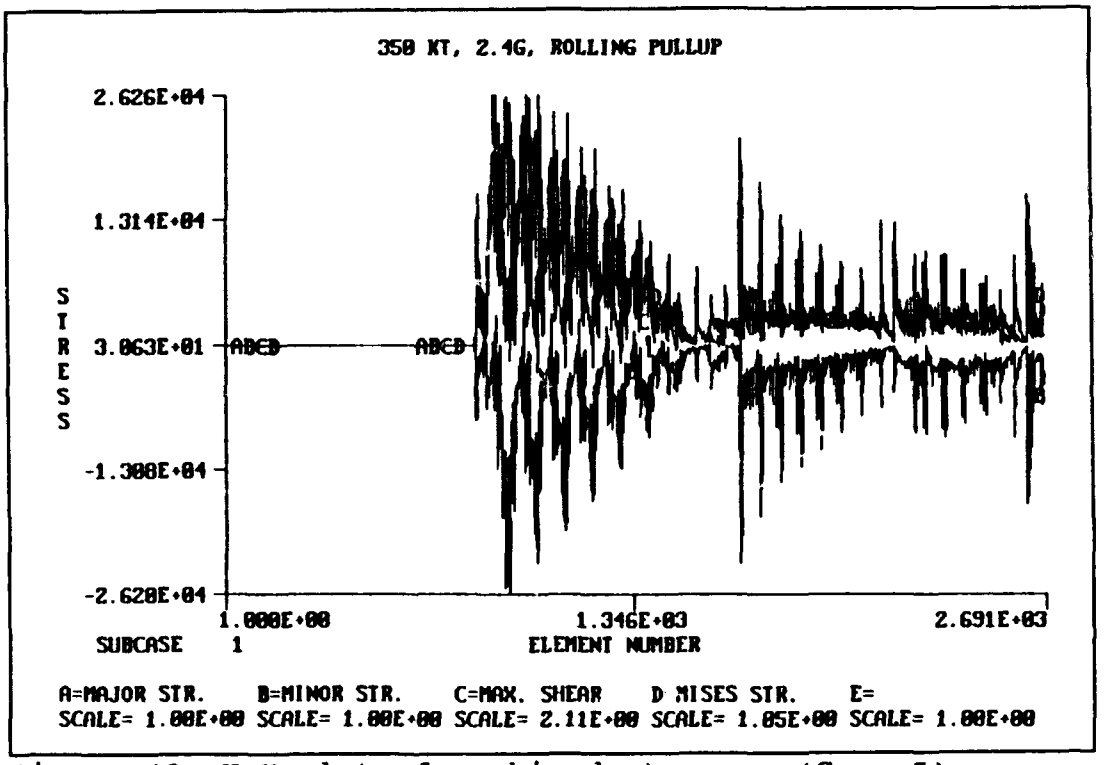

Figure 40. X-Y plot of combined stresses (Case 5).

f. Load Case 6

In order to examine the design ultimate flight load condition, load case 6 was run at 325 knots and 4.5G. The airspeed corresponds to the approximate stall speed (corner speed) for the 135,000 pound airplane gross weight.

Stress values of nearly 52 ksi may be seen in Figure 41. Note that this result exceeds the yield stress for the material (47 ksi).

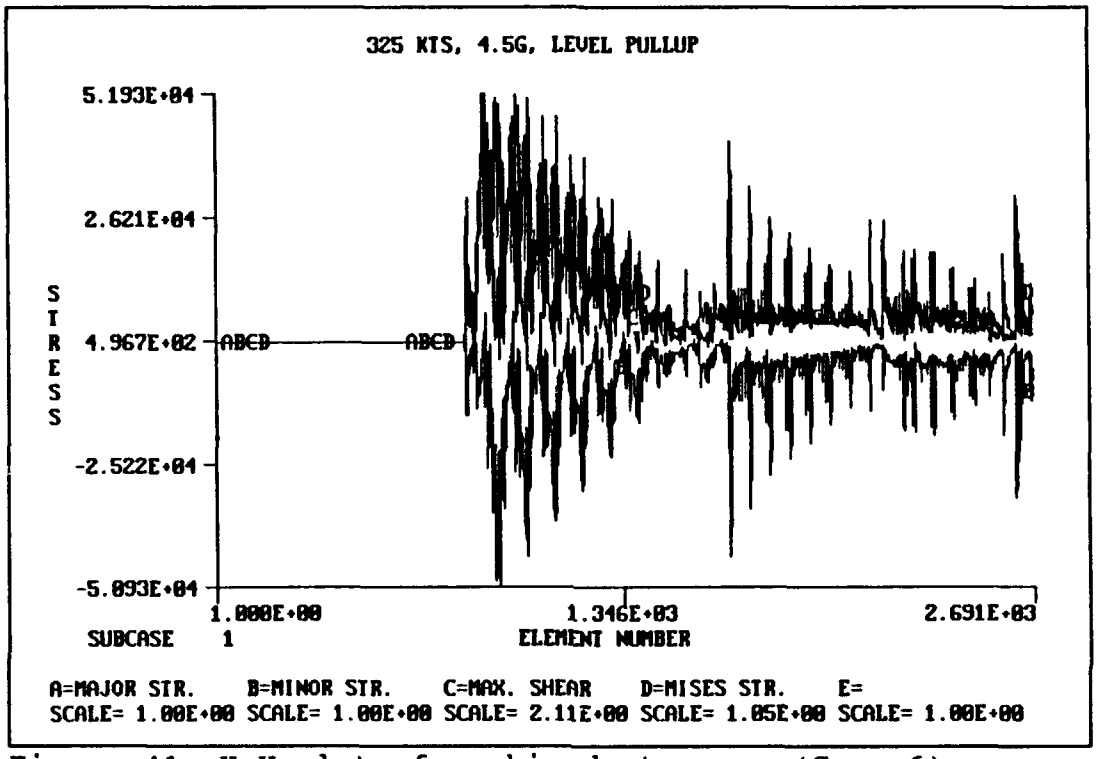

Figure 41. X-Y plot of combined stresses (Case 6).

3. Discussion

The primary factor of concern in the observed loads presented above is the apparently high level of stress in the rib legs as determined by the methods stated in the course of this writing. According to the Engineering Investigation (EI) report for the USN P-3 mishap [Ref. 21] and a preliminary report issued by Aircraft Research Laboratories of Melbourne, Australia [Ref. 22], the initial structural failure in both mishaps was believed to have occurred in the lower rib legs,

with initial failure occurring in the outboard leg and proceeding inboard in a series of sequential failures. It would appear from the results of this study that this failure sequence may have been reversed, since the highest observed stresses were in the inboard rib. Additionally, the fact that there is an intermediate rib at WS 317, only three inches from the outboard end rib (rather than the eight- to nine-inch spacing for all other ribs in the leading edge) supports the idea that the failure would likely have initiated at some other location. This close proximity of two ribs means that the load in that region would be shared, thereby reducing the stress in the outboard rib. In any case, the primary question remains as to whether there were sufficiently high stress levels in the rib legs to cause structural failure.

While the maximum observed stress levels (found here for operation within the flight envelope, occurring under load case 2 in a wings level, 3-G pullup at 135,000 pounds gross weight) were some 12 ksi below the yield stress for the material, two areas of concern must be addressed: 1) the additional effect of extending this data from the assumed 64-inch model size to the true 92-inch leading edge segment which is installed on the aircraft; and 2) the effect of stress concentrations around holes in the rib legs.

a. Extending the Structure

Proceeding under the assumption that the stress concentrations vary linearly with the length of the structure, extending the 64-inch model to the full (92-inch) length of the true structure would result in an increase in the observed stress in the lower rib leg to 51.9 ksi, which is in excess of the 47 ksi yield stress. Examining the major principal axis stresses in the lower legs of WS 256 and WS 282, this linearity would appear to hold true. Since aluminum is a ductile material, the stresses may subside as the material begins to yield, therefore, the structure may still carry the load without fracture. However, changes in the pressure distribution around the leading edge must also be considered as the structure begins to deform. Given the observed directions of the deformations as seen in the contour plots, it seems likely that the aerodynamic load would continue to increase due to the increased camber in the leading edge as it lifts perpendicular to the chord and develops a more circular form. This deformation, although initially small could add to the load, initiating a divergent stress scenario leading to failure.

b. Stress Concentrations

It is an established fact that stress concentrations around circular holes can multiply the localized stress by factors of between two and four, depending

on the directional orientation of the loading seen by the specimen. Along the inner surface of the end ribs is a continuous flange which is attached by a rivet spacing of approximately one-half inch. Additionally, there are four tapered angle stiffeners riveted to the web section of the rib. Two of these are symmetrically located on the upper and lower legs at a position approximately 52 percent of the leading edge chordwise dimension forward of the hinge. (On the outboard end rib (WS 320) this is approximately 12 inches forward of the hinge.) Around these rivet holes, stress concentrations may be assumed to occur. The occurrence of these concentrations at the onset of stress loading depends on the rivet installation procedure; i.e., the stress concentration effect is delayed if the rivet hole is placed in compression (as in a dimpled or double dimpled installation [Ref. 18]). If the hole were initially in compression, a margin or stress buffer would be provided, as the material is subjected to tension stress; i.e., the tensile stress applied must first exceed the compressive pre-stress of the rivet installation before the hole will begin to experience a stress concentration. The type of installation of the rivets under consideration is unknown by this author. Since the inside flange of the upper legs is placed under compressive loading nearly equivalent to that experienced by the lower leg in tension, the effect of compressive concentrations must also be considered. If the rivet holes were pre-stressed in

compression, this would add to the compressive stress level at this location, potentially causing the upper leg to fail first in compression. As before, this all depends on the stress reduction due to yielding which takes place in the ductile material.

In the Australian incident report, the failure sequence was described as having initiated along the line of the riveted stiffener on the lower leg of the outboard end rib as mentioned above. In addition, it goes on to say that the failure then proceeded along a line of dimples in the lower legs of the intermediate ribs, from outboard to inboard. These dimples act as stiffeners for the intermediate ribs and would also act as stress concentrations under load. None of these stiffeners, on either outboard or intermediate ribs, nor their rivet holes, are included in the finite element model employed in this study. Again, the failure sequence described is opposite of that expected from the results of this study. The RAAF determination of the failure sequence was based on the observed outboard-to-inboard bending of the rib fragments which remained attached to the structure. [Ref. 22]

VI. CONCLUSIONS AND RECOMMENDATIONS

A. CONCLUSIONS

The results of this study indicate that failure of a P-3 wing leading edge segment could be predicted to occur within the normal aircraft operating envelope providing proper account is given to the influences of wing static aeroelastic effects both upon wing span loads and torsional twists induced in the wing spar box. The location of the highest stresses are in the area of the observed failures as reported in the EI and Preliminary reports [Ref. 21 and 22]. It is reasonable to assume that stress concentrations around the rivet holes could be on the order of 1.5 or 2.0 times the observed stresses. This, combined with the effect of extending the model to the full 92-inch length, could result in stress levels in excess of the ultimate strength of the material, 60 ksi [Ref. 18].

The primary evidentiary conflict with this study is the reported location of apparent failure initiation at the outboard vice inboard end. The observed inboard bending of the rib fragments may have been induced by the upper portion departing the wing in some fashion other than that assumed. It is difficult, at best, to assess the direction in which the ribs would bend as the failure progressed.

While fatigue is potentially a contributor to this mode of failure, given the possibility of plastic strain having occurred earlier under a reduced load condition, the EI [Ref. 21] stated that no undue hardness was detected in the failed USN structure. This would indicate that no material strain hardening had taken place up to the time of failure.

Corrosion is another potential problem, particularly when dealing with aircraft operating routinely in low level overwater environments; however, no levels of corrosion which would effect the structural integrity of the leading edge were cited in the EI.

Whether or not the aircrews overstressed the aircraft by exceeding the limitations of the flight envelope cannot be concluded here. Even they may not know for sure whether this was the case. Flight experiments conducted in the 2F87F P-3 simulator at NAS Moffett Field, CA, during the course of this analysis indicate that at high gross weights and aft center of gravity conditions, it is easy to exceed the 3G limit with just a firm pull on the control yoke. The rapid onset of G overload may be imperceptible due to the rate at which it was observed to occur. The cockpit G meter is not an instrument which is normally kept in the pilot's scan.

B. RECOMMENDATIONS

This analysis should be confirmed by independent validation. If these results are verified, re-enforcement of the end rib may be feasible; alternately, some limitations should be placed on the operational flight envelope of the P-3. Covered here are some recommended procedures for validation along with approximations of interim flight envelope limits, should validation and/or repair not be possible in the near-term.

1. Validation

Since the Naval Air Systems Command, through Aerostructures, Inc., has the base model from which this finite element model was derived, it is recommended that validation be conducted with the following modifications on the existing model:

- Skin stiffness should be included in the model. The contribution of the skin to the load bearing properties of the structure is essential. Skin stiffness could be simulated by artificially increasing the thickness to simulate the double skin as was done here, or preferably, through addition of a **w** axis (quadrilateral element local coordinate system) stiffness factor which would emulate the combined stiffness of the inner and outer skins.

- Static aeroelastic twist must be included in the analysis since it was the factor contributing to the dramatic increase in inboard end rib stress. Since the NASTRAN® model is already of the appropriate length, this model would serve to verify or discount the theory that the stress concentrations would increase linearly with extended length.

- A small finite element model of the area of immediate concern (the lower leg of an end rib) should be

constructed and analyzed. This model should be of sufficient detail to include the rivet holes and stiffeners in order to examine the amount of stress concentration occurring. Any pre-stress of the rivet holes should be taken into account.

Laboratory tests of actual end ribs would prove helpful in determining the effect of the rivet holes on stress concentrations and provide data on the load levels required to cause fracture.

2. Flight Envelope Modifications

If these results are verified, the P-3 flight envelope should be restricted to prevent another mishap. If, in the estimation of NAVAIR, verification cannot be accomplished within a reasonable amount of time (six months), then it is recommended that an interim measure be taken to restrict the flight envelope until such verification or disproval can be accomplished. While the precise envelope restrictions would be developed by NAVAIR, it is recommended on the basis of the results observed here that the following limitations be applied if interim limitations are deemed appropriate:

- Reduce the maximum sustained load factor for the aircraft from 3G to 2G at all operating weights above 100,000 pounds.
- Reduce the maximum sustained load factor for the aircraft from 3G to 2.5G at all operating weights up to and including 100,000 pounds.

While these are rough estimates, they are believed to provide a sufficient margin of safety to allow safe flight without severely impacting daily P-3 operations.

LIST OF REFERENCES

1. Lockheed, California Company Report 15392, *P-3A Orion Performance and Standard Aircraft Characteristics,* 29 September, 1961, revised 15 June, 1964.

2. NAVAIR 01-75PAC-1, *NATOPS Flight Manual, Navy Model P-3C Aircraft,* 1 December, 1983.

3. Lockheed, California Company Report 30516 (L-512), *Wind Tunnel Test of Electronic Surveillance Wing Tips on the P-3C,* 5 August, 1983.

4. Schmidt, L.V., *Static Aeroelastic Effects Upon Wing Span Loads,* paper number AIAA-91-3316, American Institute of Aeronautics and Astronautics 9th Applied Aerodynamics Conference, Baltimore, MD, September, 1991.

5. Bertin, J.J., Smith, M.L., *Aerodynamics for Engineers,* p. 354, Prentice Hall, 1989.

6. Schmidt, L.V., Unpublished Notes, Naval Postgraduate School, Monterey, CA.

7. Etkin, B., *Dynamics of Flight - Stability and Control,* John Wiley and Sons, 1989.

8. NAVAIR 01-75PAA-3-1, *Structural Repair Instruction, Organization and Intermediate Level Maintenance,* 1 November, 1985.

9. Lockheed Aircraft Corporation Report 13133, *Lockheed P3V-1 Flying Qualities,* 19 November, 1959.

10. Glauert, H., *The Elements of Airfoil and Airscrew Theory,* Cambridge University Press, 1946.

11. ANC-9 Bulletin, *Aircraft Propeller Handbook,* Department of the Air Force, Department of the Navy, Department of Commerce, September, 1956.

12. Teng, N.H., *The Development of a Computer Code for the Numerical Solution of Unsteady Inviscid and Incompressible Flows Over An Airfoil,* M.S. Thesis, Naval Postgraduate School, Monterey, CA, June, 1987.

13. Nakamura, S., *Applied Numerical Methods With Software,* Prentice Hall, 1991.

14. Mac-Neal Schwendler Corporation, *MSC-PAL 2, Advanced Stress and Vibration Analysis, Reference Manual,* 1989.

15. Mac-Neal Schwendler Corporation, *MSC-PAL 2, Advanced Stress and Vibration Analysis, Application Manual,* 1989.

16. NAVAIR 01-75PAA-4-2, *Organization Maintenance, Illustrated Parts Breakdown--Landing Gear,* 1 January, 1990.

17. Engineering Alloy Digest Inc., *Alloy Digest,* Engineering Alloy Digest, Upper Montclair, NJ, 1973.

18. Bruhn, E.F., *Analysis and Design of Flight Vehicle Structures,* Tri-State Offset Company, 1956.

19. Megson, T.H.G., *Aircraft Structures for Engineering Students,* Halstead Press (a division of John Wiley and Sons), 1990.

20. Beer, F.P., Johnston Jr., E.R., *Mechanics of Materials,* McGraw Hill Book Company, 1981.

21. NAVAVNDEPOT Alameda, CA, *P-3 Final EI Response,* message dtg 081703Z July, 1988.

22. Aircraft Research Laboratory, Melbourne, Australia, *Preliminary Report on the Accident to P-3C Orion A9-754,* date unknown, received via Naval Safety Center, Norfolk, VA, facsimile transmission 19 September, 1991.

APPENDIX A

```
10   ' Program "P3SPNLD3.BAS"
     ' Solve Static Aeroelastic Spanload Problem
     '  for a wing with straight taper
     ' Vortex Lattice capability uses swept bound vortex
     '  elements
     ' Inputs consist of:
     '    AR   = Wing Aspect Ratio = B^2/S
     '    TR   = Wing Taper Ratio  = Ct/Cr
     '    SWP25 = 0.25 ch'd. sweep angle, +'ve is sweepback
     '    CEA   = Elastic axis location on const. fraction
     '             chord line
     '    MACH   = Subsonic Mach no. for aerodynamic compress.
     '           correctn.
     '    M    = No. of equal length spanwise stations, RH wing
     '    N    = No. of equal chordwise stations
     '   ** Comments **
     '   Allows Vortex Lattice solution with MxN boxes on
     '    RH wing
     '   Max. of MxN = 50:' Consistent with dimension
     '    statements
     '   N = 1 for elementary (Modified Weissinger) lifting
     '    line theory
     '   Wingspan, B, set to 1188 inches (for P3 applicatn.)
100  ' $DYNAMIC
     DIM X1(50), Y1(50), X2(50), Y2(50), X3(50), Y3(50),
     SWP(50),DIM A1(50, 50), A2(50, 50), ASYM(50, 50),
     AANT(50, 50),DIM S(50, 50), F(20, 50), G(20, 50),
     XEA(20), YEA(20), EI(20), GJ(20),DIM SWPM(50),
     DELA(50, 20), MX(20, 50), MY(20, 50),DIM ALPHA(50),
     U(20, 20), UGJ(20, 20), UEI(20, 20),DIM A(50, 50),
     XIN(50): ' for Spanload solutns. using ELU/SLVB S/R's
     DIM ALPHA1(50), ALPHA2(50), ALPHA3(50), ALPHA4(50),
     Q(50), DELCAM(5)
     OPEN "C:QBFILES\EXTRA.DAT" FOR OUTPUT AS #1
150  ' Input wing geometric information .. P3 usage
     AR = 7.539: TR = .40088: M = 10
     'PRINT : PRINT "Aspect Ratio, AR ="; AR
     'PRINT "Taper Ratio, TR ="; TR
     'PRINT "No. R.H. Wing Spanwise Stas. ="; M
     'MACH = .6: PRINT TAB(5); "Mach No. ="; MACH
     INPUT "Airspeed (knots) ="; VEL
     MACH = (VEL * 1.68781) / 1116.3
     PRINT "Mach No. =", MACH
     IF MACH > .95 THEN GOTO 151
     FC = 1! / SQR(1! - MACH ^ 2): GOTO 152
```

```
151 FC = 1!
152 ' Continue Dummy statement
    N = 5
    'PRINT "No. Chordwise Stas. ="; N
    'INPUT "No. Chordwise Stas. ="; N
    SWP25 = -1.312: 'PRINT "C/4 Sweep (deg.) ="; SWP25
    'INPUT "0.25 chd. sweep (deg.) ="; SWP25
    CEA = .4: 'PRINT "Elast. Axis Locatn., X/C ="; CEA
    'INPUT "Elastic Axis Locatn., X/C ="; CEA
    'INPUT "Dynamic Pressure, Q (psi) ="; Q
    INPUT "Is this a RIGID run? 1=Yes, 2=No, ANS=", ANS
    IF (ANS = 1) THEN
    Q = 0
    ELSE
    Q = (.7 * 2116.2 * MACH ^ 2) / 144
    END IF
    PRINT "Q =", Q
    KMAX = M * N
    '
    ' Calculate propeller thrust per engine (using curve fit
    ' from 2F87F P-3 simulator data)
    THRUST = (5849 - 5.069 * VEL)
    ' Calculate velocity boost due to prop slipstream
    v = VEL * 1.68781
    V1 = (-v + SQR((v ^ 2 + (4 * .05 * THRUST / (143.14 *
       .0023769))))) * 10
    ' Use velocity boost to find boosted Q (Q1)
    Q1 = (.5 * .0023769 * (v + V1) ^ 2) / 144
    IF (ANS = 1) THEN
      Q1 = 0
    END IF
    '
    ' Set up Q as a vector with boosted pressure (Q1) in
    ' region behind propellers
    FOR I = 1 TO KMAX
    Q(I) = Q: NEXT I
    FOR I = 11 TO 35
    Q(I) = Q1: NEXT I
    '
    PI = 4! * ATN(1!): ' Establish constant
    SWP25 = SWP25 * PI / 180!: ' Convert sweep to radians

180 ' Print header
    'GOSUB 1100
    'FOR MM = 1 TO 4



200 ' Determine Initial Wing Geometry
    B = 1188!:    ' DEFAULT Value of P3 Wing Span, inches
```

```
    DELB = .5 * B / M: 'Spanwise spacing increments of
    '                  vortex elements
    CR = 2! * B / (AR * (1! + TR)): ' Root Chord, inches
    S = B ^ 2 / AR: ' Wing Area, sq. in.
    TANLE = TAN(SWP25) + (.5 * CR * (1! - TR)) / B:
    ' Tangent L.E. sweep
    ' Develop Mean Aero. Chord information
    MAC = 2! * CR * ((1! + TR) - (TR / (1! + TR))) / 3!:
    ' Cmac, inches
    IF TR = 1! THEN GOTO 210
    YMAC = .5 * B * (1! - (MAC / CR)) / (1! - TR): GOTO 211
210 YMAC = .5 * B
211 XMAC25 = (YMAC * TANLE) + .25 * MAC

250 ' Determine coords. for wing vortex lattice corners &
    ' control pts.
    CONST1 = 1! - TR
    FOR I = 1 TO M
    C1 = CR * (1! - (CONST1 * (I - 1!) / M)): 'Total wing
    ' chord, inbd. vortex
    C2 = CR * (1! - (CONST1 * I / M)):  ' Wing chord, outbd.
    ' vortex
    C3 = CR * (1! - (CONST1 * (I - .5) / M)): ' Chord at
    ' control point sta.
    DELC1 = C1 / N: DELC2 = C2 / N: DELC3 = C3 / N
    YEA(I) = (I - .5) * DELB:  ' Create "M" Elastic axis
    ' coordinates
    XEA(I) = YEA(I) * TANLE + CEA * C3
    FOR J = 1 TO N
    K = (I - 1) * N + J: 'Create Vortex Lattice numbering
    ' scheme
    Y1(K) = (I - 1) * DELB: Y2(K) = Y1(K) + DELB
    Y3(K) = Y1(K) + (.5 * DELB)
    X1(K) = DELC1 * (J - .75) + Y1(K) * TANLE
    X2(K) = DELC2 * (J - .75) + Y2(K) * TANLE
    X3(K) = DELC3 * (J - .25) + Y3(K) * TANLE
    TANSWP = (X2(K) - X1(K)) / (Y2(K) - Y1(K))
    SWP(K) = ATN(TANSWP)
    TANSWPM = FC * TANSWP
    SWPM(K) = ATN(TANSWPM)
    NEXT J
    NEXT I
    ' Tangent of Elastic Axis Sweep, etc.
    DELEA = (XEA(2) - XEA(1)): REA = SQR(DELEA ^ 2 + DELB^2)
    TANEA = DELEA / DELB: SINEA = DELEA / REA
    COSEA=DELB/REA
    WRITE #1, Q
    INPUT "ENTER G LOAD, n =", NZ
    'Calculate required CL
    CLREQD = (NZ * 135000) / (.7 * 2116.2 * MACH ^ 2 * 1300)
    PRINT "CLREQD =", CLREQD
```

```
    WRITE #1, NZ
270 ' Bring in EI(I) and GJ(I) values for Structural model
    ' I = 1 (Root Sta.) & I = M (Tip Sta.), M = 10 by
    ' default
    ' EI Data, Est. for P3 wing
    DATA 8.30E+10, 6.80E+10, 5.27E+10, 4.10E+10, 2.80E+10
    DATA 2.00E+10, 1.33E+10, 0.85E+10, 0.55E+10, 0.35E+10
    FOR I = 1 TO M: READ EI(I): NEXT I
    ' GJ Data, Est. for P3 wing
    DATA 7.50E+10, 5.25E+10, 3.90E+10, 2.90E+10, 2.10E+10
    DATA 1.30E+10, 0.85E+10, 0.65E+10, 0.35E+10, 0.25E+10
    FOR I = 1 TO M: READ GJ(I): NEXT I

300 'Develop Aerodynamic Influence Coefficients
    ' A1(K1,K2) = RH Wing
    ' A2(K1,K2) = LH Wing
    FOR K1 = 1 TO KMAX: ' K1 Sta. is at the Control Point
    FOR K2 = 1 TO KMAX: ' K2 Sta. is at the Vortex Station
    NUM1 = X3(K1) - X1(K2): NUM2 = X3(K1) - X2(K2)
    NUM1 = FC * NUM1: NUM2 = FC * NUM2
    ' Bring in Prandtl-Glauert factor
    DEN1 = Y3(K1) - Y1(K2): DEN2 = Y3(K1) - Y2(K2)
    R1 = SQR(NUM1 ^ 2 + DEN1 ^ 2): R2 = SQR(NUM2^2+DEN2^2)
    ' Find trig. functns for orthogonal transformation on
    ' swept bound vortex
    SINSWP = SIN(SWPM(K2)): COSSWP = COS(SWPM(K2))
    H = NUM1 * COSSWP - DEN1 * SINSWP
    Y1ROT = NUM1 * SINSWP + DEN1 * COSSWP
    Y2ROT = NUM2 * SINSWP + DEN2 * COSSWP
    COSTHET1 = Y1ROT / R1: COSTHET2 = -Y2ROT / R2
    ' Logic Check to avoid division by zero
    IF (ABS(H)) <= .001 THEN GOTO 310
    DELWBD = (COSTHET1 + COSTHET2) / H: GOTO 311
310 DELWBD = 0!:    ' No downwash contributn. from bound
    '               vortex
311 ' Dummy statement space
    COS1 = NUM1 / R1: COS2 = NUM2 / R2
    DELWLH = (1! + COS1) / DEN1
    DELWRH = (1! + COS2) / DEN2
    A1(K1, K2) = (DELWLH + DELWBD - DELWRH) / (8! * PI)
    NEXT K2
    NEXT K1

    ' ** Similar logic for LH Wing Panel Aero. Influence
    '    coeffs.

315 FOR K1 = 1 TO KMAX: ' K1 Sta. is at the Control Point
    FOR K2 = 1 TO KMAX: ' K2 Sta. is at the Vortex Station
    NUM2 = X3(K1) - X1(K2): NUM1 = X3(K1) - X2(K2)
    NUM2 = FC * NUM2: NUM1 = FC * NUM1
    ' Bring in Prandtl-Glauert factor
```

```
    DEN2 = Y3(K1) + Y1(K2): DEN1 = Y3(K1) + Y2(K2)
    R1 = SQR(NUM1 ^ 2 + DEN1 ^ 2): R2 = SQR(NUM2^2+DEN2^2)
    ' Find trig. functns for orthogonal transformation on
    ' swept bound vortex
    SINSWP = -SIN(SWPM(K2)): COSSWP = COS(SWPM(K2))
    H = NUM1 * COSSWP - DEN1 * SINSWP
    Y1ROT = NUM1 * SINSWP + DEN1 * COSSWP
    Y2ROT = NUM2 * SINSWP + DEN2 * COSSWP
    COSTHET1 = Y1ROT / R1: COSTHET2 = -Y2ROT / R2
    ' Logic Check to avoid division by zero
    IF (ABS(H)) <= .001 THEN GOTO 320
    DELWBD = (COSTHET1 + COSTHET2) / H: GOTO 321
320 DELWBD = 0!:    ' No downwash contributn. from bound
    '                 vortex
321 ' Dummy statement space
    COS1 = NUM1 / R1: COS2 = NUM2 / R2
    DELWLH = (1! + COS1) / DEN1
    DELWRH = (1! + COS2) / DEN2
    A2(K1, K2) = (DELWLH + DELWBD - DELWRH) / (8! * PI)
    ASYM(K1, K2) = A1(K1, K2) + A2(K1, K2)
    AANT(K1, K2) = A1(K1, K2) - A2(K1, K2)
    NEXT K2
    NEXT K1

400 ' Determine Struct. Infl. Matrix, based on test of Q > 0
    ' Note: Q = 0 psi case is rigid wing situation
    IF Q > 0! THEN GOSUB 3000

    ' Skip the option for Sym. or Anti-Symm. Soln.
    'GOTO 800: 'Symm. solution branch

700 ' Select Symmetric or Antisymmetric Solution
    INPUT "Symm. or AntiSymm. Prob., S/A"; P$
710 IF P$ = "S" THEN GOTO 800
    IF P$ = "A" THEN GOTO 900
    GOTO 1000
800 ' Find Additional Loading
    ' GOTO 805: ' Branch to find effect of wing washout
    ' Introduce Additional type of alpha
    INPUT "ENTER AOA IN RADIANS, AOA =", AOA
    FOR K = 1 TO KMAX: ALPHA(K) = AOA: NEXT K
    'GOTO 805
    'PRINT "Elastic wing, Alpha = ", ALPHA(1)
    WRITE #1, ALPHA(1)
    '
    ' Introduce alpha due to built-in geometric twist
    ' 0.0 deg. at root, linearly to -2.5 deg. at tip
    WASH = -2.5 * PI / 180!
    FOR I = 1 TO M
    ETA = (I - .5) / M: DELWASH = ETA * WASH
    FOR J = 1 TO N
```

```
      K = (I - 1) * N + J: ' Create panel numbering
      ALPHA1(K) = DELWASH: NEXT J
      NEXT I
      'GOTO 805
      '
      ' Introduce alpha (rad.) due to eng./prop assbly.
      ' dead-wgt.
      DATA -0.0012, -0.0042, -0.0084, -0.0138, -0.0189
      DATA -0.0240, -0.0318, -0.0366, -0.0366, -0.0366
      ' Read dead-wgt. alphas one at a time..
      FOR I = 1 TO M
      READ DELALPH
      FOR J = 1 TO N
      K = (I - 1) * N + J: ' Create panel numbering
      ALPHA2(K) = NZ * DELALPH: NEXT J
      NEXT I
      '
      ' Introduce alpha (rad.) due to camber
      DATA -.0525, -.0240, 0.0, .0420, .0730
      ' Read in alphas due to camber at the root (WS = 0)
      FOR I = 1 TO N
      READ DELCAM(I)
      NEXT I
      ' Calculate the fifty slopes (one per control point) as
      ' airfoil varies from 14% to 12% thickness from root to
      ' tip
      FOR I = 1 TO M
      FOR J = 1 TO N
      K = (I - 1) * N + J
      ALPHA3(K) = DELCAM(J) * (1! - (I - .5) / (7 * M))
      NEXT J
      NEXT I
      '
      ' Introduce alpha (rad.) due to aileron float angle
      ' Calculate aileron float angle (rad) based on velocity
      ' (kts)
      FLAIL = -(1.4548 - .0090025 * VEL + .0000444 * VEL ^ 2)
            * .01745
      FOR I = 1 TO KMAX
      ALPHA4(K) = 0!: NEXT I
      ALPHA4(39) = .2 * FLAIL
      ALPHA4(44) = .2 * FLAIL: ALPHA4(49) = .2 * FLAIL
      ALPHA4(35) = .35 * FLAIL
      ALPHA4(40) = FLAIL: ALPHA4(45) = FLAIL: ALPHA4(50)=FLAIL

805   ' Combine angles by choice for net alpha distrib.
      INPUT "Enter type of run desired: 0 = Additional only,
      1= Washout only, 2 = Dead wt only, 3 = Camber only,
      4= Aileron float only, 5 = Complete solution, TYPE =", T
      WRITE #1, T
```

```
FOR I = 1 TO KMAX
IF (T = 0) THEN
ALPHA(I) = ALPHA(I): 'Additional loading selection
ELSEIF (T = 1) THEN
ALPHA(I) = ALPHA1(I): ' Washout alpha selection
ELSEIF (T = 2) THEN
ALPHA(I) = ALPHA2(I): ' Dead-wgt. induced alpha
'                       selection
ELSEIF (T = 3) THEN
ALPHA(I) = ALPHA3(I): ' Camber alpha section
ELSEIF (T = 4) THEN
ALPHA(I) = ALPHA4(I): ' Aileron float selection
ELSEIF (T = 5) THEN
ALPHA(I) = ALPHA(I) + ALPHA1(I) + ALPHA2(I) + ALPHA3(I)
         + ALPHA4(I): ' Complete wing selection
END IF
XIN(I) = ALPHA(I)
FOR J = 1 TO KMAX
A(I, J) = ASYM(I, J) - S(I, J) * Q(I): NEXT J
NEXT I
'
' Find Spanload Soln. L/Q from XIN(KMAX)
GOSUB 2000
' S/R returns XIN(I) as L/Q vector of length KMAX
LIFT = 0!: MOMENT = 0!: FOR I = 1 TO KMAX
LIFT = LIFT + XIN(I)
MOMENT = MOMENT + XIN(I) * (XMAC25 - .5 * (X1(I) +
       X2(I))): NEXT I
' Find Lift & Moment Coefficient
CL = LIFT * 2! * DELB / S
'
CM = MOMENT * 2! * DELB / (S * MAC)
NP = .25 - (CM / CL)
CLTOT = CLREQD - CL
PRINT "CL ="; CL; ", CM ="; CM; ",CLTOT ="; CLTOT
'PRINT "Neut. Pt. at (% Cmac)"; NP: PRINT
GOSUB 1100: ' Print Header
CAVE = .5 * CR * (1! + TR)
FOR I = 1 TO M: ' Sum up L/Q at eta value to get CLC
ETA = (I - .5) / M: CLC = 0!
FOR J = 1 TO N: K = (I - 1) * N + J
CLC = CLC + XIN(K)
NEXT J
' Find struct. twist due to airloads at front panel for
' sta. "I"
TWIST = 0!: J2 = (I - 1) * N + 1
FOR K = 1 TO KMAX
TWIST = TWIST + S(J2, K) * Q(I) * XIN(K): ' Struct twist
' due to airload
NEXT K
```

```
    C3 = CR * (1! - (CONST1 * (I - .5) / M)): ' Chord at
    ' control point sta.
    CLSECT = CLC / C3
    CLC = CLC / (CL * CAVE)
    GOSUB 1210: ' Print eta, cLc/CLCave, cL(sect) & struct.
    '             twist
    NEXT I
    GOTO 990

900 ' Anti-Symmetric Solution Branch
    ' Set up alpha for roll damping due to pB/2V = HELIX
    INPUT "Enter run desired: 0=Roll helix,
           1=Aileron deflection, RUN=", R
    ' Calculate available Pb/2V (rad) at specified velocity
    ' (kts)
    HELIX = (.21009 - .0008744 * VEL + .000001 * VEL ^ 2)
    IF (R = 1) GOTO 905
    FOR I = 1 TO M
    ALPDAMP = (I - .5) / M
    ' Multiply alpha for roll damping by available roll
    ' helix angle (rad) at given velocity (kts)
    ALPDAMP = ALPDAMP * HELIX
    FOR J = 1 TO N
    K = (I - 1) * N + J: XIN(K) = ALPDAMP: NEXT J
    NEXT I
    GOTO 908

905 ' Use following statement for aileron control
    ' effectiveness
    FOR I = 1 TO KMAX: XIN(I) = 0!: NEXT I
    ' Calculate aileron deflection (rad) available at given
    ' velocity (kts)
    DELAIL = -(90.30699 - .65754 * VEL + .001771 * VEL ^ 2 -
           .0000016 * VEL ^ 3) * .01745
    ' Deduct float angle from available control wheel
    ' aileron deflection
    FLAIL = -(1.4548 - .0090025 * VEL + .0000444 * VEL ^ 2)
          * .01745
    DELAIL = DELAIL - FLAIL
    XIN(39) = .2 * DELAIL: XIN(44) = .2 * DELAIL
    XIN(49) = .2 * DELAIL
    XIN(35) = .35 * DELAIL
    XIN(40) = DELAIL: XIN(45) = DELAIL: XIN(50) = DELAIL

908 ' Solve Spanload Problem
    FOR I = 1 TO KMAX: FOR J = 1 TO KMAX
    A(I, J) = AANT(I, J) - S(I, J) * Q(I): NEXT J
    NEXT I
    ' Use S/R ELU/SLVB to solve anti-symm L/Q
    GOSUB 2000
    ROLL = 0!: FOR I = 1 TO KMAX
```

```
    ROLL = ROLL + XIN(I) * Y3(I): NEXT I
    CROLL = -ROLL * 2! * DELB / (S * B)
    IF (R = 0) THEN
    PRINT "Roll Damping Deriv. CLP ="; CROLL / HELIX
    ELSE
    PRINT "Aileron Control Deriv., CLa =", CROLL / DELAIL
    END IF

910 'IF Q > 0 THEN GOTO 915
    'CROLLQ0 = CROLL

915 ' Dummy Skip Statement
    'EROLL = CROLL / CROLLQ0
    'GOSUB 1200:  ' Print results
    ' Branch for cLc,CLsect,Twist
    GOSUB 1100: ' Print Header
    CAVE = .5 * CR * (1! + TR)
    FOR I = 1 TO M  'Sum up L/Q at ETA to get CLC
    ETA = (I - .5) / M: CLC = 0!
    FOR J = 1 TO N: K = (I - 1) * N + J
    CLC = CLC + XIN(K)
    NEXT J
    ' Find struct. twist due to airloads at front panel for
    ' sta. "I"
    TWIST = 0!: J2 = (I - 1) * N + 1
    FOR K = 1 TO KMAX
    TWIST = TWIST + S(J2, K) * Q(I) * XIN(K)
    ' Struct twist due to airload
    NEXT K
    C3 = CR * (1! - (CONST1 * (I - .5) / M)): ' Chord at
    ' control point sta.
    CLSECT = CLC / C3
    'CLC = CLC / (CL * CAVE)
    GOSUB 1210: ' Print eta, cLc, cL(sect) & struct. twist
    NEXT I

    'GOSUB 1100
    'CAVE = .5 * CR * (1! + TR)
    'FOR I = 1 TO M:  ' Defaulted for N = 1 (Chrdwse sta.)
    'ETA = (I - .5) / M
    'CLC = XIN(I) / CAVE: GOSUB 1200
    'NEXT I


990 ' Q = Q + 1!
    'NEXT MM
    'GOTO 700


1000 END
```

```
1100 ' S/R to Print header, whole selection shown
     'PRINT TAB(3); "Mach No."; TAB(14); "CLalpha"; TAB(25);
     '              "CmCl"; TAB(35); "N.P."; TAB(45); "Clp"
     'PRINT TAB(5); "Q, psi"; TAB(14); "CLalpha"; TAB(25);
     '              "CmCl"; TAB(35); " N.P."; TAB(45);
     '              "Elift"; TAB(55); "Del-NP"
     'PRINT TAB(10); "Roll Control Evaluation, Mid Ail. at
     '                0.05"
     'PRINT TAB(5); "Q, psi"; TAB(15); "Croll"; TAB(25);
     '              "Eroll"
     PRINT
     PRINT TAB(6); "2Y/B"; TAB(13); "Clc/CLcave"; TAB(26);
     '          "Cl"; TAB(35); "Twist"; TAB(45); "Degrees"
     RETURN
1200 ' S/R to Print results, whole selection shown
     'PRINT USING "#####.####"; Q; CL; CM; NP; ELIFT; DELNP
     'PRINT USING "#####.####"; Q; CROLL; EROLL
1210 PRINT USING "#####.####"; ETA; CLC; CLSECT; TWIST;
               TWIST / .01745
     WRITE #1, ETA, CLC, CLSECT, TWIST, TWIST / .01745
     RETURN

2000 ' S/R ELU
     ' Tri-Diagonalizes the input matrix A(KMAX,KMAX)
     ' Input Column vector, XIN(KMAX), gets replaced by
     ' the output which is returned to the main program
     NM1 = KMAX - 1
     FOR K = 1 TO NM1: KP1 = K + 1
     FOR I = KP1 TO KMAX
     G = -A(I, K) / A(K, K): A(I, K) = G
     FOR J = KP1 TO KMAX
     A(I, J) = A(I, J) + G * A(K, J): NEXT J
     NEXT I
     NEXT K
     GOSUB 2050:  ' Use S/R SLVB for next step
     RETURN

2050 ' S/R SLVB
     ' Solves the Tri-Diagonalized matrix [A] obtained
     ' from ELU by back substitution
     NM1 = KMAX - 1: NP1 = KMAX + 1
     FOR K = 1 TO NM1
     KP1 = K + 1
     FOR I = KP1 TO KMAX
     XIN(I) = XIN(I) + A(I, K) * XIN(K)
     NEXT I
     NEXT K
     XIN(KMAX) = XIN(KMAX) / A(KMAX, KMAX)
     FOR K = 2 TO KMAX
     I = NP1 - K
     J1 = I + 1
```

```
      FOR J = J1 TO KMAX
      XIN(I) = XIN(I) - A(I, J) * XIN(J)
      NEXT J
      XIN(I) = XIN(I) / A(I, I)
      NEXT K
      RETURN

3000 'S/R to Determine [S] Structural Infl. Coeff. matrix
      '
3010 ' Generate [My] and [Mx] matrices, order M x KMAX
      ' First get diagonal elements
      K = 1: FOR I = 1 TO M: FOR J = 1 TO N
      MY(I, K) = .5 * (XEA(I) - X1(K) - .75 * DELB *
                TAN(SWP(K)))
      MX(I, K) = .25
      K = K + 1: NEXT J
      NEXT I
      ' Now get Upper triangular elements
      VALUE = 1!: FOR L = 1 TO M - 1
      K = L * N + 1: K2 = M - L
      FOR I = 1 TO K2: FOR J = 1 TO N
      MY(I, K) = XEA(I) - X1(K) - .5 * DELB * TAN(SWP(K))
      MX(I, K) = VALUE: K = K + 1: NEXT J
      NEXT I
      VALUE = VALUE + 1!: NEXT L
      ' Test circuit
      ' PRINT "Print out of MX(I,J)"
      ' FOR I = 1 TO M: FOR J = 1 TO KMAX
      ' PRINT USING "##.##"; MX(I, J);
      ' NEXT J
      ' PRINT : NEXT I

3020 ' Generate [DELA(I,J)], order KMAX x M
      K = 1
      FOR I = 1 TO M: FOR J = 1 TO N
      DELA(K, I) = 1!
      K = K + 1: NEXT J
      NEXT I
      ' Test circuit
      ' PRINT "Print out of DELA(I,J)"
      ' FOR I = 1 TO KMAX: FOR J = 1 TO M
      ' PRINT USING "##.##"; DELA(I, J);
      ' NEXT J
      ' PRINT : NEXT I


3030 ' Generate [U(I,J)] square matrix, order M x M
      FOR I = 1 TO M: FOR J = 1 TO M
      IF I = J THEN U(I, J) = .5
      IF I < J THEN U(I, J) = 0!
      IF I > J THEN U(I, J) = 1!
```

```
      NEXT J
      NEXT I
      ' Test circuit
      ' FOR I = 1 TO M: FOR J = 1 TO M
      ' PRINT USING "##.##"; U(I, J);
      ' NEXT J
      ' PRINT : NEXT I

3040  ' Generate UGJ(I,J) & UEI(I,J) matrices, order M x M
      ' Embed DELB^2 type of constants
      DELB2 = DELB ^ 2: TANDELB2 = TANEA * DELB2
      FOR I = 1 TO M: FOR J = 1 TO M
      ' DELB2 = 1!: GJ(J) = 6! - J : ' for test circuit
      UGJ(I, J) = DELB2 * U(I, J) / GJ(J)
      UEI(I, J) = TANDELB2 * U(I, J) / EI(J): NEXT J
      NEXT I    = TANDELB2 * U(I, J) / EI(J): NEXT J
      'Test Circuit
      ' PRINT "Sample of UGJ(I,J)"
      ' FOR I = 1 TO M: FOR J = 1 TO M
      ' PRINT USING "##.##"; UGJ(I, J);
      ' NEXT J
      'PRINT : NEXT I

3050  ' Start gathering terms for [S] matrix assembly
      DELSIN = DELB * SINEA: DELCOS = DELB * COSEA
      FOR I = 1 TO M: FOR J = 1 TO KMAX
      F(I, J) = 0!: G(I, J) = 0!
      FOR K = 1 TO M
      F(I, J) = F(I, J) + UGJ(I, K) * (COSEA * MY(K, J) +
              DELSIN * MX(K, J))
      G(I, J) = G(I, J) + UEI(I, K) * (SINEA * MY(K, J) -
              DELCOS * MX(K, J))
      NEXT K
      NEXT J
      NEXT I
3060  ' Form the [S] matrix, order KMAX x KMAX
      FOR I = 1 TO KMAX: FOR J = 1 TO KMAX
      S(I, J) = 0!
      FOR K = 1 TO M
      S(I, J) = S(I, J) + DELA(I, K) * (F(K, J) + G(K, J)):
      NEXT K
      NEXT J
      NEXT I
      ' [S] matrix is now available
      RETURN
```

APPENDIX B

```
C     P-3 LEADING EDGE FAILURE ANALYSIS
C     TWO DIMENSIONAL PANEL METHOD

      PROGRAM PANEL

C.....THIS FORTRAN PROGRAM ITERATIVELY COMPUTES THE PRESSURE
C     AND FORCE DISTRIBUTION AROUND THE P-3 AIRFOIL AT 24
C     SELECTED WING STATIONS AND WRITES A LOAD FILE FOR USE
C     IN MSC PAL2 FINITE ELEMENT ANALYSIS SOFTWARE.  INPUT
C     CONSISTS OF THE AIRFOIL COORDINATES (X,Y) FROM A FILE
C     CALLED P3.DAT, THE 24 WING STATION LOCATIONS IN
C     INCHES AND THE NODE NUMBERS FROM THE FINITE ELEMENT
C     MODEL AT WHICH FORCES AND CONSTRAINTS WILL BE APPLIED.
C     OUTPUT CONSISTS OF THE PAL2 LOAD FILE (LE.LD), A
C     TABULAR FILE IDENTIFYING THE COEFFICIENT OF PRESSURE,
C     DYNAMIC PRESSURE AND FORCES AT A GIVEN PANEL MID POINT
C     ON THE LEADING EDGE OF THE AIRFOIL.  SECTION LIFT
C     COEFFICIENT (Cl) IS MATCHED TO AN INPUT Cl REQUIREMENT
C     (GENERATED BY AN AEROELASTIC SPAN LOAD ANALYSIS
C     PROGRAM) THROUGH ITERATION OF ANGLE OF ATTACK.

      PARAMETER(N=53,M=N+1,PI=3.14159265,RHO=.0023769,
     +          PAMB=14.7)
      REAL X(M),Y(M),THETA(M),BETA(M,M),R(M,M),XM(M),YM(M),
     +     A(100,101),AN(M,M),BN(M,M),AT(M,M),BT(M,M),
     +     SUMBN(M,M),SUMB1,SUMB2,SUMA(M),SUMB(M),VTAN(M),
     +     Q(M),CP(M),P(M),NUM(M),DEN(M),ALPHA,V,VEL,AOA,
     +     CY(M),CX(M),CM(M),FY(M),FX(M),VTOT(N),CYT,CXT,CMT
     +     FYT,FXT,CD,CL,CLRQD(100),WS(100),XML(M),YML(M),
     +     LOADM(M),INTWIST,OUTWIST,TWIST,XTOPDIS,XBOTDIS,
     +     XDISTOP(48),XDISHIN(24),ZDISTOP(48),ZDISHIN(24)
      INTEGER K,I,J,NODE(100,100),NTOP(100),NHIN(100)

      OPEN(UNIT=51,FILE='P3.DAT',STATUS='UNKNOWN')
      OPEN(UNIT=57,FILE='DUMP.DAT',STATUS='UNKNOWN')
      OPEN(UNIT=58,FILE='WS.DAT',STATUS='UNKNOWN')
      OPEN(UNIT=60,FILE='LE.LD',STATUS='UNKNOWN')
      OPEN(UNIT=61,FILE='TOP.DAT',STATUS='UNKNOWN')
      OPEN(UNIT=62,FILE='HINGE.DAT',STATUS='UNKNOWN')
      OPEN(UNIT=63,FILE='NODESa.DAT',STATUS='UNKNOWN')
      OPEN(UNIT=64,FILE='NODESb.DAT',STATUS='UNKNOWN')
      OPEN(UNIT=65,FILE='NODESc.DAT',STATUS='UNKNOWN')
```

```
C.....READ IN AIRFOIL DATA

      DO 10 K=1,N
        READ(51,500) X(K),Y(K)
   10 CONTINUE
  500 FORMAT(2F10.6)

      X(N+1)=X(1)
      Y(N+1)=Y(1)

C.....READ IN FINITE ELEMENT NODE NUMBERS FOR LATER USE
C     (READ AS NODE(PANEL NO.,RIB))

      DO 12 I=17,36
        READ(63,575) (NODE(I,J),J=1,8)
        READ(64,575) (NODE(I,J),J=9,16)
        READ(65,575) (NODE(I,J),J=17,24)
   12 CONTINUE
  575 FORMAT(9I5)

C.....WRITE HEADER FOR FINITE ELEMENT LOAD FILE

      WRITE(60,590)

C.....REQUEST AND RECEIVE AIRSPEED INPUT

      PRINT*,'ENTER VELOCITY IN KNOTS (XXX.XX)'
      READ*,VEL
      V = VEL*1.6878

C.....REQUEST AND RECEIVE FRONT SPAR TWIST ANGLES

      PRINT*,'ENTER TWIST AT 2Y/B=.35 (rad)(.XXXX)'
      READ*,TWIST35
      PRINT*,'ENTER TWIST AT 2Y/B=.45 (rad)(.XXXX)'
      READ*,TWIST45
      PRINT*,'ENTER TWIST AT 2Y/B=.55 (rad)(.XXXX)'
      READ*,TWIST55


C.....CALCULATE CHORD LENGTH OF P-3 WING AT SELECTED WING
C     STATIONS


C.....SET UP OUTER LOOP TO ITERATIVELY CALCULATE PRESSURES
C     FOR A SERIES OF WING STATIONS
```

```
C.....INPUT WING STATIONS, Cl AND LOAD MULTIPLIER FROM FILE
C     WS.DAT AND CALCULATE CHORD LENGTH AT THE WING STATION

  502 FORMAT(F7.1,F8.4,F6.2)
      DO 15 L=1,24
        READ(58,502) WS(L),CLRQD(L),LOADM(L)
        PRINT*,'ITERATION=',L
        PRINT*,'WS=',WS(L)
        PRINT*,'CLRQD=',CLRQD(L)
        CHORD = 227.*(1-(0.6*(2.*WS(L)/1188.)))
        PRINT*,'CHORD=',CHORD

C.....CALCULATE THE THICKNESS FRACTION AT A GIVEN WING
C     STATION (USE TO LINEARLY VARY AIRFOIL THICKNESS WITH
C     WING STATION)

      DTHICK = 1-((1-(12./14.))*(2.*WS(L)/1188.))
      PRINT*,'THICKNESS RATIO =',DTHICK

C.....SCALE THE THICKNES OF THE AIRFOIL AT EACH WING STATION
C     BY THE THICKNESS FRACTION

      DO 16 K=1,N
        Y(K)=Y(K)*DTHICK
   16 CONTINUE

C.....SET STARTING ALPHA

      ALPHA = (PI/180.)

C.....SET COUNTER START FOR AOA ITERATION

      KOUNT = 1

C.....BEGIN ITERATION OF ALPHA TO MATCH CLREQD = CL

 1100 CONTINUE

C.....FIND NORMALIZED MID-POINT OF PANEL

      DO 30 I=1,N-1
        XM(I)=0.5*(X(I)+X(I+1))
        YM(I)=0.5*(Y(I)+Y(I+1))

C.....FIND MID-POINT OF PANEL IN INCHES

      XML(I)=XM(I)*CHORD
      YML(I)=YM(I)*CHORD
```

```
C.....CALCULATE THETA (ANGLE BETWEEN PANEL AND CHORD LINE)

      NUM(I)=Y(I+1)-Y(I)
      DEN(I)=X(I+1)-X(I)
      THETA(I)=ATAN2(NUM(I),DEN(I))

C.....CALCULATE R (DISTANCE BETWEEN PANEL MID-POINTS)

      DO 20 J=1,N
        R(I,J)=SQRT((XM(I)-X(J))**2+(YM(I)-Y(J))**2)

C.....CALCULATE BETA  (ANGLE AT MID POINT OF PANEL I,
C     ENCLOSING END POINTS OF PANEL J)

        BETA(I,J)=ATAN2(((YM(I)-Y(J+1))*(XM(I)-X(J))
     #                -((XM(I)-X(J+1)))*(YM(I)-Y(J))),
     #                 ((XM(I)-X(J+1))*(XM(I)-X(J))
     #                 +(YM(I)-Y(J+1))*(YM(I)-Y(J))))


   20    CONTINUE
   30 CONTINUE

C.....CALCULATE AUGMENTED "A" MATRIX

      SUMB1=0.0
      SUMB2=0.0
      DO 50 I=1,N-1
        SUMBN(I,N)=0.0
      DO 40 J=1,N-1
        IF (I.EQ.J) THEN
          AN(I,J)=0.5
          AT(I,J)=0.0
          BN(I,J)=0.0
          BT(I,J)=0.5
        ELSE

AN(I,J)=(SIN(THETA(I)-THETA(J))*LOG(R(I,J+1)/R(I,J))
     #             +COS(THETA(I)-THETA(J))*BETA(I,J))/(2*PI)

BN(I,J)=(COS(THETA(I)-THETA(J))*LOG(R(I,J+1)/R(I,J))
     #             -SIN(THETA(I)-THETA(J))*BETA(I,J))/(2*PI)
          AT(I,J)=-BN(I,J)
          BT(I,J)=AN(I,J)
        END IF
        SUMBN(I,N)=SUMBN(I,N) + BN(I,J)
        IF (I.EQ.1) THEN
          SUMB1=SUMB1 + BT(1,J)
        ELSEIF (I.EQ.N-1) THEN
          SUMB2=SUMB2 + BT(N-1,J)
        END IF
```

```
      A(I,J) = AN(I,J)
      A(I,N) = SUMBN(I,N)
      A(N,J) = AT(1,J) + AT(N-1,J)
      A(N,N) = SUMB1 + SUMB2
   40    CONTINUE
   50 CONTINUE

      DO 60 I=1,N-1
        A(I,N+1) = -V*SIN(ALPHA-THETA(I))
   60 CONTINUE

        A(N,N+1)=-V*(COS(ALPHA-THETA(1))+
     +            COS(ALPHA-THETA(N-1)))

      CALL GAUSS(N,A)

      GAMMA=0.0
      DO 80 I=1,N
        Q(I)=A(I,N+1)
        GAMMA=A(N,N+1)
   80 CONTINUE

      DO 100 I=1,N-1
        SUMA(I)=0.0
        SUMB(I)=0.0
      DO 90 J=1,N-1
        SUMA(I)=SUMA(I)+Q(J)*AT(I,J)
        SUMB(I)=SUMB(I)+BT(I,J)
        VTOT(I)=SUMA(I)+GAMMA*SUMB(I)+V*COS(ALPHA-THETA(I))
        VTAN(I)=VTOT(I)/V
        CP(I)=1.0-(VTAN(I))**2.0
        P(I)=((CP(I)*0.5*RHO*(V**2.))/144.)
   90 CONTINUE
  100 CONTINUE

C.....CALCULATE FORCE COEFFICIENTS (CX,CY) AND FORCES (FX=
C     CHORDWISE, FY=NORMAL TO CHORD) AT PANEL MID POINT

      CYT=0
      CXT=0
      CMT=0
      FXT=0
      FYT=0
      DO 110 I=1,N-1
        CY(I)=-1.0*CP(I)*(X(I+1)-X(I))
        CX(I)=CP(I)*(Y(I+1)-Y(I))

C.....MULTIPLY BY CHORD FOR FULL SCALE SOLUTION

        FY(I)=CHORD*CY(I)*0.5*RHO*(V**2.)/144
```

```
        FX(I)=CHORD*CX(I)*0.5*RHO*(V**2.)/144
        CM(I)=CP(I)*((X(I+1)-X(I))*XM(I)+
     +         (Y(I+1)-Y(I))*YM(I))
        CYT=CYT+CY(I)
        CXT=CXT+CX(I)
        FYT=FYT+FY(I)
        FXT=FXT+FX(I)
  110 CONTINUE

C.....GET FORCE TOTALS FORWARD OF FRONT SPAR (.15C)

      FYNT=0.0
      FXNT=0.0
      DO 115 I=18,35
        FYNT=FYNT+FY(I)
        FXNT=FXNT+FX(I)
  115 CONTINUE

C.....CALCULATE APPROXIMATE TOTAL FORCES ON COMPLETE LE
C     SECTION (BETWEEN NACELLES) BY TAKING FORCES AT
C     MID POINT * 92 INCHES

      IF (L.EQ.7) THEN
        FYTOT=FYNT*92
        FXTOT=FXNT*92
      ENDIF

C.....PERFORM AXIS ROTATION TO FIND CL

      CL=CYT*COS(ALPHA)-CXT*SIN(ALPHA)

C.....PERFORM ITERATION OF ANGLE OF ATTACK

      DIFF=.0001
      CLDIFF=CLRQD(L)-CL
      KILL=50
      DELTA=0.1745
      IF (KOUNT.GT.KILL) THEN
        PRINT*,'COUNTER EXCEEDED'
        GOTO 111
      ELSEIF (CLDIFF.GT.DIFF) THEN
        PRINT'(I3,2F10.6)',KOUNT,ALPHA,CL
        KOUNT=KOUNT+1
        ALPHA=ALPHA+(DELTA*ABS(CLDIFF))
        GOTO 1100
      ELSEIF (CLDIFF.LT.0.0) THEN
        PRINT'(I3,2F10.6)',KOUNT,ALPHA,CL
        KOUNT=KOUNT+1
        ALPHA=ALPHA-(DELTA*ABS(CLDIFF))
        GOTO 1100
      ELSE
```

```
        PRINT'(4F10.5)',ALPHA,CL,FXNT,FYNT
        WRITE(57,570) VEL,WS(L),ALPHA,CLRQD(L),CL,FXNT,FYNT
        WRITE(57,560)
      ENDIF

C.....WRITE PRESSURES AND FORCES TO OUTPUT FILES

      DO 120 I=17,36
        WRITE(57,580) I,XM(I),XML(I),YML(I),CP(I),P(I),
     +                FX(I)*LOADM(L),FY(I)*LOADM(L)
  120 CONTINUE

C.....WRITE LOADING FILE (LE.LD) FOR FINITE ELEMENT
APPLICATION(PAL2).

      FX(17)=FX(17)*0.5
      FY(17)=FY(17)*0.5
      FX(23)=FX(23)+0.5*FX(24)
      FY(23)=FY(23)+0.5*FY(24)
      FX(25)=FX(25)+0.5*FX(24)
      FY(25)=FY(25)+0.5*FY(24)
      FX(26)=FX(26)+FX(27)
      FY(26)=FY(26)+FY(27)
      FX(28)=FX(28)+0.5*FX(29)
      FY(28)=FY(28)+0.5*FY(29)
      FX(30)=FX(30)+0.5*FX(29)
      FY(30)=FY(30)+0.5*FY(29)
      FX(36)=FX(36)*0.5
      FY(36)=FY(36)*0.5
      DO 125 I=17,36
        J=I
      IF (I.LE.23) THEN
        WRITE(60,591) NODE(J,L),FX(I)*LOADM(L),
     +                NODE(J,L),FY(I)*LOADM(L)
      ELSEIF (I.EQ.25) THEN
        WRITE(60,591) NODE(J,L),FX(I)*LOADM(L),
     +                NODE(J,L),FY(I)*LOADM(L)
      ELSEIF (I.EQ.26) THEN
        WRITE(60,591) NODE(J,L),FX(I)*LOADM(L),
     +                NODE(J,L),FY(I)*LOADM(L)
      ELSEIF (I.EQ.28) THEN
        WRITE(60,591) NODE(J,L),FX(I)*LOADM(L),
     +                NODE(J,L),FY(I)*LOADM(L)
      ELSEIF (I.GE.30) THEN
        WRITE(60,591) NODE(J,L),FX(I)*LOADM(L),
     +                NODE(J,L),FY(I)*LOADM(L)
      ENDIF
  125 CONTINUE
```

```
  560 FORMAT(2X,'PANEL',3X,'XM(I)',4X,'XML(I)',4X,'YML(I)',
     +       5X,'CP(I)',5X,'P(I)',6X,'FX(I)',5X,'FY(I)')
  570 FORMAT(//,2X,'VEL=',F10.1,/,2X,'WS=',F10.3,/,2X,
     +     'ALPHA=',F10.5,/,2X,'CLRQD=',F10.5,/,2X,'CL=',
     +     F10.5,/,2X,'FXNT=',F10.5,/,2X,'FYNT=',F10.5,/)
  580 FORMAT(2X,I3,7F10.5)
  590 FORMAT(1X,'FORCES AND MOMENTS APPLIED 0')
  591 FORMAT(1X,'FX',I7,F10.5,/,1X,'FZ',I7,F10.5)
  111 CONTINUE
   15 CONTINUE

C.....CALCULATE TWIST DISPLACEMENTS OF FINITE ELEMENT NODES

      INTWIST=0.82155*(TWIST45-TWIST35)+TWIST35
      OUTWIST=0.89371*(TWIST55-TWIST45)+TWIST45
      TWIST=OUTWIST-INTWIST
      XTOPDIS=TWIST*8.8
      XBOTDIS=(-1.0)*XTOPDIS

      DO 130 I=1,24
        J=I-1
        XDISTOP(2*I-1)=(XTOPDIS/23.)*J
        XDISTOP(2*I)=(XTOPDIS/23.)*J
        XDISHIN(I)=(XBOTDIS/23)*J
        TT=(TWIST/23.)*J
        XT=(XTOPDIS/23.)*J
      IF (TT.LE.0625) THEN
        ZDISTOP(2*I)=0.5*TT*XT
      ELSE
        ZDISTOP(2*I)=(-0.5)*(TT-.125)*XT
      END IF
        ZDISTOP(2*I-1)=(-0.5)*TT*(XT+1.0)
        ZDISHIN(I)=0.5*TT*XT
  130 CONTINUE

      WRITE(57,555) FXTOT,FYTOT
  555 FORMAT(/,2X,'APPROX TOTAL FX(92")=',F10.1,
     +       /,2X,'APPROX TOTAL FY(92")=',F10.1)

C.....READ AND WRITE NODES AND CORRESPONDING BOUNDARY
C     CONDITIONS IN FINITE ELEMENT LOAD

      WRITE(60,597)
      READ(61,592) (NTOP(I),I=1,48)
      READ(62,601) (NHIN(I),I=1,24)
      WRITE(60,593) (NTOP(I),I=1,48)
      WRITE(60,5931) (NTOP(I),XDISTOP(I),I=1,48)
```

```
C.....ENFORCE Y-AXIS DISPLACEMENT CONSTRAINT ALONG FRONT
C     EDGE OF SPAR CAP FLANGE ONLY.  (RELEASE BACK EDGE TO
C     SIMULATE SINGLE LINE OF SCREW FASTENERS.)

      WRITE(60,5932) (NTOP(2*I),I=1,24)
      WRITE(60,5933) (NTOP(I),ZDISTOP(I),I=1,48)
      WRITE(60,594) (NHIN(I),XDISHIN(I),I=1,24)
      WRITE(60,599) (NHIN(I),I=1,24)
      WRITE(60,600) (NHIN(I),ZDISHIN(I),I=1,24)
      WRITE(60,595) (NHIN(I),I=1,24)
      WRITE(60,596) (NHIN(I),I=1,24)
      WRITE(60,598)
  592 FORMAT(I5)
  601 FORMAT(I5)
  593 FORMAT(1X,'RA',I7,1X,'0')
 5931 FORMAT(1X,'TX',I7,1X,F8.4)
 5932 FORMAT(1X,'TY',I7,1X,'0')
 5933 FORMAT(1X,'TZ',I7,1X,F8.4)
  594 FORMAT(1X,'TX',I7,1X,F8.4)
  599 FORMAT(1X,'TY',I7,1X,'0')
  600 FORMAT(1X,'TZ',I7,1X,F8.4)
  595 FORMAT(1X,'RX',I7,1X,'0')
  596 FORMAT(1X,'RZ',I7,1X,'0')
  597 FORMAT(1X,'-- BLANK LINE --',/,
     +       1X,'DISPLACEMENTS APPLIED 0')
  598 FORMAT(1X,'-- BLANK LINE --',/,
     +       1X,'SOLVE',/,1X,'QUIT')

      STOP
      END


      SUBROUTINE GAUSS(N,A)

C.....THIS SUBROUTINE PERFORMS GAUSS ELIMINATION WITH
C     PIVOTING.

      INTEGER PV                        ! PIVOT INDEX.
      DIMENSION A(100,101)
      EPS=1.0
   10 IF (1.0+EPS.GT.1.0) THEN
      EPS=EPS/2.0
      GOTO 10
      END IF
      EPS=EPS*2.0
      EPS2=EPS*2.0
      DO 1010 I=1,N-1
        PV=I
      DO J=I+1,N
      IF (ABS(A(PV,I)).LT.ABS(A(J,I))) PV=J
```

```
      END DO
      IF (PV.EQ.I) GOTO 1050
      DO JC=1,N+1
        TM=A(I,JC)
        A(I,JC)=A(PV,JC)
        A(PV,JC)=TM
      END DO
 1050 IF (A(I,I).EQ.0) GOTO 1200  ! KICK OUT IF SINGULAR
      DO JR=I+1,N          ! ELIMINATION OF BELOW DIAGONAL.
      IF (A(JR,I).NE.0.0) THEN
        R=A(JR,I)/A(I,I)
      DO KC=I+1,N+1
        TEMP=A(JR,KC)
        A(JR,KC)=A(JR,KC) - R*A(I,KC)
      IF (ABS(A(JR,KC)).LT.EPS2*TEMP) A(JR,KC)=0.0

C.....IF THE RESULT OF SUBTRACTION IS SMALLER THAN 2 TIMES
C     EPS TIMES THE ORIGINAL VALUE, IT IS SET TO ZERO.

      END DO
      END IF
 1060 END DO
 1010 CONTINUE

      IF (A(N,N).EQ.0) GOTO 1200
      A(N,N+1)=A(N,N+1)/A(N,N)
      DO NV=N-1,1,-1      ! BEGIN BACKWARD SUBSTITUTION.
        VA=A(NV,N+1)
      DO K=NV+1,N
        VA=VA-A(NV,K)*A(K,N+1)
      END DO
        A(NV,N+1)=VA/A(NV,NV)
      END DO
      RETURN

 1200 PRINT*,'MATRIX IS SINGULAR'

      STOP
      END
```

INITIAL DISTRIBUTION LIST

1.	Defense Technical Information Center Cameron Station Alexandria, VA 22304-6145	2
2.	Superintendent, Naval Postgraduate School Library, Code 0142 Monterey, CA 93943-5002	2
3.	Superintendent, Naval Postgraduate School Dept. of Aeronautics & Astronautics, Code AA Monterey, CA 93943-5000	1
4.	Superintendent, Naval Postgraduate School Professor Louis V. Schmidt, Code AA/Sc Monterey, CA 93943-5000	2
5.	Superintendent, Naval Postgraduate School Professor Richard M. Howard, Code AA/Ho Monterey, CA 93943-5000	1
6.	Superintendent, Naval Postgraduate School Aviation Safety Programs, Code 034 ATTN: CDR Stuart Schreckengast Monterey, CA 93943-5000	1
7.	Commander, Naval Air Systems Command AIR-530 ATTN: Mr. J.C. McKeown Washington, DC 20361-5300	1
8.	Commander, Naval Safety Center Code 112A ATTN: LT Brian Craddock NAS Norfolk, VA 23511-5796	1
9.	Commanding Officer, Patrol Squadron Thirty-One Code 00A ATTN: Dr. Henry H. Smith NAS Moffett Field, CA 94035-5000	1

10. LCDR Richard B. Bobbitt, USN 1
551 Hyannis Drive
Sunnyvale, CA 94087

11. LCDR Dennis A. Lott 2
P.O. Box 175
Windsor, NY 13865